Habilitation à diriger des recherches

université PARIS-SACLAY

Cold atom experiments on correlations in magnetic and light-induced dipoles

Habilitation à diriger des recherches de l'Université Paris-Saclay

présentée et soutenue à Palaiseau, le 30 mai 2024, par

Igor FERRIER-BARBUT

Composition du jury

Mathilde HUGBART Directrice de recherche, Institut de physique de Nice	Rapportrice
Leticia TARRUELL Professeure des universités, Institut des sciences photoniques	Rapportrice
Giovanni MODUGNO Professeur des universités, Université de Florence	Rapporteur
David CLEMENT Maitre de conférences, Institut d'optique	Examinateur
Jacqueline BLOCH Directrice de recherche, Centre pour les nanosciences et nanotechnologies	Examinatrice

Remerciements

Ce mémoire présente mes travaux de recherche depuis ma soutenance de thèse jusqu'aujourd'hui, ils ont été rendus possibles par de nombreuses personnes que je remercie ici avec beaucoup de plaisir.

Pour mon post-doctorat à Stuttgart, j'ai bénéficié d'un accueil particulièrement bienveillant de la part de Tilman Pfau et son groupe. Les étudiants d'alors, Thomas, Holger Matthias et Matthias m'ont tout de suite fait une place en m'intégrant activement l'équipe ce qui m'a permis d'être tout de suite très à l'aise avec eux et dans mon rôle de postdoc. Tilman m'a donné beaucoup de responsabilités très tôt, je lui en suis extrêmement reconnaissant. J'ai énormément appris en physique à ses côtés découvrant une approche très riche de la physique expérimentale.

Depuis mon arrivée au LCF, de nombreuses personnes ont été importantes. En premier lieu, Antoine qui m'a accueilli dans son groupe. J'apprends tous les jours en le côtoyant mais je suis surtout impressionné par sa capacité à prêter toute son attention à ses étudiants et collègues en toute circonstance. Ça a entre autres permis que je trouve une place dans le groupe et un travail au quotidien dont je suis très heureux. Je prends aussi beaucoup de plaisir à interagir Thierry et à apprendre à ses côtés. La qualité de ses méthodes de travail et ses connaissances sont impressionnantes, et nourrissent continuellement mon travail. Giovanni a eu une place importante en tant que postdoc, ce qui n'était pas chose facile. Il a su se rendre indispensable à notre équipe par sa force de travail et ses qualités humaines que j'apprécie beaucoup. La présence de Florence dans le groupe est précieuse, à la fois pour le développement des expériences pour les mettre sur les rails vers des beaux succès, et par l'attention bienveillante qu'elle porte à tous ses collègues, qui cimente aussi un bel esprit de groupe. Je remercie aussi Daniel, je bénéficie de la qualité de son travail et de ses questions sur mon travail. Merci aussi à Yvan de m'avoir en quelque sorte légué sa place. Je profite pour finir énormément de la présence de Patrick, qui nous porte une attention de tous les instants et nous rend le travail facile.

Les doctorantes et doctorants jouent un rôle majeur au quotidien. Merci à Toni de m'avoir presque accueilli sur sa manip pour la mener ensemble vers de beaux résultats. Merci infiniment à Damien puis Britton et aussi Sam, qui portent avec brio le poids de devoir construire la nouvelle manip. Leurs qualités et leur travail ont permis sa mise en route avec succès, et je suis impressionné par l'excellente ambiance qui y règne. J'espère développer une aussi bonne relation avec les nouveaux thésards de notre groupe, Sara et compères. Merci aussi à tous les membres du groupe sur la partie Rydberg avec qui j'interagit au quotidien,. Ils contribuent à une ambiance de groupe que j'aime beaucoup, et je suis toujours curieux de discuter des résultats magistraux de leur travail.

Je remercie aussi les personnes avec qui j'ai travaillé pour l'enseignement et la fête de la science au sein de l'institut, Matthieu, Marc, Sylvie etc. Je souhaite finalement appuyer sur le soutient de la structure administrative du LCF et de l'IOGS dont nous bénéficions, qui nous permet de travailler dans les meilleures conditions.

Merci enfin à mes amis et ma famille, ma maman mes soeurs depuis toujours, Raphaëlle qui montre qu'on peut faire avec enthousiasme un metier qui a du sens, Alix et Saskia qui me permettent d'oublier un peu le travail.

À mon père.

Introduction

My PhD was carried out at Laboratoire Kastler Brossel, in the physics department of ENS Paris, under the joint supervision of Christophe Salomon and Frédéric Chevy. We were concerned in good part with the study of superfluidity in quantum gases that interacted via the usual van der Waals interaction.

After that, I joined the 5th institute of Physics at the university of Stuttgart, in the group of Tilman Pfau. There I was a member of the team that studied experimentally dipolar quantum gases, that is quantum gases made of atoms that interact not only via the short-range van der Waals interaction, but also through a magnetic dipole-dipole interaction. Experiments on these dipolar quantum gases were initiated in Stuttgart in the early 2000s, first with Chromium atoms. Shortly before I joined the team in December 2014, they had completed building a new experimental setup, and had achieved Bose-Einstein condensation of Dysprosium, the second realization after the first in Benjamin Lev'ĂŹs group in Urbana Champaign. From then on, during the three-and-a-half years that my postdoctoral stay lasted, we performed experiments on dipolar Bose-Einstein condensates in the regime where the magnetic dipole-dipole interaction dominates, gradually gaining control of interactions and understanding the resulting many-body state. This led to the discovery of an unforeseen phenomenon : the existence of quantum droplets whose stability can only be understood by accounting for quantum fluctuations beyond mean-field theory. Understanding the nature of dipolar quantum droplets and characterising their main features occupied us for the duration of my postdoc, and led us to predict the possibility of obtaining spontaneous structure formation while maintaining superfluidity. This was observed soon after I left the Stuttgart team, and the study of these IJdipolar supersolidsĂİ as they are now called is a very active area.

Then I joined in October 2018 the ĂAtoms team of the Quantum Optics group at Laboratoire Charles Fabry, Institut d'ĂŹOptique in Palaiseau, headed by Antoine Browaeys. I started by working in the so-called ĂIJCyclopixĂİ lab that was built by Antoine together with Yvan Sortais who has since started a new group on industrial photonics at LCF. This new research was the occasion for me to study a new type of dipole-dipole interactions : light-induced dipole-dipole interactions. We are interested in the internal state of the atoms. And we are concerned with non-conservative problems i.e. with dissipation in the form of collective spontaneous emission from the atoms. This can be put in contrast with the Rydberg array experiments carried out in the group by Antoine and Thierry Lahaye, who study also spin systems but so far only in the conservative case (at least when one ignores experimental imperfections and the finite lifetime of Rydberg levels). Cyclopix produces dense clouds of rubidium in an optical tweezer. With these we study the collective light-matter interaction of dense two-level atom ensembles, where the interatomic distance is on the order of the wavelength of the light or smaller. We have observed the two hallmarks of collective spontaneous emission : superradiance and subradiance. We are pursuing studies with the general goal to elucidate the relationship between atomic correlations in the medium and properties of the light it radiates : intensity, coherence, correlations.

To explore these problems, we will continue research on Rb dense ensembles as they have shown themselves a remarkable platform. I also started a new lab thanks to an ANR JCJC and ERC Starting Grant, with the aim to produce arrays of Dy atoms and study collective light-matter interactions in ordered ensembles, where theoretical predictions are more easily obtained. Structuring the ensemble should also lead to an enhanced light-matter coupling. The intended advantage of this new setup is to offer access to new observables (direct measurement of the atomic state) and new tools (sub-wavelength spacing, local addressing of the atomic resonance). This setup was

started in the spring 2021. We have now obtained single atoms of Dy in tweezer arrays, and I review the progress towards these goals in the last part of the manuscript.

Table des matières

1 Bose Einstein condensates of magnetic dipoles

1.1 Introduction

Degenerate gases have allowed remarkable progress in the understanding of interaction effects in many-body systems [Bloch et al., 2008]. Most studies were using the van der Waals interaction between ground state atoms. A few experimental teams are studying instead effects of *magnetic dipole-dipole interactions* (DDI) in quantum gases [Lahaye et al., 2009, Chomaz et al., 2016]. The first experiments were performed on chromium Bose-Einstein condensates in the group of Tilman Pfau in Stuttgart. For this, one relies on species with a sizeable magnetic moment such as Cr and lanthanide atoms, in particular erbium and dysprosium. I joined the Stuttgart group for my postdoc working on the new Dy setup that had started producing BECs.

Let us first review the interactions taking place in these dipolar Bose-Einstein condensates (dBECs) before explaining the phenomena that we investigated.

1.2 Interactions in a dipolar Bose-Einstein condensate

The van der Waals interaction has a short range, in ultracold conditions ($\sim$ sub mK) it is effectively a contact interaction :

$$V(\boldsymbol{r}) = g\,\delta(\boldsymbol{r}) = \frac{4\pi\hbar^2}{m}\,a\,\delta(\boldsymbol{r}), \tag{1}$$

and its strength is given by the scattering length a which can be varied through Feshbach resonances [Chin et al., 2010]. Atoms also possess a magnetic moment $\boldsymbol{\mu}$, which gives rise to the magnetic dipole-dipole interaction between two atoms :

$$V_{\mathrm{dd}}(\boldsymbol{\mu}_1, \boldsymbol{\mu}_2, \boldsymbol{r}) = \frac{\mu_0}{4\pi}\frac{\boldsymbol{\mu}_1\cdot\boldsymbol{\mu}_2 - 3(\boldsymbol{\mu}_1\cdot\boldsymbol{u}_r)(\boldsymbol{\mu}_2\cdot\boldsymbol{u}_r)}{r^3}. \tag{2}$$

This interaction potential leads to quantum magnetism effects between atomic spins $\boldsymbol{J}$, $\boldsymbol{\mu} = g_J\mu_{\mathrm{B}}\boldsymbol{J}$ which implement an XXZ hamiltonian [de Paz et al., 2013, Hazzard et al., 2014]. Quantum magnetism with magnetic dipole-dipole interactions has been studied in numerous experiments reviewed in [Chomaz et al., 2022]. In contrast, in the experiments that will be presented here, a strong magnetic field polarizes the atoms to their maximal Zeeman state so that the internal state is frozen and we will study the effects of the dipole-dipole interaction on external degrees of freedom. In these conditions the DDI takes the form :

$$V_{\mathrm{dd}}(r,\theta) = \frac{\mu_0\mu^2}{4\pi\, r^3}\left(1 - 3\cos^2\theta\right) \tag{3}$$

where θ denotes the angle between the magnetic field orienting the dipoles and the interatomic separation $\boldsymbol{r}$. For Dy, $J = 8$ in the ground state and $\mu = 9.93\,\mu_{\mathrm{B}}$.

The ground state and excitations of dBECs can be analysed using the mean-field approximation [Lahaye et al., 2009, Dalibard, 2024]. This level of approximation was enough to describe the studies performed on chromium dBECs prior to the introduction of lanthanides. These phenomena

are encapsulated in the dispersion relation of elementary excitations in a condensate of density n_0 :

$$\varepsilon(\boldsymbol{p}) = \sqrt{\frac{p^2}{2m}\left(2gn_0(1+\varepsilon_{\mathrm{dd}}(3\cos^2\alpha - 1)) + \frac{p^2}{2m}\right)}, \tag{4}$$

with α the angle between the excitation propagation direction $\boldsymbol{p}$ and the magnetic field $\boldsymbol{B}$. The factor $\varepsilon_{\mathrm{dd}}$ compares the magnitudes of contact and dipole interactions : $\varepsilon_{\mathrm{dd}} = \frac{a_{\mathrm{dd}}}{a}$ with the dipolar length $a_{\mathrm{dd}} = \frac{\mu_0\mu^2 m}{12\pi\hbar^2}$. A particular phenomenon called dipolar collapse was observed when the DDI dominates over the contact interaction ($\varepsilon_{\mathrm{dd}} > 1$) : the DDI (3) favors a head-to-tail distribution of dipoles, and when the dipole interaction dominates interactions are effectively attractive, leading to a collapse of the BEC on itself. According to expression (4), mean-field stability is ensured by having $\varepsilon_{\mathrm{dd}} < 1$ so that $\varepsilon(\boldsymbol{p})$ is always real for all angles α. The dipolar collapse was observed with Cr by tuning the scattering length down to the regime $\varepsilon_{\mathrm{dd}} > 1$ in [Lahaye et al., 2008].

The results that I present below have been obtained during the PhD thesis of several graduate students. During my time in the Stuttgart group, I particularly co-supervised several of them : Matthias Schmitt who worked on interactions in Dy and quantum droplets, Matthias Wenzel who worked on quantum droplets and anisotropic superfluidity and later Fabian Böttcher who worked on droplets and superfluidity.

1.2.1 Understanding interactions in Dy

As our setup reached low enough temperatures to obtain dBECs of Dy, one had to know the scattering length to make sense of our observations, and produce stable dBECs. Theoretically calculating the scattering length of Dy as a function of magnetic field is beyond reach because there is a tremendous number of Feshbach resonances due to the complexity of its atomic structure and in particular a partially-filled sub-merged $4f$ shell [Kotochigova & Petrov, 2011]. The first experimental Feshbach spectra of Dy at low magnetic field [Baumann et al., 2014] showed that Dy has a very high density of Feshbach resonances. With extended measurements up to hundreds of Gauss [Maier et al., 2015b, Maier et al., 2015a], we confirmed this high density (about 5 resonances per gauss for bosonic isotopes and up to 20 per gauss for the fermionic ones which have a hyperfine structure). We also verified that the Feshbach spectrum presents chaotic characteristics as observed beforehand on Er [Frisch et al., 2014], which makes predictions practically impossible. With these experimental benchmarks we were able to find regions of magnetic field where the dBECs are stable, and where $\varepsilon_{\mathrm{dd}}$ can be tuned between $\varepsilon_{\mathrm{dd}} < 1$ and $\varepsilon_{\mathrm{dd}} > 1$, which is where we observed dipolar quantum droplets, presented in section 1.3.

1.2.2 Anisotropic superfluidity

Another feature of dBECs that one can extract from (4) is that the speed of sound $c = \lim_{p\to 0} \frac{\varepsilon(p)}{p}$ is anisotropic. This was observed also on chromium dBECs by Bragg spectroscopy in ref. [Bismut et al., 2012] by the LPL group in Villetaneuse. In terms of superfluidity, according to Landau's criterion, the dispersion relation (4) gives the critical velocity below which a small, weakly-coupled impurity can move without friction in a BEC :

$$v_c = \min \frac{\varepsilon(\boldsymbol{p})}{\boldsymbol{p}\cdot\hat{\boldsymbol{v}}} \tag{5}$$

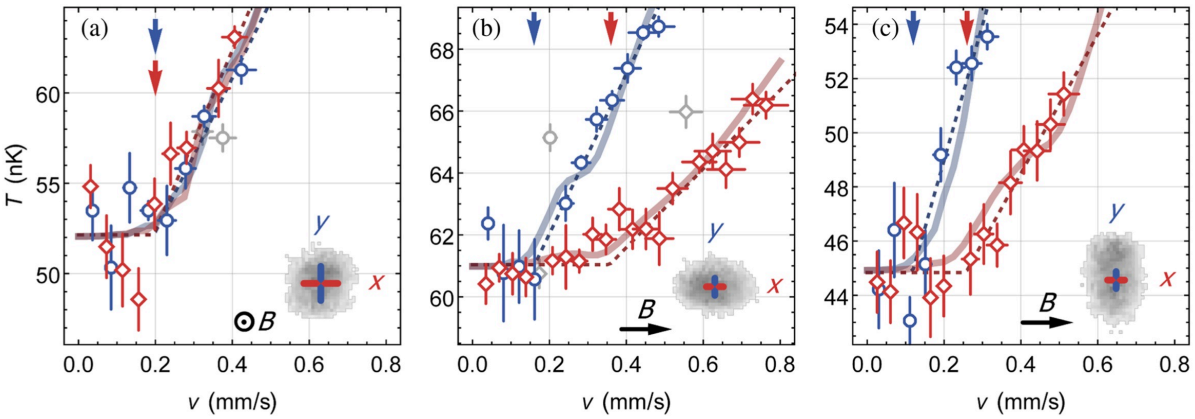

Figure 1 – **Anisotropic superfluidity.** Temperature measurements after vibrating a laser impurity in a ^{162}Dy BEC. Diamonds : impurity motion along x, circles : along y. In (a) the field is perpendicular to the plane of motion, while in (b) and (c) it is in the plane. In (a), the heating is independent of the direction of motion, while in (b) and (c) it is clearly anisotropic, and this anisotropy is not given by the cloud shape : it remains the same while the cloud aspect ratio is inverted between (b) and (c). Excellent agreement can be seen with simulations of the dipolar Gross-Pitaevskii equation. Figure from [Wenzel et al., 2018].

with $\hat{\boldsymbol{v}}$ the unit vector pointing in the direction of motion. Thus, the anisotropic sound velocity was predicted to result in a critical velocity that depends on the direction of motion with respect to the magnetic field [Yu, 2017]. We set out to observe this manifestation of dipolar interaction in a dBEC, using a BEC of the isotope ^{162}Dy. The impurity was mimicked by an attractive laser beam (wavelength 532 nm) focused down to a waist of about $w_0 \simeq 1.5\,\mu$m. The dipolar BEC Thomas-Fermi radii in the plane perpendicular to the laser propagation axis were in the range $4 - 6\,\mu$m. This meant that the excitations created by this impurity were not only elementary excitations but could also be macroscopic (e.g. vortices). Thus (5) does not directly apply to calculate the critical velocity. However, by vibrating back and forth the impurity, and measuring the heating that this induced, we did observe a threshold in velocity showing the existence of a superfluid critical velocity [Wenzel et al., 2018]. What is more, we did observe the expected anisotropy for this critical velocity : if the the field points along z and the motion of the impurity is in the $x - y$ plane, then the threshold is independent of the direction of motion in this plane. If the field is now in the plane (along x), then the critical velocity is lower in the field direction (x) than perpendicular to it (y), as can be seen in Fig. 1. The experimental results were in excellent agreement with the result of simulations of the experimental protocol with the dipolar Gross-Pitaevskii equation.

These results showed how dipolar interactions can modify collective phenomena in Bose-Einstein condensates, here with a clear anisotropy induced in superfluid flow. Next we will see that the combined influence of contact and dipole interactions leads to a new stable ground-state solution for the dBEC, in the "mean-field unstable" region where $\varepsilon_{\rm dd} > 1$.

1.3 Dipolar quantum droplets

The mean-field (MF) treatment of interacting Bose-Einstein condensates accounts properly for the ground-state energy only in the regime where $\sqrt{n_0 a^3} \ll 1$ [Pitaevskii & Stringari, 2016]. The

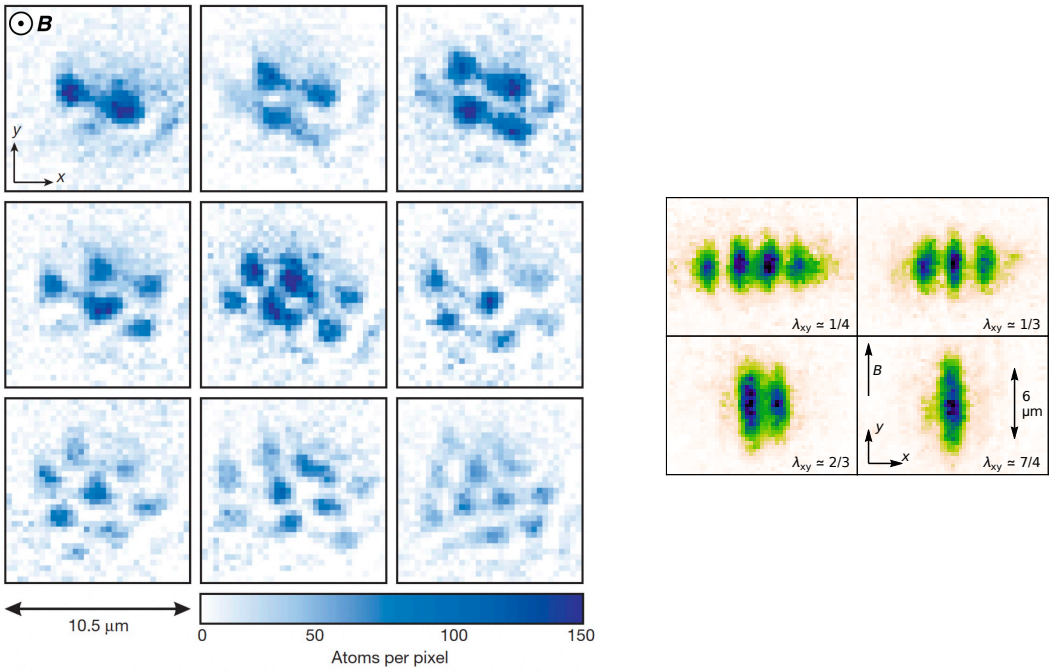

Figure 2 – **Absorption images of dipolar quantum droplets of dysprosium.** Left : Atomic images taken along the magnetic field (pointing along the z axis), which shows the geometric arrangement formed by dipolar quantum droplets in 2D, images taken at variable atom number, from about 5000 atoms (top left) to about 15000 (bottom right). Figure from [Kadau et al., 2016]. Right : Side view of quantum droplets. Here the magnetic field points along the y axis. The ratio of harmonic trapping frequencies $\lambda_{xy} = \omega_x/\omega_y$ is indicated in the different panels. As the confinement along y is increased, the droplets are compressed, and split in several droplets to minimize their energy. Figure from [Wenzel et al., 2017].

proper ground state energy can be calculated via the Bogolyubov treatment, and one obtains the following result : $E_0 = V\frac{gn_0^2}{2}(1+\alpha_{\mathrm{LHY}}\sqrt{n_0a^3})$. The first term is simply the mean-field energy, and the second with $\alpha_{\mathrm{LHY}} = 128/15\sqrt{\pi}$ was first calculated by [Lee et al., 1957] in the absence of dipole-dipole interactions. This beyond mean-field (BMF) term is small compared to the mean-field interaction term.

The BMF term can be in fact of similar magnitude if one introduces a second interaction, *competing* with the short-range interaction. It was proposed theoretically in the key work of [Petrov, 2015]. Here we will only summarize the final results, more details can be found in [Petrov, 2015, Ferrier-Barbut, 2019, Böttcher et al., 2020, Dalibard, 2024]. With two interactions the energy becomes :

$$E_0 = V\frac{n_0^2}{2}[\delta g + g\alpha'_{\mathrm{LHY}}\sqrt{n_0a^3})], \tag{6}$$

with δg, the sum of coupling constants for the two interactions. When one is repulsive, the other attractive they compete and δg can be made small, and even negative. Very roughly, in a dipolar BEC we have $\delta g \approx g(1-\varepsilon_{\mathrm{dd}})$ so indeed, for $\varepsilon_{\mathrm{dd}} > 1$ the effective mean-field interaction is attractive. However it is also *reduced* in magnitude, and then the BMF term can play a role. With two interactions α'_{LHY} remains positive, and it is *amplified* with respect to the single interaction case : $\alpha'_{\mathrm{LHY}} > \alpha_{\mathrm{LHY}}$. While α_{LHY} is known since the seminal work of [Lee et al., 1957], it was extended much more recently in [Lima & Pelster, 2011, Lima & Pelster, 2012] to account for the effect of dipolar interactions. For dBECs they obtained [1] : $\alpha'_{\mathrm{LHY}} \approx \alpha_{\mathrm{LHY}}(1+\frac{3}{2}\varepsilon_{\mathrm{dd}}^2)$.

Thus, in the case $\delta g < 0$, a new phase arises. The energy is minimized at finite density, at the equilibrium between mean-field *attraction*, dominant at low density, and beyond mean-field *repulsion* taking over at high density. Rather than filling the whole volume available, the dBEC will form finite-density self-bound droplets, which is why it is considered a liquid phase. This liquid phase was predicted for binary mixtures with contact interactions in [Petrov, 2015]. We observed it soon later in Dy dBECs in 2015-2016 : First we reported stable structures where MF theory was predicting collapse in [Kadau et al., 2016]. Then we identified in [Ferrier-Barbut et al., 2016] that these were indeed quantum droplets, stabilized from MF collapse by the BMF term, observed as well by the Innsbruck group in Er dBEC [Chomaz et al., 2016]. And we finally observed their self-bound nature in [Schmitt et al., 2016]. This liquid phase was also observed in binary mixtures following the original proposal [Cabrera et al., 2018, Semeghini et al., 2018]. This discovery of a new phase was a surprise and an achievement in itself, but it also opened the possibility for the observation of a remarkable phenomenon in droplet arrays.

The subsequent observation of phase-coherent "supersolid" droplet arrays

It was known since early numerical works [Yi & You, 2000, Góral et al., 2000] that dipolar Bose-Einstein condensates should exhibit spontaneous structure formation. This structure formation occurs in constrained geometry where external trapping along the dipoles' axis competes with their tendency to form elongated structures along the field. This comes hand in hand with the existence of a local "roton" minimum in the dispersion relation of trapped dBECs demonstrated theoretically in the milestone paper [Santos et al., 2003], see [Chomaz et al., 2022] for more details. The Innsbruck group has performed a series of work which clearly demonstrated the minimum in the dispersion relation [Chomaz et al., 2018, Petter et al., 2019], while we had experimentally observed spontaneous structure formation in [Kadau et al., 2016] with the creation of stable microscopic

1. Formally, α'_{LHY} takes real values only for $\varepsilon_{\mathrm{dd}} \leqslant 1$, the existence of an imaginary part is due to the presence of unstable collective modes. However these are cutoff by the finite size of the liquid droplets that form. To my knowledge no self-consistent calculation of α'_{LHY} accounting for the spectrum in a finite-size system has been performed.

crystal-like structures.

The result of spontaneous structure formation is an array of stable droplets, which repel each other to form crystal-like structures. This observation made it possible to study the fate of superfluidity in the presence of spontaneous structure formation. The goal was to obtain *supersolidity* : the coexistence of (i) superfluidity across the whole sample i.e. phase coherence between different droplets and (ii) long-range spatial order i.e. the breaking of a continuous translation symmetry in the thermodynamic limit. In [Wenzel et al., 2017] we theoretically found a regime where this coexistence should occur, but it proved hard to reach and we couldn't observe phase coherence experimentally. In [Roccuzzo & Ancilotto, 2019], a better regime was identified, that can be reached smoothly from a uniform dBEC by tuning the scattering length to induce the softening of a roton minimum. This then quickly led to the three subsequent reports of the observation of phase coherence across droplets in small 1D chains : [Tanzi et al., 2019, Chomaz et al., 2019, Böttcher et al., 2019]. Since then these new phase-coherent arrays have been explored in numerous exciting studies [Böttcher et al., 2020, Tanzi et al., 2019, Biagioni et al., 2023, Chomaz et al., 2022], and new interesting directions arise, for instance increasing the system size to approach the thermodynamic limit, or changing dimensionality.

1.4 Publications

I reproduce here a selected number of publications from my work in Stuttgart, the complete list can be found at the end of this report in section 3.9.

Anisotropic Superfluid Behavior of a Dipolar Bose-Einstein Condensate

Matthias Wenzel, Fabian Böttcher, Jan-Niklas Schmidt, Michael Eisenmann, Tim Langen, Tilman Pfau, and Igor Ferrier-Barbut*

5. Physikalisches Institut and Center for Integrated Quantum Science and Technology (IQST), Universität Stuttgart, Pfaffenwaldring 57, 70569 Stuttgart, Germany

(Received 12 April 2018; published 17 July 2018)

We present transport measurements on a dipolar superfluid using a Bose-Einstein condensate of ^{162}Dy with strong magnetic dipole-dipole interactions. By moving an attractive laser beam through the condensate we observe an anisotropy in superfluid flow. This observation is compatible with an anisotropic critical velocity for the breakdown of dissipationless flow, which, in the spirit of the Landau criterion, can directly be connected to the anisotropy of the underlying dipolar excitation spectrum. In addition, the heating rate above this critical velocity reflects the same anisotropy. Our observations are in excellent agreement with simulations based on the Gross-Pitaevskii equation and highlight the effect of dipolar interactions on macroscopic transport properties, rendering dissipation anisotropic.

DOI: 10.1103/PhysRevLett.121.030401

The discovery of superfluidity in liquid helium [1] is a hallmark of quantum physics at the macroscopic scale. The famous Landau criterion [2] relates the transport properties of a superfluid, namely, the maximal velocity for frictionless flow v_c, to its spectrum of elementary collective excitations. As a consequence, features of the system's excitation spectrum are reflected in the transport properties of the superfluid. In the context of ultracold atoms, superfluidity and the breakdown thereof have been studied by moving microscopic impurities, i.e., single atoms, which are realized by either stimulated Raman transitions [3] or with atomic mixtures [4], allowing a direct comparison to Landau's criterion. Other experiments with macroscopic impurities, e.g., laser beams or optical lattices, explored superfluidity in a trapped Bose-Einstein condensate [5,6], a two-dimensional Bose gas [7], or a Fermi gas in the BEC-BCS crossover regime [8,9]. In the latter case, a reduced critical velocity with respect to the prediction of Landau's criterion is observed.

In the spirit of these pioneering experiments, we perform the first transport measurements on a dipolar Bose-Einstein condensate (dBEC), a superfluid with anisotropic interactions. We observe that the anisotropy of the dispersion relation is reflected in both the anisotropy of the critical velocity and the heating rate above this threshold. Our measurements are in excellent agreement with dynamical simulations of the extended Gross-Pitaevskii equation (eGPE) [10], taking into account finite-size effects of the trapped dBEC as well as the characteristics of the moving impurity.

In order to illustrate the behavior of a dBEC we first focus on the homogeneous gas, where the excitation spectrum

$$\omega(\boldsymbol{k}) = k\sqrt{\left(\frac{\hbar k}{2m}\right)^2 + \frac{gn_0}{m}(1 + \varepsilon_{dd}(3\cos^2\alpha - 1))} \quad (1)$$

is known analytically [11]. It exhibits an anisotropic dependency on the angle α between excitations with wave vector $\boldsymbol{k}$ and the polarization direction $\boldsymbol{B}$; see Fig. 1(a). In a dBEC with a density n_0 atoms with mass m are subject to the contact interaction, characterized by the scattering length a_s via $g = 4\pi\hbar^2 a_s/m$, as well as the dipolar interaction, defined by the dipolar length $a_{dd} = \mu_0\mu_m^2 m/12\pi\hbar^2$ via the magnetic moment μ_m. The ratio $\varepsilon_{dd} = a_{dd}/a_s$ of these two length scales describes the

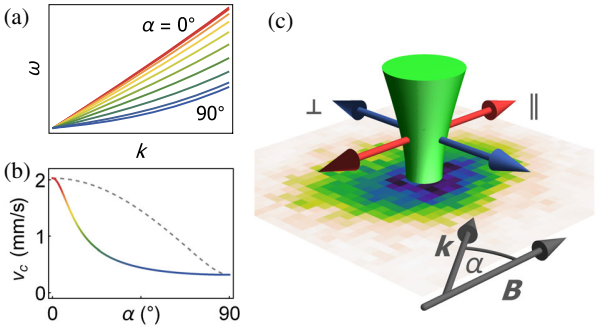

FIG. 1. Probing anisotropic critical velocity. (a) Excitation spectrum of a homogeneous dipolar Bose gas. The speed of sound v_s depends on the direction of the excitation $\boldsymbol{k}$ with respect to the dipole polarization $\boldsymbol{B}$, denoted by the angle α. (b) The critical velocity v_c (solid), as given by Eq. (2), becomes anisotropic and is in general lower than v_s (dashed). (c) Schematic of the experiment. We drag an attractive laser beam through a dipolar condensate perpendicular ($\alpha = 90°$, blue) and parallel ($\alpha = 0°$, red) to the magnetic field direction.

relative dipolar strength. The anisotropy of the dipolar excitation spectrum has been confirmed experimentally by Bragg spectroscopy of a chromium dBEC [12].

The Landau criterion [2] then relates the anisotropy of the excitation spectrum to the breakdown of superfluidity, since quasiparticles cannot be emitted by an impurity moving at a velocity v smaller than the critical velocity $v_c = \min[\omega(k)/k]$ in an isotropic fluid. For anisotropic interactions the excitation wave vector $\boldsymbol{k}$ does not necessarily coincide with the direction of movement $\hat{\boldsymbol{v}}$ of the impurity [13]. In its generalized form the Landau criterion therefore becomes $v_c = \min[\omega(\boldsymbol{k})/(\boldsymbol{k}\cdot\hat{\boldsymbol{v}})]$. Applied to the dipolar dispersion relation in Eq. (1), it yields an anisotropic critical velocity

$$v_c(\alpha) = \left(\frac{\sin(\alpha)^2}{v_{s,\perp}^2} + \frac{\cos(\alpha)^2}{v_{s,\parallel}^2}\right)^{-1/2}, \tag{2}$$

see Fig. 1(b) (solid line). In general, the acquired v_c is lower than the speed of sound $v_s(\alpha) = \omega(k)/k|_{k\to 0}$ (dashed line) and only coincides with it for a movement parallel $v_{s,\parallel} = v_s(0°)$ or perpendicular $v_{s,\perp} = v_s(90°)$ to the polarization axis. For ^{162}Dy with a scattering length $a_s = 141(17)a_0$ [14] and a dipolar length $a_{dd} = 131a_0$ the critical velocity ranges from $v_{s,\perp} = 0.32$ to $v_{s,\parallel} = 2.0$ mm/s for a typical density $n_0 = 10^{20}$ m^{-3} as shown in Fig. 1(b).

In a confined dipolar system the situation changes since such a system is additionally subject to roton softening [15–17] at finite momentum k. This collective excitation softening influences v_c [18]. In this context the anisotropy of the critical velocity was first predicted in [19] for a quasi-2D dBEC. In order to fully account for such confinement-induced effects and other experimental features, full numerical simulations are required.

Here, we perform experiments aimed at measuring the dependence of superfluid flow on the transport direction. Our experimental procedure is as follows, see Fig. 1(c). Starting with the setup described in Ref. [20] we focus an attractive laser beam ($\lambda = 532$ nm, along $\hat{z}$) on a trapped dBEC of ^{162}Dy atoms. The beam has a waist of $w_0 \approx 1.5$ μm and power of $P_0 \approx 1.3$ μW. Using the theoretical value of the dynamical polarizability, we estimate the potential depth to $V_0 \approx 0.5$ μ, with μ being the chemical potential of the gas. This "stirring beam" can be moved transversally over a few μm in the imaging plane by means of two electro-optical deflectors. In order to measure superfluid properties we move the beam at a constant velocity $v = 4r_s f_s$ given by the stirring amplitude r_s, which is the displacement with respect to the cloud center, and the frequency f_s of a single cycle. The position $r(t)$ of the stirring beam is thus a triangular periodic function centered around zero with amplitude r_s. There is a finite acceleration at the turning points of the triangular motion, leading to the emission of sound waves and thus small heating for velocities below the critical one [21]. A minor misalignment leads to a difference in stirring amplitudes for x and y, but is fully accounted for as detailed in Ref. [22]. We probe the high-density region avoiding thermal wings by choosing an amplitude $r_s/R_{\mathrm{TF}} = 0.15$–$0.35$, with R_{TF} being the Thomas-Fermi radius of the dBEC. Most of the measurements are carried out in a harmonic trapping potential with frequencies $f_x = 52(1)$ Hz $\approx f_y = 49(1)$ Hz, $f_z = 168(1)$ Hz with almost cylindrical symmetry along $\hat{z}$. In this trap we prepare a dBEC at a condensed fraction of 0.7 with 1×10^4 to 2×10^4 atoms in total. Then—while moving the beam continuously—the power of the stirring beam is ramped up within 25 ms, kept constant for a time $t_{\mathrm{stir}} = 1$ s, and ramped down within 25 ms followed by an additional 200 ms for thermalization of the sample. Finally, we extract the temperature T of the sample from *in situ* images; see Ref. [22]. Because of finite-size effects and experimental noise, our data cannot be considered as a clear proof of superfluidity, but it is in excellent agreement with superfluid flow. To quantify the anisotropy of superfluid flow and compare with simulations we extract the critical velocity v_c with a fit function $T(v) = T_0 + ht_{\mathrm{stir}}(v/v_c - 1)\Theta(v - v_c)$. It is constant in the dissipationless regime below v_c and increases linearly with a given heating rate $\dot{T} = h(v/v_c - 1)$ above v_c, determined by the heating coefficient h.

In order to take the inhomogeneity and finite-size effects of the BEC as well as the finite extent and depth of the stirring beam into account, we conduct dynamic simulations of the extended Gross-Pitaevskii equation [10,20], which are explained in detail in Ref. [22]. The gain in total energy per atom $\Delta E/N$ of a single cycle of the beam's movement is scaled by the number of oscillations $t_{\mathrm{stir}}f_s$ in the experiment, thus assuming an identical increase in energy induced by the subsequent stirring cycles. Furthermore, there is a nonlinear relation between energy and temperature even for the noninteracting Bose gas [23]. Since the observed change in temperature is less than 20%, we assume a linear relation in this regime. Altogether, the simulation data are thus mapped to a temperature $T = T_0 + ct_{\mathrm{stir}}f_s\Delta E/Nk_B$ with the Boltzmann constant k_B. To get agreement between experimental data and simulations we use the coefficient c as a fit parameter scaling only the temperature axis. For the data presented in Fig. 2, the factor c is in the range of 0.02–0.05 pointing towards a much weaker heating induced by the subsequent stirring cycles. This parameter also takes into account the mentioned relation between energy and temperature, the uncertainty in the potential depth and finite-temperature effects lowering the superfluid fraction [26]. A finite-temperature theory would probably allow us to include such effects and further model the introduced coefficient properly. We emphasize that the rescaling procedure we use here does not influence the critical velocity, which we extract by applying the same fit function as used for the experimental data. With the evaluation procedure at hand we now turn to the measurements.

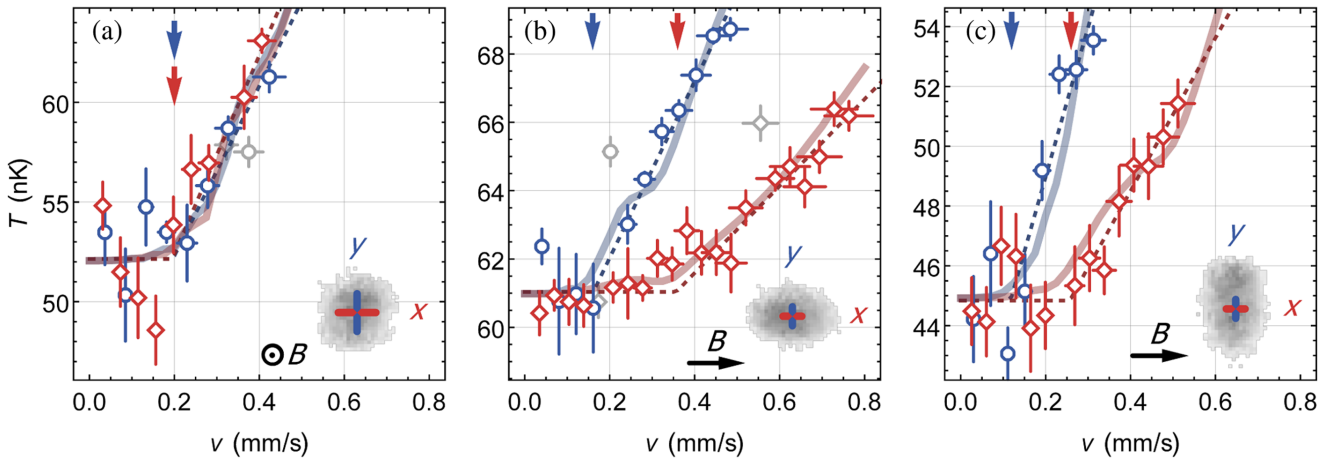

FIG. 2. Temperature of the dBEC after stirring for (a) the isotropic case with $\boldsymbol{B}\|\hat{\boldsymbol{z}}$ and (b) the anisotropic case with $\boldsymbol{B}\|\hat{\boldsymbol{x}}$ in an almost cylindrical trap. In (c) the trap is additionally reshaped to invert the cloud aspect ratio. The stirring beam is moved along the x (red squares) or y (blue circles) axis, as illustrated in the insets with example *in situ* images. Critical velocities are extracted by a linear fit (dashed) and marked with arrows. In (a) the response is isotropic with $v_x = 0.20(5)$ and $v_y = 0.20(7)$ mm/s, while we observe a clear difference in (b) with $v_\perp = 0.16(2)$ mm/s along $\hat{\boldsymbol{y}}$ and $v_\parallel = 0.36(3)$ mm/s along $\hat{\boldsymbol{x}}$. In (c) we extract $v_\perp = 0.12(3)$ and $v_\parallel = 0.26(4)$ mm/s proving that the observed anisotropy remains even when inverting the anisotropy of the atomic cloud. Data points with stirring frequency matching the trapping frequencies (gray) are excluded from the analysis. Simulations of the eGPE for a single stirring cycle (solid lines) show excellent agreement with the experiment. See text for further parameters.

In a first reference measurement we apply the magnetic field $\boldsymbol{B}\|\hat{\boldsymbol{z}}$. The problem is therefore isotropic in the xy plane and moving the laser defect along $\hat{\boldsymbol{x}}$ or $\hat{\boldsymbol{y}}$ is expected to give the same critical velocity. For both stirring directions along $\hat{\boldsymbol{x}}$ (red diamonds) and $\hat{\boldsymbol{y}}$ (blue circles) we observe the typical threshold in heating of the dBEC when the velocity of the stirring beam is increased, see Fig. 2(a). The response is clearly isotropic. Both the critical velocity and the heating coefficient coincide. From the fits (dashed lines) we extract the critical velocity $v_x = 0.20(5)$ and $v_y = 0.20(7)$ mm/s with heating coefficients $h_x = 8(5)$ and $h_y = 9(8)$ nK/s, respectively. For this measurement the stirring frequency is varied between $f_s = 3$ and 60 Hz. Data points with stirring frequency at the transversal trap frequency (gray) are excluded from the analysis, since the coupling to the center-of-mass oscillation in the trap can influence the energy transfer. The agreement with the simulation data (solid lines) is remarkable. We extract a critical velocity of $v_{x,\mathrm{sim}} = v_{y,\mathrm{sim}} = 0.21(1)$ mm/s in excellent agreement with the presented experimental values.

We now turn to the anisotropic case with the magnetic field $\boldsymbol{B}\|\hat{\boldsymbol{x}}$ pointing along one of the stirring directions. Because of magnetostriction the cloud is deformed to an aspect ratio of $\kappa = R_x/R_y = 1.4$ [11] in the imaging plane with Thomas-Fermi radii $R_x = 6.0$ and $R_y = 4.3$ μm. In this configuration the cloud is elongated along the magnetic field; thus the mean dipolar interaction is predominantly attractive and therefore the peak density $n_0 = 1.7 \times 10^{20}\mathrm{m}^{-3}$ is a factor of 2 higher as compared to the previous case. More importantly, the dispersion relation becomes anisotropic when comparing the stirring directions along $\hat{\boldsymbol{x}}\|\boldsymbol{B}$ and $\hat{\boldsymbol{y}}\perp\boldsymbol{B}$. In consequence, we directly observe a factor of 2 difference in critical velocity, as shown in Fig. 2(b). The extracted values are $v_\perp = 0.16(2)$ and $v_\parallel = 0.36(3)$ mm/s with heating coefficients $h_\perp = 4.2(9)$ and $h_\parallel = 4.5(9)$ nK/s, that agree within the experimental error. The difference in heating rates $\dot{T} = h(v/v_c - 1)$, as given by the slope in the figure, can thus be fully attributed to the anisotropy of the critical velocity. From this fact we infer that the anisotropy in both critical velocity and heating rate share a common cause in the anisotropy of collective excitations. Comparing to simulation data yields excellent agreement, as can be seen in Fig. 2(b). We stress that a single fit parameter c is used for both curves. The anisotropy in heating rate is thus very well reproduced by the simulation. We further extract $v_{\perp,\mathrm{sim}} = 0.16(1)$ and $v_{\parallel,\mathrm{sim}} = 0.35(2)$ mm/s in excellent agreement with the experiment.

In order to ensure that the observed anisotropy is not trivially caused by the anisotropic cloud shape, we invert the aspect ratio of the cloud to $\kappa = R_x/R_y \approx 1.4^{-1}$ by adjusting the trapping potential. The trap frequencies in this case are $\{f_x, f_y, f_z\} = \{81(2), 39(1), 140(1)\}$ Hz counteracting the magnetostriction along the magnetic field axis $\boldsymbol{B}\|\hat{\boldsymbol{x}}$. This leads to measured sizes $R_x = 4.3$ and $R_y = 5.8$ μm of the condensate. The extracted critical velocities are $v_\perp = 0.12(3)$ and $v_\parallel = 0.26(4)$ mm/s again with compatible heating coefficients $h_\perp = 6(3)$ and $h_\parallel = 7(3)$ nK/s, as shown in Fig. 2(c). The observed anisotropy of transport remains in the same direction even though the cloud aspect ratio was inverted, providing conclusive evidence that it

arises directly from the dipolar anisotropy. Once again for this data set, excellent agreement with simulations is found.

We further compare the measured v_c to the speed of sound v_s of the homogeneous dipolar gas introduced in Eq. (2). For the given peak density the latter is $v_{s,\perp} = 0.42$ and $v_{s,\parallel} = 2.6$ mm/s, respectively. The measured critical velocity $v_c/v_s = 0.1$–0.4 is thus well below the expected speed of sound in the cloud center. This value is in agreement with the critical velocity measured in the pioneering experiment with a contact-interacting BEC [6]. An obvious effect lowering the measured v_c is the inhomogeneuos density distribution both along the beam and transversally [27]. Vortex formation is a dominant effect for repulsive obstacles lowering the density, but should be suppressed in our experiment with an attractive beam [28]. Yet, the macrosocopic size of the beam can influence the measured critical velocity as well [29].

In conclusion, we performed the first transport measurements on a dipolar BEC. The strong dipole-dipole interaction of dysprosium atoms renders the excitation spectrum of the dBEC, and thus the critical velocity for the breakdown of superfluidity, anisotropic. We investigate the latter by measuring the heating caused by moving an attractive laser beam through the condensate. We find excellent agreement comparing our data taken at a sizable thermal fraction to dynamic simulations of the eGPE, which is a zero temperature theory. We therefore deduce that the effect of thermal excitations has a negligible influence on the critical velocity in our experiment. As discussed earlier, roton softening of the excitation spectrum can decrease the critical velocity [18]. Yet, for the current set of experiments with dipolar strength of $\varepsilon_{dd} < 1$ in conjunction with a weak confinement along the magnetic field this effect is likely negligible. Increasing both quantities could lead to an observable reduction of the critical velocity, which is an interesting perspective for future studies. An anisotropic dispersion relation is expected to have many more implications on hallmark properties of superfluids, e.g., on vortices in rotating systems. In future experiments we expect to find an anisotropic density distribution around a vortex core [30]. Furthermore, this effect induces anisotropic vortex-vortex interactions [31] leading to transitions between vortex lattices of different symmetries [32].

We thank A. Pelster and A. Balaž for valuable discussions as well as Z.-Q. Yu for pointing us to the generalized form of the Landau criterion. This work is supported by the German Research Foundation (DFG) within FOR2247 under Pf381/16-1, Pf381/20-1, and HBFG INST41/1056-1. This project has received funding from the European Union's Horizon 2020 research and innovation programme under the Marie Skłodowska-Curie Grants agreement No. 703419 and No. 746525 (I. F. B. and T. L. respectively). T. L. acknowledges support from the Alexander von Humboldt Foundation through a Feodor Lynen Fellowship.

*i.ferrier-barbut@physik.uni-stuttgart.de

[1] P. L. Kapitsa, Viscosity of liquid helium below the λ-point, Nature (London) **141**, 74 (1938).
[2] L. Landau, Theory of the superfluidity of helium II, Phys. Rev. **60**, 356 (1941).
[3] A. P. Chikkatur, A. Görlitz, D. M. Stamper-Kurn, S. Inouye, S. Gupta, and W. Ketterle, Supression and Enhancement of Impurity Scattering in a Bose-Einstein Condensate, Phys. Rev. Lett. **85**, 483 (2000).
[4] M. Delehaye, S. Laurent, I. Ferrier-Barbut, S. Jin, F. Chevy, and C. Salomon, Critical Velocity and Dissipation of an Ultracold Bose-Fermi Counterflow, Phys. Rev. Lett. **115**, 265303 (2015).
[5] C. Raman, M. Köhl, R. Onofrio, D. S. Durfee, C. E. Kuklewicz, Z. Hadzibabic, and W. Ketterle, Evidence for a Critical Velocity in a Bose-Einstein Condensed Gas, Phys. Rev. Lett. **83**, 2502 (1999).
[6] R. Onofrio, C. Raman, J. M. Vogels, J. R. Abo-Shaeer, A. P. Chikkatur, and W. Ketterle, Observation of Superfluid Flow in a Bose-Einstein Condensed Gas, Phys. Rev. Lett. **85**, 2228 (2000).
[7] R. Desbuquois, L. Chomaz, T. Yefsah, J. Léonard, J. Beugnon, C. Weitenberg, and J. Dalibard, Superfluid behaviour of a two-dimensional Bose gas, Nat. Phys. **8**, 645 (2012).
[8] D. E. Miller, J. K. Chin, C. A. Stan, Y. Liu, W. Setiawan, C. Sanner, and W. Ketterle, Critical Velocity for Superfluid Flow across the BEC-BCS Crossover, Phys. Rev. Lett. **99**, 070402 (2007).
[9] W. Weimer, K. Morgener, V. P. Singh, J. Siegl, K. Hueck, N. Luick, L. Mathey, and H. Moritz, Critical Velocity in the BEC-BCS Crossover, Phys. Rev. Lett. **114**, 095301 (2015).
[10] M. Wenzel, F. Böttcher, T. Langen, I. Ferrier-Barbut, and T. Pfau, Striped states in a many-body system of tilted dipoles, Phys. Rev. A **96**, 053630 (2017).
[11] T. Lahaye, C. Menotti, L. Santos, M. Lewenstein, and T. Pfau, The physics of dipolar bosonic quantum gases, Rep. Prog. Phys. **72**, 126401 (2009).
[12] G. Bismut, B. Laburthe-Tolra, E. Maréchal, P. Pedri, O. Gorceix, and L. Vernac, Anisotropic Excitation Spectrum of a Dipolar Quantum Bose Gas, Phys. Rev. Lett. **109**, 155302 (2012).
[13] Z. Q. Yu, Landau criterion for an anisotropic Bose-Einstein condensate, Phys. Rev. A **95**, 033618 (2017).
[14] Y. Tang, W. Kao, K.-Y. Li, S. Seo, K. Mallayya, M. Rigol, S. Gopalakrishnan, and B. L. Lev, Thermalization near Integrability in a Dipolar Quantum Newton's Cradle, Phys. Rev. X **8**, 021030 (2018).
[15] L. Santos, G. V. Shlyapnikov, and M. Lewenstein, Roton-Maxon Spectrum and Stability of Trapped Dipolar Bose-Einstein Condensates, Phys. Rev. Lett. **90**, 250403 (2003).
[16] R. N. Bisset, D. Baillie, and P. B. Blakie, Roton excitations in a trapped dipolar Bose-Einstein condensate, Phys. Rev. A **88**, 043606 (2013).
[17] L. Chomaz, R. M. W. van Bijnen, D. Petter, G. Faraoni, S. Baier, J. H. Becher, M. J. Mark, F. Wächtler, L. Santos, and F. Ferlaino, Observation of roton mode population in a dipolar quantum gas, Nat. Phys. **14**, 442 (2018).
[18] R. M. Wilson, S. Ronen, and J. L. Bohn, Critical Superfluid Velocity in a Trapped Dipolar Gas, Phys. Rev. Lett. **104**, 094501 (2010).

[19] C. Ticknor, R. M. Wilson, and J. L. Bohn, Anisotropic Superfluidity in a Dipolar Bose Gas, Phys. Rev. Lett. **106**, 065301 (2011).
[20] M. Schmitt, M. Wenzel, F. Böttcher, I. Ferrier-Barbut, and T. Pfau, Self-bound droplets of a dilute magnetic quantum liquid, Nature (London) **539**, 259 (2016).
[21] B. Jackson, J. F. McCann, and C. S. Adams, Dissipation and vortex creation in Bose-Einstein condensed gases, Phys. Rev. A **61**, 051603 (2000).
[22] See Supplemental Material at http://link.aps.org/supplemental/10.1103/PhysRevLett.121.030401 for details on the imaging, calibration and simulation procedure, which contains Refs. [10,11,20,23–25].
[23] L. Pitaevskii and S. Stringari, *Bose-Einstein Condensation and Superfluidity* (Oxford University Press, New York, 2016).
[24] H. Kadau, M. Schmitt, M. Wenzel, C. Wink, T. Maier, I. Ferrier-Barbut, and T. Pfau, Observing the Rosensweig instability of a quantum ferrofluid, Nature (London) **530**, 194 (2016).
[25] K. Glaum and A. Pelster, Bose-Einstein condensation temperature of dipolar gas in anisotropic harmonic trap, Phys. Rev. A **76**, 023604 (2007).
[26] M. Ghabour and A. Pelster, Bogoliubov theory of dipolar Bose gas in a weak random potential, Phys. Rev. A **90**, 063636 (2014).
[27] P. O. Fedichev and G. V. Shlyapnikov, Critical velocity in cylindrical Bose-Einstein condensates, Phys. Rev. A **63**, 045601 (2001).
[28] V. P. Singh, W. Weimer, K. Morgener, J. Siegl, K. Hueck, N. Luick, H. Moritz, and L. Mathey, Probing superfluidity of Bose-Einstein condensates via laser stirring, Phys. Rev. A **93**, 023634 (2016).
[29] J. S. Stießberger and W. Zwerger, Critical velocity of superfluid flow past large obstacles in Bose-Einstein condensates, Phys. Rev. A **62**, 061601 (2000).
[30] S. Yi and H. Pu, Vortex structures in dipolar condensates, Phys. Rev. A **73**, 061602 (2006).
[31] B. C. Mulkerin, R. M. W. van Bijnen, D. H. J. O'Dell, A. M. Martin, and N. G. Parker, Anisotropic and Long-Range Vortex Interactions in Two-Dimensional Dipolar Bose Gases, Phys. Rev. Lett. **111**, 170402 (2013).
[32] N. R. Cooper, E. H. Rezayi, and S. H. Simon, Vortex Lattices in Rotating Atomic Bose Gases with Dipolar Interactions, Phys. Rev. Lett. **95**, 200402 (2005).

LETTER

doi:10.1038/nature16485

Observing the Rosensweig instability of a quantum ferrofluid

Holger Kadau[1], Matthias Schmitt[1], Matthias Wenzel[1], Clarissa Wink[1], Thomas Maier[1], Igor Ferrier-Barbut[1] & Tilman Pfau[1]

Ferrofluids exhibit unusual hydrodynamic effects owing to the magnetic nature of their constituents. As magnetization increases, a classical ferrofluid undergoes a Rosensweig instability[1] and creates self-organized, ordered surface structures[2] or droplet crystals[3]. Quantum ferrofluids such as Bose–Einstein condensates with strong dipolar interactions also display superfluidity[4]. The field of dipolar quantum gases is motivated by the search for new phases of matter that break continuous symmetries[5,6]. The simultaneous breaking of continuous symmetries such as the phase invariance in a superfluid state and the translational symmetry in a crystal provides the basis for these new states of matter. However, interaction-induced crystallization in a superfluid has not yet been observed. Here we use *in situ* imaging to directly observe the spontaneous transition from an unstructured superfluid to an ordered arrangement of droplets in an atomic dysprosium Bose–Einstein condensate[7]. By using a Feshbach resonance to control the interparticle interactions, we induce a finite-wavelength instability[8] and observe discrete droplets in a triangular structure, the number of which grows as the number of atoms increases. We find that these structured states are surprisingly long-lived and observe hysteretic behaviour, which is typical for a crystallization process and in close analogy to the Rosensweig instability. Our system exhibits both superfluidity and, as we show here, spontaneous translational symmetry breaking. Although our observations do not probe superfluidity in the structured states, if the droplets establish a common phase via weak links, then our system is a very good candidate for a supersolid ground state[9–11].

Research in condensed matter physics is driven by the discovery of novel phases of matter, in particular, phases simultaneously displaying different types of order. A prime example is the supersolid state, which features crystalline order and superfluidity simultaneously [9–11]. This state has been elusive and claims of its discovery in helium[12,13] have been withdrawn recently[14]. One of the requirements for spontaneous spatially ordered structure formation in the ground state of a many-body system is the existence of long-range interactions such as those present in ferrofluids. As a consequence of these interactions, a magnetized ferrofluid forms stationary surface waves due to competition between gravitational or magnetic trapping, dipolar interaction and surface tension. This effect is known as the normal-field instability or Rosensweig instability[2] and leads to stable droplet patterns on a superhydrophobic surface[3]. For ferrofluids, the dispersion relation of surface excitations has a minimum at finite momentum, resembling the well-studied roton spectrum in liquid helium[15]. However, the physical interpretation of this minimum is very different for ferrofluids and helium. The origin of the dispersion-relation minimum for a ferrofluid is an energy gain due to the attractive part of the dipolar interaction resulting in a clustering of polarized dipoles in a head-to-tail configuration in periodic structures. Such roton-induced structures have also been discussed for quantum ferrofluids[8,16]. In close similarity with a classical ferrofluid, a competition exists between the harmonic trapping, dipolar interaction and contact interaction in a quantum ferrofluid. For increasing relative dipolar interaction, the roton instability can lead to a periodic perturbation of the atomic density distribution, which is closely connected to the Rosensweig instability[17]. However, it was believed that these rotonic structures would be unstable, owing to subsequent instabilities of the forming droplets[18].

Here we cool down the most magnetic element—dysprosium (Dy)[19], with a magnetic moment of $\mu = 9.93\mu_B$, where μ_B is the Bohr magneton—and generate a Bose–Einstein condensate (BEC)[7]. We observe an angular roton instability[16,18] and find subsequent droplet formation yielding triangular structures with surprisingly long lifetimes. We use two key tools to study these self-organized structures. First, we use a magnetic Feshbach resonance[20] to tune the contact interaction (see Extended Data Fig. 1) and to induce the droplet formation. Second, we use a microscope with high spatial resolution to detect the atomic density distribution *in situ*.

The first prediction of structured ground states in a dipolar BEC dates back to the early days of quantum gases[21]; the first mechanical effects were seen with chromium atoms[22]. There, the dipolar attraction deforms the compressible gas and its shape is balanced by a repulsive contact interaction, described by the scattering length a. To compare the strengths of the contact and dipolar interaction, we introduce a length scale that characterizes the magnetic dipole–dipole interaction strength: $a_{dd} = \mu_0\mu^2 m/(12\pi\hbar)$ (ref. 2), where μ_0 is the vacuum permeability, m is the atomic mass and $\hbar$ is the reduced Planck constant. By tuning the scattering length a with a Feshbach resonance such that $a < a_{dd}$, the dipolar attraction dominates the repulsive contact interaction and an instability of a dipolar gas can occur[4,23]. However, in a pancake-shaped trap, the dipoles sit mainly side-by-side and predominantly repel each other, owing to the anisotropy of the dipole–dipole interaction, and hence the dipolar BEC is stabilized. In such a pancake-shaped configuration, the roton instability, which occurs at a finite wavelength, is predicted[8,16].

For our experiments, we used the isotope ^{164}Dy with a dipolar length of $a_{dd} = 132a_0$, where a_0 is the Bohr radius. This dipolar length is already greater than the background scattering length $a_{bg} = 92(8)a_0$ (where the errors in parentheses here and elsewhere represent one standard deviation), which is the value far from Feshbach resonances[24,25]. To obtain a stable BEC, we tuned the scattering length to $a \approx a_{dd}$ using a magnetic field of $B = 6.962(3)$ G in the vicinity of a Feshbach resonance located at $B_0 = 7.117(3)$ G. We then obtained typically 15,000 atoms in nearly pure Dy BECs (see Methods section). The atoms were trapped in a radially symmetric, pancake-shaped trap with harmonic frequencies of $(\nu_x, \nu_y, \nu_z) = (46, 44, 133)$ Hz, and the external magnetic field aligned the magnetic dipoles in the axial z direction. Subsequently, we tuned the magnetic field such that $B \lesssim 6.9$ G, which reduced a to $a_{bg} < a_{dd}$, resulting in an angular roton instability[16] that triggered the transition to ordered states (Fig. 1a). We then observed the formation of droplets that arranged in ordered structures using *in situ* phase-contrast polarization imaging along the z direction with a spatial resolution of 1 μm.

[1]5. Physikalisches Institut and Center for Integrated Quantum Science and Technology, Universität Stuttgart, Pfaffenwaldring 57, 70569 Stuttgart, Germany.

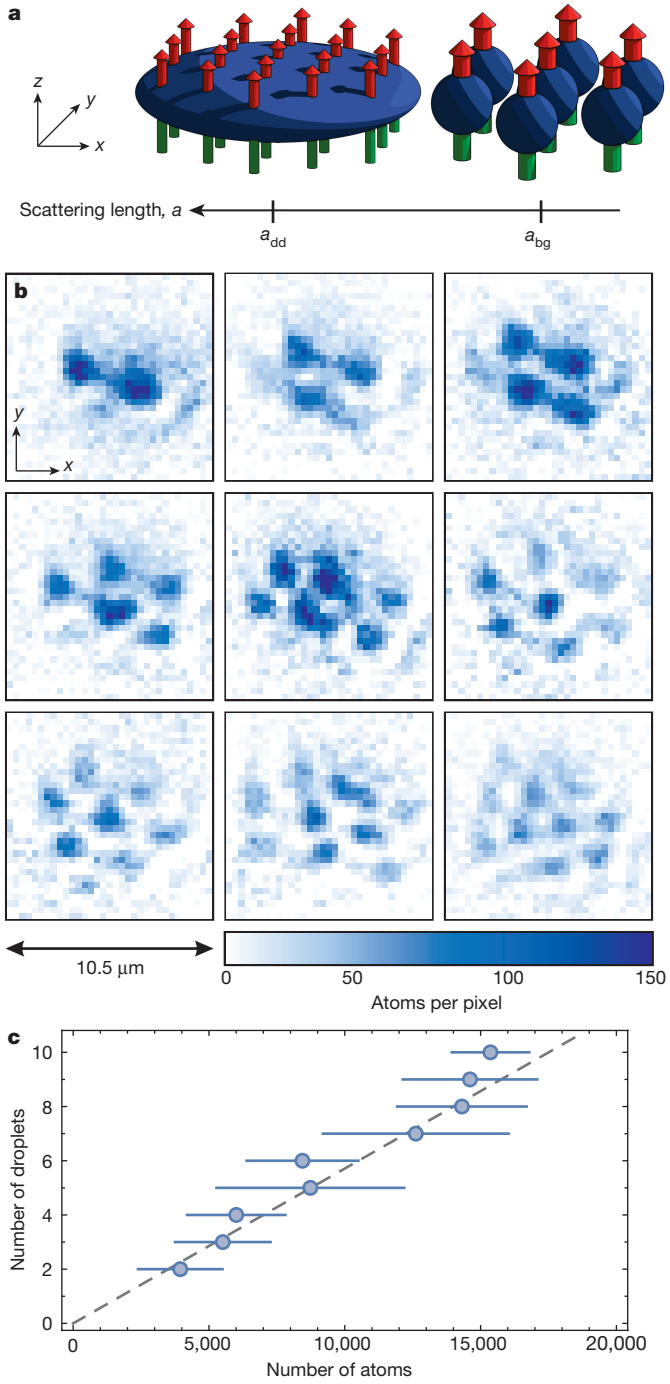

Figure 1 | Growth of a microscopic droplet crystal. a, Schematic of the experimental procedure. We prepared a stable, strongly dipolar Dy BEC with $a \approx a_{dd}$ in a pancake-shaped trap (left). By decreasing the scattering length a, we induced an instability close to $a \approx a_{bg}$. Following this instability, the atoms clustered to droplets in a triangular pattern (right). **b**, Representative single samples of droplet patterns imaged *in situ*, with droplet numbers, N_d, ranging from two to ten. **c**, We used a set of 112 realizations with different numbers of droplets and atoms for a statistical analysis. The plot shows the mean number of atoms as a function of the number of droplets N_d, with error bars indicating the standard deviation. The fitted linear relation (grey dashed line) has a slope of 1,750(300) atoms per droplet. This shows that increasing the number of atoms results in growth of the microscopic droplet crystal.

In Fig. 1b, we show typical *in situ* images of the resultant triangular patterns for the quantum ferrofluid with different numbers of droplets, N_d, ranging from two to ten. To analyse the average number of atoms per droplet, we count the number of droplets N_d in relation to the total number of atoms. Figure 1c indicates a linear dependence between N_d and the number of atoms, with a slope of 1,750(300) atoms per droplet. For $N_d = 2$, we observe a droplet distance of $d = 3.0(4)\,\mu m$. The droplets, which have a large effective dipole moment of $N_d\mu$, strongly repel each other while the radial trapping applies a restoring force. Hence, the distance d can be calculated using a simplified one-dimensional classical system by minimizing the energy of the system.

We assume two strongly dipolar particles with 1,750 times the mass and magnetic moment of a Dy atom that are confined in a harmonic trap. For our experimental parameters, these particles minimize their energy with a distance of $d = 3.3\,\mu m$, in agreement with the observed distance. For $N_d > 2$, the droplets arrange mostly in triangular structures, and form a microscopic crystal with a droplet distance of $d = 2$–$3\,\mu m$. Owing to the isotropy of the repulsion between droplets in the radial plane, we expect the triangular configuration to have the lowest energy. Because of the repelling dipolar force between the droplets, we observe in the radial direction nearly round, discrete droplets with possible weak overlap to neighbouring ones.

Comparing our quantum ferrofluid with a classical ferrofluid, very similar behaviour and patterns have been observed on a superhydrophobic surface[3]. In this classical-ferrofluid system, a single droplet first deforms as the external magnetic field increases, and then divides into two droplets when some critical field is reached. For a quantum ferrofluid, a single droplet should be unstable for $a < a_{dd}$, owing to the attractive part of the dipolar interaction, and so should collapse. Although, the counteracting quantum pressure—the zero-point energy that exists as a result of an external trapping potential—can compensate attraction and prevent collapse[26], mean field calculations[18] predict this not to be the case. Our observation of stable droplet ensembles is therefore striking, and further work is needed to understand their stability. A possible stabilizing effect is that of quantum fluctuations, leading to beyond mean-field effects[27]. Such stabilization has been suggested in a similar situation of competing attraction and repulsion[28], and an increased effect of quantum fluctuations has been calculated for strongly dipolar gases[29].

As further quantitative statistical analysis, we computed the Fourier spectrum $S(k)$ of the obtained images (Fig. 2a–c). The patterns are visible as a local maximum in $S(k)$ at finite momentum $k = 2\pi/d \approx 2.5\,\mu m^{-1}$, whereas the spectrum of a BEC monotonically decreases with k. We define the spectral weight

$$SW = \sum_{k=1.5\,\mu m^{-1}}^{5\,\mu m^{-1}} S(k)$$

which is a quantity that represents the strength of the structured states, and normalize it such that a BEC has $SW_{BEC} = 1$. After a quench of the interactions from $a \approx a_{dd}$ to $a \approx a_{bg}$, we statistically investigated the pattern-formation time and the lifetime of these patterns (Fig. 2d). We repeated this measurement 13 times and found statistically that the pattern is fully developed after 7 ms, and has a 1/e lifetime of about 300 ms. The decay of the droplet structure is accompanied by a decrease in the number of atoms, with a 1/e lifetime of about 130 ms, while the residual thermal cloud is constant. Owing to the decreasing number of atoms, the structures evolve back to lower numbers of droplets, N_d, until they merge back into one droplet (insets of Fig. 2d). In comparison, because we measured lifetimes of a non-structured BEC of more than 5 s, we assume increased three-body losses as a reason for the reduced lifetime. One indication of this is the measured atomic peak density for droplets of $n \gtrsim 5 \times 10^{20}\,m^{-3}$, which is greater than the density of a BEC, $n \approx 10^{20}\,m^{-3}$.

To explore the nature of this instability, we performed the following experimental sequence, depicted in Fig. 3a. We prepared the BEC close to the Feshbach resonance with $a \approx a_{dd}$ and ramped the magnetic field linearly to varying values near the instability point. We ensured that the structures were formed within 10 ms, even for values of the magnetic

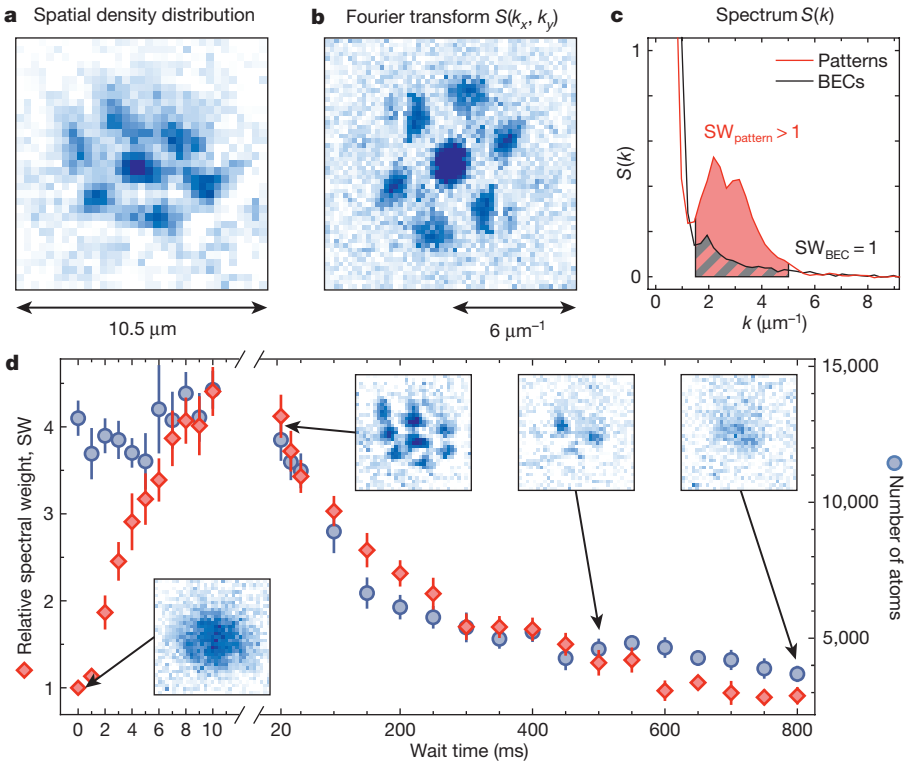

Figure 2 | Evaluation of the structures and lifetime analysis. a–c, Illustration of our statistical evaluation procedure. We began with the spatial density distribution (**a**), and then calculated the absolute value of the two-dimensional Fourier transform $S(k_x, k_y)$ (**b**) and radially averaged over $k = (k_x^2 + k_y^2)^{1/2}$ to obtain the spectrum $S(k)$ (**c**). We removed the white noise from the spectrum $S(k)$ such that $S(k) = 0$ for $k > 7\,\mu m^{-1}$, which corresponds to structures below our resolution. The spectra in **c** represent an average of 13 images for both BECs and patterns at a wait time of 10 ms. For patterns in the spatial density distribution, we observe an enhanced signal for $k \approx 2.5\,\mu m^{-1}$ in the spectrum (red line), whereas the spectrum of BECs (black line) shows monotonic decay for increasing momentum. We define the sum of these spectra over a momentum range as the relative spectral weight SW (shaded areas, as defined in the text), which is a quantity for the strength of the structured states. **d**, We performed a sudden quench (over 0.5 ms) of the BEC below the instability to $B = 6.656(3)$ G, for varying wait times. To determine the creation time and the lifetime of the patterns, we plot the relative spectral weight SW (red diamonds) against wait time. Each point is an average of 13 realizations, with error bars indicating the standard error. The plot shows rapid pattern formation within 7 ms and a surprisingly long 1/e lifetime of about 300 ms. This lifetime seems to be limited by a decrease in the number of atoms (blue circles). The insets are typical spatial density distributions of single samples before pattern formation (BEC; bottom left), and at three different wait times.

field close to the stability threshold, and waited at the chosen value for twice this time. Figure 3b shows a clear hysteresis for the way down in magnetic field compared to the return. For the return, we observe the same spectral weights as for the way down, but for magnetic fields that are about 20 mG greater. This demonstrates that our system features bistability in the transition region. We expect that the transition from one state to the other is driven by thermal excitations or weak currents due to overlapping droplets. In the thermodynamic limit, such behaviour is a clear signature of a first-order phase transition and a latent heat in the crystallization process.

To verify that we are dealing with a transition to a ground state and not a metastable state resulting from quench dynamics, we performed forced evaporative cooling at a constant magnetic field far away from any Feshbach resonance with $a \approx a_{bg}$. We observed very similar self-organized structures, which were visible for temperatures near the expected critical temperature for the phase transition to a BEC.

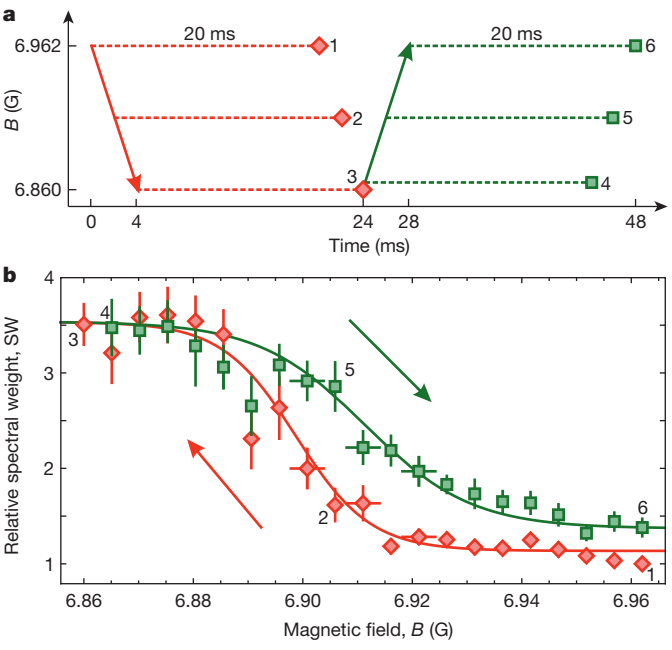

Figure 3 | Hysteresis of pattern formation. a, A timeline of the experiment in which we observed hysteresis. We prepared the Dy BEC close to the Feshbach resonance at $B = 6.962(3)$ G and ramped down the magnetic field linearly to different values, with a constant change rate, the lowest of which was $B = 6.860(3)$ G. To ensure that the structures had enough time to form, we waited for 20 ms at each value before imaging the atomic sample *in situ*. For the way back, we first waited at the lowest field value for 20 ms and then increased the magnetic field with the same ramp speed to higher values, once again holding for 20 ms at each value before imaging the sample *in situ*. **b**, Hysteresis plot for the structured patterns, which shows the spectral weight SW against magnetic field as it is decreased (red diamonds and line) and then increased (green squares and line). Each point is an average of 14 realizations, with the vertical error bars indicating standard errors. We determined the long-term field stability to be 3 mG, as shown by the horizontal error bars for selected points. A clear hysteresis is visible, although the total time is twice as long for the way back. The labels 1–6 in **a** and **b** indicate data points at particular field values to help the understandability; the lines in **b** serve as a guide to the eye.

Because structures can melt back into a BEC, and because we observed evaporative cooling to patterns, it is quite plausible that the droplets are superfluid individually. Whether they share the same phase via weak links or lose their mutual phase coherence will have to be investigated in future experiments. Another open question is the creation dynamics of a self-organized structure. It will be interesting to study phonons in such a droplet crystal, which we expect to have eigenfrequencies of the order of many inverse lifetimes. We also expect that these phonons will be coupled to collective Josephson oscillations via weak links[30].

Online Content Methods, along with any additional Extended Data display items and Source Data, are available in the online version of the paper; references unique to these sections appear only in the online paper.

Received 12 August; accepted 17 November 2015.
Published online 1 February 2016.

1. Rosensweig, R. *Ferrohydrodynamics* Ch. 7.1 (Cambridge Univ. Press, 1985).
2. Cowley, M. D. & Rosensweig, R. E. The interfacial stability of a ferromagnetic fluid. *J. Fluid Mech.* **30,** 671–688 (1967).
3. Timonen, J. V. I., Latikka, M., Leibler, L., Ras, R. H. A. & Ikkala, O. Switchable static and dynamic self-assembly of magnetic droplets on superhydrophobic surfaces. *Science* **341,** 253–257 (2013).
4. Lahaye, T. *et al.* Strong dipolar effects in a quantum ferrofluid. *Nature* **448,** 672–675 (2007).
5. Lahaye, T., Menotti, C., Santos, L., Lewenstein, M. & Pfau, T. The physics of dipolar bosonic quantum gases. *Rep. Prog. Phys.* **72,** 126401 (2009).
6. Baranov, M. A., Dalmonte, M., Pupillo, G. & Zoller, P. Condensed matter theory of dipolar quantum gases. *Chem. Rev.* **112,** 5012–5061 (2012).
7. Lu, M., Burdick, N. Q., Youn, S. H. & Lev, B. L. Strongly dipolar Bose-Einstein condensate of dysprosium. *Phys. Rev. Lett.* **107,** 190401 (2011).
8. Santos, L., Shlyapnikov, G. V. & Lewenstein, M. Roton-Maxon spectrum and stability of trapped dipolar Bose-Einstein condensates. *Phys. Rev. Lett.* **90,** 250403 (2003).
9. Andreev, A. F. & Lifshitz, I. M. Quantum theory of defects in crystals. *Sov. Phys. JETP* **29,** 1107–1113 (1969).
10. Chester, G. V. Speculations on Bose-Einstein condensation and quantum crystals. *Phys. Rev. A* **2,** 256–258 (1970).
11. Leggett, A. J. Can a solid be "superfluid"? *Phys. Rev. Lett.* **25,** 1543–1546 (1970).
12. Kim, E. & Chan, M. H. W. Probable observation of a supersolid helium phase. *Nature* **427,** 225–227 (2004).
13. Kim, E. & Chan, M. H. W. Observation of superflow in solid helium. *Science* **305,** 1941–1944 (2004).
14. Kim, D. Y. & Chan, M. H. W. Absence of supersolidity in solid helium in porous Vycor glass. *Phys. Rev. Lett.* **109,** 155301 (2012).
15. Henshaw, D. G. & Woods, A. D. B. Modes of atomic motions in liquid helium by inelastic scattering of neutrons. *Phys. Rev.* **121,** 1266–1274 (1961).
16. Ronen, S., Bortolotti, D. C. E. & Bohn, J. L. Radial and angular rotons in trapped dipolar gases. *Phys. Rev. Lett.* **98,** 030406 (2007).
17. Saito, H., Kawaguchi, Y. & Ueda, M. Ferrofluidity in a two-component dipolar Bose-Einstein condensate. *Phys. Rev. Lett.* **102,** 230403 (2009).
18. Wilson, R. M., Ronen, S. & Bohn, J. L. Angular collapse of dipolar Bose-Einstein condensates. *Phys. Rev. A* **80,** 023614 (2009).
19. Maier, T., Kadau, H., Schmitt, M., Griesmaier, A. & Pfau, T. Narrow-line magneto-optical trap for dysprosium atoms. *Opt. Lett.* **39,** 3138–3141 (2014).
20. Maier, T. *et al.* Emergence of chaotic scattering in ultracold Er and Dy. *Phys. Rev. X* **5,** 041029 (2015).
21. Góral, K., Rzążewski, K. & Pfau, T. Bose-Einstein condensation with magnetic dipole-dipole forces. *Phys. Rev. A* **61,** 051601 (2000).
22. Stuhler, J. *et al.* Observation of dipole-dipole interaction in a degenerate quantum gas. *Phys. Rev. Lett.* **95,** 150406 (2005).
23. Koch, T. *et al.* Stabilization of a purely dipolar quantum gas against collapse. *Nature Phys.* **4,** 218–222 (2008).
24. Tang, Y., Sykes, A., Burdick, N. Q., Bohn, J. L. & Lev, B. L. *s*-wave scattering lengths of the strongly dipolar bosons ^{162}Dy and ^{164}Dy. *Phys. Rev. A* **92,** 022703 (2015).
25. Maier, T. *et al.* Broad universal Feshbach resonances in the chaotic spectrum of dysprosium atoms. *Phys. Rev. A* **92,** 060702(R) (2015).
26. Bradley, C. C., Sackett, C. A. & Hulet, R. G. Bose-Einstein condensation of lithium: observation of limited condensate number. *Phys. Rev. Lett.* **78,** 985–989 (1997).
27. Lee, T. D., Huang, K. & Yang, C. N. Eigenvalues and eigenfunctions of a Bose system of hard spheres and its low-temperature properties. *Phys. Rev.* **106,** 1135–1145 (1957).
28. Petrov, D. S. Quantum mechanical stabilization of a collapsing Bose-Bose mixture. *Phys. Rev. Lett.* **115,** 155302 (2015).
29. Lima, A. R. P. & Pelster, A. Quantum fluctuations in dipolar Bose gases. *Phys. Rev. A* **84,** 041604 (2011).
30. Saccani, S., Moroni, S. & Boninsegni, M. Excitation spectrum of a supersolid. *Phys. Rev. Lett.* **108,** 175301 (2012).

Acknowledgements We thank A. Griesmaier for support at the early stage of the experiment and D. Zajec, D. Peter, H. P. Büchler and L. Santos for discussions. This work is supported by the German Research Foundation (DFG) within SFB/TRR21. H.K. acknowledges support by the 'Studienstiftung des deutschen Volkes'.

Author Contributions All authors discussed the results, made critical contributions to the work and contributed to the writing of the manuscript.

Author Information Reprints and permissions information is available at www.nature.com/reprints. The authors declare no competing financial interests. Readers are welcome to comment on the online version of the paper. Correspondence and requests for materials should be addressed to H.K. (h.kadau@physik.uni-stuttgart.de) or T.P. (t.pfau@physik.uni-stuttgart.de).

Observation of Quantum Droplets in a Strongly Dipolar Bose Gas

Igor Ferrier-Barbut, Holger Kadau, Matthias Schmitt, Matthias Wenzel, and Tilman Pfau
5. Physikalisches Institut and Center for Integrated Quantum Science and Technology, Universität Stuttgart, Pfaffenwaldring 57, 70550 Stuttgart, Germany

(Received 13 January 2016; revised manuscript received 15 February 2016; published 23 May 2016)

Quantum fluctuations are the origin of genuine quantum many-body effects, and can be neglected in classical mean-field phenomena. Here, we report on the observation of stable quantum droplets containing ~800 atoms that are expected to collapse at the mean-field level due to the essentially attractive interaction. By systematic measurements on individual droplets we demonstrate quantitatively that quantum fluctuations mechanically stabilize them against the mean-field collapse. We observe in addition the interference of several droplets indicating that this stable many-body state is phase coherent.

DOI: 10.1103/PhysRevLett.116.215301

Uncertainties and fluctuations around mean values are one of the key consequences of quantum mechanics. At the many-body level, they induce corrections to mean-field theory results, altering the many-body state, from a classical factorizable to an entangled state. Owing to their versatility, ultracold atom experiments offer numerous examples of interesting many-body states [1]. Among these systems, bosonic superfluids are well studied. They are described in the weakly interacting regime by a mean-field energy density proportional to the square of the particle density n^2, with a negative prefactor in the attractive case. Since the seminal work of Lee, Huang, and Yang [2], it is known that interactions lead to a repulsive correction $\propto n^{5/2}$ owing to quantum fluctuations. Therefore, an equilibrium between these two contributions can in principle stabilize an attractive Bose gas [3]. A similar stabilization mechanism using quantum fluctuations was proposed for an attractive Bose-Bose mixture in Ref. [4], which leads to the formation of droplets. In this reference liquidlike droplets are defined as the result of a competition between an attractive n^2 and a repulsive $n^{2+\alpha}$ term in the energy functional. Besides liquid helium droplets [5], such functionals are also used to describe atomic nuclei [6]. Here, we study a strongly dipolar Bose gas where the attractive mean-field interaction is due to the dipole-dipole interaction (DDI). This system is known to be unstable in the mean-field approximation [7]. We however show here that beyond mean-field effects lead to the stabilization of droplets. Our investigations are aimed at probing strongly dipolar Bose gases of ^{164}Dy, which are characterized by a dipolar length $a_{\mathrm{dd}} = \mu_0\mu^2 m/12\pi\hbar^2 \simeq 131a_0$, where a_0 is the Bohr radius with $\mu = 9.93\mu_B$ Dy's magnetic dipole moment in units of the Bohr magneton μ_B, $\hbar$ the reduced Planck constant, and m the atomic mass. The additional short-range interaction of ^{164}Dy, characterized by the scattering length a has been the focus of several papers [8–11], and the background scattering length was measured to be $a_{\mathrm{bg}} = 92(8)a_0$, modulated by many Feshbach resonances. Thus, away from Feshbach resonances at the mean-field level the dipolar interaction dominates with $\varepsilon_{\mathrm{dd,bg}} = a_{\mathrm{dd}}/a_{\mathrm{bg}} \simeq 1.45$. In a previous work [12], we have reported the observation of an instability of a dipolar Bose-Einstein condensate (BEC); the resulting state of this instablity is characterized by the existence of apparent droplets. These droplets cannot be explained by a stabilization by one-body quantum pressure [13], and as such are not solitons in the strict sense.

Here, we isolate these droplets to unravel their nature. To perform our study systematically, we place them in a waveguide. This relaxes their confinement in one direction (along x) and thus suppresses the effect of dipolar repulsion between the droplets. The waveguide is a single optical dipole trap that creates a tight confinement around the x axis with frequencies $\nu_y = 123(5)$ Hz, $\nu_z = 100(10)$ Hz. The release in this waveguide is performed in the following way (details of the ramping procedures can be found in Ref. [14]): we create a BEC containing $\sim 10 \times 10^3$ atoms in a crossed optical dipole trap at a magnetic field along the vertical (z) axis $B_{\mathrm{BEC}} = 6.962(10)$ G; we then lower the field to $B_1 = 6.656(10)$ G in 1 ms, from which a wait time of 15 ms follows. At $B = B_1$ [$B = B_{\mathrm{BEC}}$] using $a_{\mathrm{bg}} = 92a_0$ and our knowledge of the Feshbach resonances [14], we get $a = 95(13)a_0$ [$a = 115(20)a_0$]. Then, one dipole trap is turned off and the other one ramped-up to higher power in 1 ms. The trap has a too weak confinement to hold the atoms in the x direction and the cloud starts moving. We then image it as function of time in the waveguide t_{WG} using high-resolution (1 μm) imaging. We observe the following, illustrated in Fig. 1. First, the condensed fraction remains fragmented into up to six droplets and down to one droplet. Some atoms originally in the BEC do not form droplets; this fraction of atoms is hard to quantify since it is hard to tell apart from a thermal fraction in our images. Second, during the evolution time the initial confinement energy is turned into relative kinetic energy and these droplets move away from each other. We observe an *in situ*

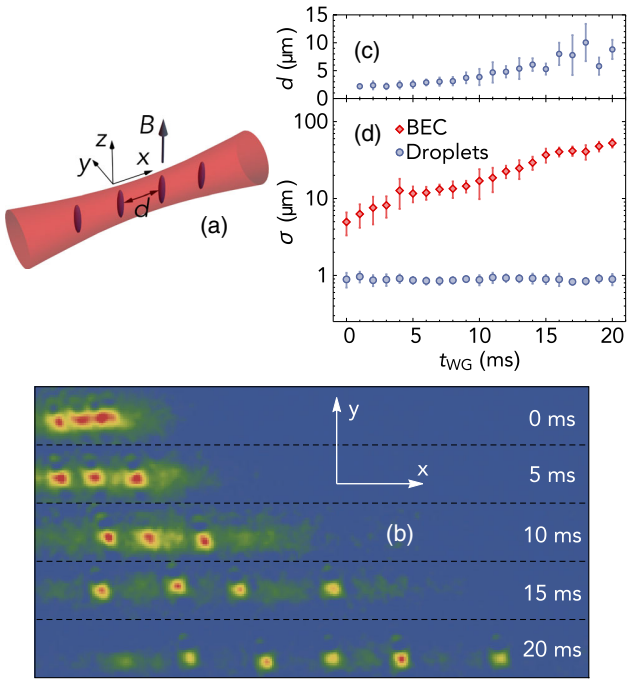

FIG. 1. Quantum droplets of a dipolar Bose gas in a waveguide. (a) Schematic representation of the droplets in the waveguide; the elongation along z is represented; their separation d is indicated. (b) Examples of *in situ* optical density (OD) images after release in the waveguide at the magnetic field $B_1 = 6.656(10)$ G. Images taken at times $t_{\mathrm{WG}} = 0, 5, 10, 15, 20$ ms (top to bottom). The OD is normalized to the maximal OD in each image to improve visibility. (c) Evolution of the mean separation d between the droplets as a function of time. (d) Blue circles: evolution of the width σ obtained from a Gaussian fit to their density profiles (average of transverse and axial radii). Red diamonds: evolution of the size of a BEC for comparison. The data in panels (c) and (d) are obtained by averaging at least four experimental realizations; the error bars indicate the statistical standard deviation The convention for the axes used through the Letter is indicated in panel (a).

size limited by our resolution (Gaussian width $\sigma \simeq 900$ nm roughly identical in the x and y directions), which does not evolve during 20 ms. If we perform the same sequence but keeping the field at B_{BEC}, we observe that the BEC does not separate into droplets and expands as a whole in the waveguide; in 20 ms its axial size is increased by a factor 10 [Fig. 1(d), red diamonds]. At $B = B_1$, the number of atoms in the droplets is $N = 800(200)$. The facts that a single droplet appears to be stable and, when there are several of them, that their size does not significantly increase while their distance is multiplied by 4, indicates that they are self-confining. Note that we also observe these droplets on the low-field side of a resonance at $B = 1.2$ G.

Since the confinement is too weak in the long direction to observe droplets for longer times, we perform a second set of experiments keeping a very weak confinement in the x direction ($\nu_x = 14.5(1)$ Hz, see Ref. [14]); thus, the trapping potential takes a prolate cigar shape still perpendicular to $\vec{B}$ with an aspect ratio $\nu_{y,z}/\nu_x \simeq 8$. We observe that in this trap, the droplets equilibrate at long times $t > 100$ ms at an average relative distance $d = 2.5(5)$ μm, obtained from ten experimental realizations. Furthermore, when we first adiabatically load a BEC in the prolate trap and then ramp from B_{BEC} to B_1, we observe the same distance. This distance is smaller than the length obtained by a simple analysis assuming pointlike dipoles in a harmonic trap $l_x = (3N\mu_0\mu^2/2\pi m\omega_x^2)^{1/5} \simeq 4.5$ μm, indicating that the droplets cannot be considered as pointlike. With a more refined analysis developed in Ref. [14] using a Gaussian ansatz with radial symmetry around z for the density distribution inside a droplet, we calculate the dipole-dipole repulsion. We thus obtain that a distance of $d = 2.5(5)$ μm is obtained for elongated droplets with $\sigma_z = 2.5(5)$ μm and a radial size $\sigma_r \lesssim 500$ nm. Finally, we observe lifetimes of several hundreds of milliseconds, similar to what we reported in Ref. [12], which confirm a strong stabilization mechanism.

Given the strong elongation of the droplets along the z direction, the dipolar interaction is mainly attractive and since $\epsilon_{\mathrm{dd}} = a_{\mathrm{dd}}/a > 1$ this attraction is stronger than the short-range repulsion, such that overall the interactions are mainly attractive. The droplets are thus expected to be unstable at the mean-field level [20]. We observe that first the gas locally collapses, before this collapse is arrested at high densities finally forming droplets. This means that the density dependence of the stabilizing mechanism is stronger than that of the mean-field two-body interactions. Importantly, our present work shows that this mechanism is local and not due to any long-range effect between droplets. Two works have postulated the existence of a three-body conservative repulsion [21,22] with mean-field energy density $\propto n^3$.

However, these works neglect beyond mean-field effects. As stated above the energy density e for these effects is $e \propto n^{5/2}$. This correction has been measured in contact-interacting Bose gases [23,24]. Here, we must take both contact repulsion and the DDI into account. Using the results of Refs. [25–27] the beyond mean-field correction to the chemical potential $\mu = (\partial e/\partial n)$ for a dipolar gas is given by $\mu_{\mathrm{bmf}} \simeq (32gn/3\sqrt{\pi})\sqrt{na^3}(1 + \frac{3}{2}\epsilon_{\mathrm{dd}}^2)$, where we have taken the lowest order expansion of the Q_5 function of Ref. [27] since ϵ_{dd} is close to 1. Doing this we effectively neglect the imaginary part, which is very small compared to the real part, such that a long lifetime is still ensured, though it is only in a metastable equilibrium. This beyond mean-field term is to be compared with the mean-field contact interaction contribution $\mu_{c,\mathrm{mf}}$ and the DDI one $\mu_{\mathrm{dd,mf}}$. Using a Thomas-Fermi approximation (which neglects kinetic energy) for a droplet with a Gaussian density distribution, the contribution at the center of the droplet is $\mu_{c,\mathrm{mf}} = gn_0$ for the contact interaction where

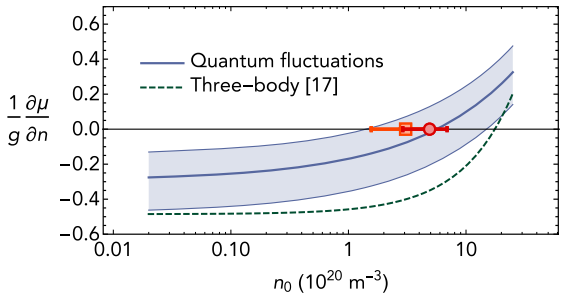

FIG. 2. Derivative of the chemical potential with respect to density as a function of density, at the center of a droplet using a Gaussian ansatz (1) ($g = 4\pi\hbar^2 a/m$). The blue shaded region expresses our uncertainty on the scattering length. Negative values imply mechanical instability. The experimental value obtained from expansion measurements (Fig. 4) is shown as a red circle assuming a Gaussian distribution and as an orange square assuming an inverted parabola. The dashed line shows the same quantity obtained using a three-body repulsion using parameters from Ref. [22], which stabilizes at a higher density.

$g = 4\pi\hbar^2 a/m$ and n_0 is the peak density. The dipolar interaction contribution is $\mu_{\mathrm{dd,mf}} = -g n_0 \epsilon_{\mathrm{dd}} f_{\mathrm{dip}}(\kappa)$ [28] with $\kappa = \sigma_r/\sigma_z$; it thus depends on the elongation of the droplet along the field direction through the function $f_{\mathrm{dip}}(\kappa)$, which can be found in Ref. [14]. Using an aspect ratio equal to our experimental upper bound $\kappa = 0.2$ one has $f_{\mathrm{dip}}(\kappa) = 0.83$ such that the dipolar attraction dominates the mean-field contributions for $\epsilon_{\mathrm{dd}} \geq 1.2$ or $a \leq 110 a_0$ [29]. The mechanical stability condition is $(\partial\mu/\partial n) \geq 0$. At the center in the Gaussian ansatz we get

$$\left.\frac{\partial\mu}{\partial n}\right|_{\mathbf{r}=0} = g\left(1 - \epsilon_{\mathrm{dd}} f_{\mathrm{dip}}(\kappa) + 16\sqrt{n_0 a^3/\pi}\left(1 + \frac{3}{2}\epsilon_{\mathrm{dd}}^2\right)\right), \tag{1}$$

where n_0 is the peak density. Note that if one assumes an inverted-parabola density distribution, then one obtains the same result [30]. We plot this function in Fig. 2 using $a = 95(13) a_0$ and $\kappa = 1/10$ [this κ value is a factor of 2 below the experimental upper bound; it yields $f_{\mathrm{dip}}(\kappa) = 0.94$]. One can clearly see that since ϵ_{dd} is close to 1, though the attraction dominates, the two mean-field contributions nearly balance each other, which leads to a major role for beyond mean-field effects, a very similar situation to the one considered in Ref. [4]. From Eq. (1) one easily derives that the central density stabilizes at the value

$$n_0 = \frac{\pi}{a^3}\left(\frac{\epsilon_{\mathrm{dd}} f_{\mathrm{dip}}(\kappa) - 1}{16(1 + 3\epsilon_{\mathrm{dd}}^2/2)}\right)^2; \tag{2}$$

thus, in our approximation, stability is reached at densities $n_0 \gtrsim 10^{20}$ m^{-3}. Equation (2) is striking because the central density does not depend on atom number but only on a and very weakly on κ [31], which is characteristic of a liquidlike state. Neglecting quantum fluctuations and assuming a three-body repulsion ($\mu_{\mathrm{3b,mf}} = \hbar\kappa_3 n^2/2$), this density becomes $n_0 = g(\epsilon_{\mathrm{dd}} f_{\mathrm{dip}}(\kappa) - 1/\hbar\kappa_3)$. Using parameters from Ref. [22] ($a = 82.6 a_0$, $\kappa_3 = 5.87 \times 10^{-39}$ m^6/s) we get $n_0 = 17 \times 10^{20}$ m^{-3}, in very good agreement with full simulation results [22]; at these densities, however, beyond mean-field effects cannot be neglected. In addition such a high value for κ_3 is very hard to justify. It is very probable that κ_3, which is the real part of the three-body coupling constant, lies close to its imaginary part, which is the three-body recombination constant L_3. Observing the lifetime of the BECs, we have an upper bound $L_3 \lesssim 10^{-41}$ m^6/s, which implies an experimentally irrelevant stabilizing density $n_0 > 10^{23}$ m^{-3}. Our experimental observations developed above imply a lower bound on the central density $n_0 \geq 10^{20}$ m^{-3}; given our imaging resolution, we cannot observe smaller droplet radii and higher densities. For a better estimate of the density, we turn to expansion experiments.

The mechanisms at work in the droplets can indeed be further explored by observing their time-of flight expansion in free space. In principle, pure liquid droplets in the absence of trapping should reach an equilibrium with an absence of growth [4,21]. On the other hand, time-of-flight expansion under a dipolar interaction is nontrivial but well studied [32,33], and it is modified by beyond mean-field effects [27]; these effects are isotropic and counteract magnetostriction. Mean-field hydrodynamic equations could not describe the expansion of our droplets. In our experiment, we perform such measurements by turning off the waveguide trap after 4 ms. In order to keep the atoms at the focal position of our imaging system, we apply a magnetic field gradient that compensates gravity, and image the atoms at various times after release, Figs. 4(a) and 4(b). We record thus the size in the x and y direction as a function of time. The sizes undergo a linear growth with rates $\dot{\sigma}_x = 0.17(3)\ \mu$m/ms, $\dot{\sigma}_y = 0.24(3)\ \mu$m/ms [14]. We qualitatively express the expansion dynamics in terms of the released energy $E_i = \frac{1}{2} m \dot{\sigma}_i^2$ [34]; we get $E_y = 0.09(1)\hbar\omega_y$, $E_x = 0.045(4)\hbar\omega_y$. Such energies are remarkably low, which demonstrates that kinetic energy plays only a marginal role, as expected; however, a full theory is presently not available to describe the free-space dynamics after release.

To circumvent the absence of a model for free-space dynamics, we perform a new set of experiments. It consists of the same procedure, but at the time of release, the magnetic field is quenched (in 50 μs) from B_1 to a higher value B_{ToF} inducing a change in scattering length $\Delta a = a(B_{\mathrm{ToF}}) - a(B_1)$, while the DDI remains unchanged. In this case, the expansion rate is strongly increased. Given the quench time, the initial density does not have time to

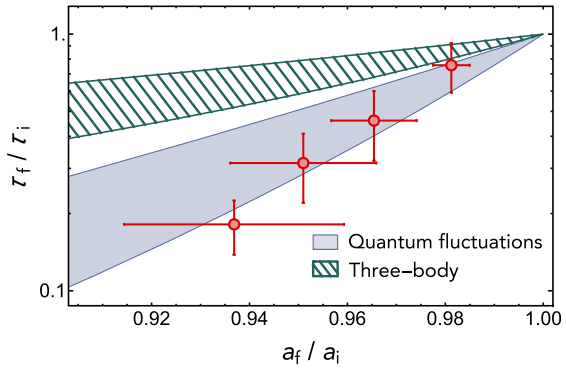

FIG. 3. Ratio of the lifetime $\tau_f/\tau i$ of the droplets between scattering lengths a_f and a_i. We use here $a_i = 94(12)a_0$ obtained at $B_i = 6.573(5)$ G. The data points are taken down to $B_f = 6.159(5)$ G. The filled blue and green hatched areas represent the expected scaling using quantum fluctuations and three-body repulsion, respectively, taking into account the uncertainty range on the droplets' aspect ratio: $0 \leq \kappa \leq 0.2$.

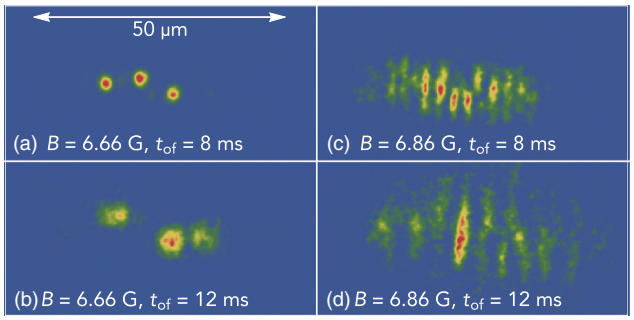

FIG. 4. Time-of-flight expansion measurements. The field is held at $B_1 = 6.656(10)$ G until release when it is quenched to a different value. (a),(b) Images where the field is kept at B_1 during expansion and (c),(d) quenched to 6.86 G. In (a) and (b) one sees expanding droplets, whereas in (c) and (d) they overlap and clear interference fringes appear along the x axis while we can still measure the expansion size in the y direction.

adapt to the interaction quench. One thus expects that the change in released energy is given by $\Delta E \simeq \frac{1}{N}\int d\vec{r}\frac{\Delta g}{2}n^2 = \Delta g n_0/4\sqrt{2}$, where we have used again a Gaussian ansatz, and $\Delta g = 4\pi\hbar^2\Delta a/m$. Since we are dealing with the difference in total energy here, the variation of the beyond mean-field corrections is negligible. Thus, since $\Delta a(B)$ is known, we can extract a value for n_0 from the observed change in ΔE. From these measurements detailed in Ref. [14], given our uncertainty on $a(B)$ we obtain $n_0 = 4.9(2.0) \times 10^{20}$ m^{-3}. If instead of the Gaussian ansatz we use an inverted parabola, then we get $\Delta E = 2\Delta g n_0/7$, from which we obtain $n_0 = 3.0(1.5) \times 10^{20}$ m^{-3}. Both values are compatible with the lower bound extracted from *in situ* imaging; we represent them in Fig. 2. The measured density is thus in agreement with the stabilizing density due to quantum fluctuations.

However, this does not probe the scaling behavior of the density as a function of a. As evident in Eq. (2), this scaling is very strong. In turn, three-body recombination in the droplets scales very strongly with a; indeed, since the density does not depend on atom number, three-body losses lead to an exponential decay with a lifetime $\tau = 1/L_3\langle n^2\rangle$ [14]. In particular, τ decreases when a decreases. To cancel the uncertainties on L_3 and on the exact density distribution one simply needs to measure the ratio in lifetime τ_f/τ_i between two different scattering lengths or magnetic fields B_i and B_f, which, assuming a constant L_3, is simply given by $\tau_f/\tau_i = (\langle n_i^2\rangle/\langle n_f^2\rangle) = (n_{0,i}^2/n_{0,f}^2)$. One can easily show that for a fixed κ this ratio is a function of only two parameters $[(a_f/a_i),(a_{dd}/a_i)]$; in particular assuming three-body repulsion, it is independent of κ_3; we give this function in Ref. [14]. Thus, using a fixed $a_i = 94(12)a_0$ [$B_i = 6.573(5)$ G], in Fig. 3 we represent τ_f/τ_i vs a_f/a_i. This figure is striking; while we vary the scattering length by less than 10%, the lifetime is divided by a factor of 5. Furthermore, the data points are incompatible with the scaling predicted by three-body repulsion while without any fit parameter they follow the scaling predicted using quantum fluctuation within the experimental uncertainties. The small deviation to lower lifetimes can be accounted for by a weak variation of L_3 [35]. This demonstrates unambiguously that quantum fluctuations constitute the stabilizing mechanism. The conclusion we drew here is reinforced by numerical simulations reported in [36] of which we have recently become aware. Finally, we observe that the droplets have internal phase coherence. Indeed, for "fast" expansion dynamics obtained when quenching B during the time of flight, the size of the expanding droplets becomes comparable to or larger than their relative distance so that neighboring ones overlap. In this case we observe matter-wave interference fringes as exemplified in Figs. 4(c) and 4(d). The presence of these fringes demonstrates that each droplet individually is phase coherent and thus superfluid. Their observation opens the door to studies of the relative phase coherence between droplets. In the present case we do not observe fringe patterns that allow us to measure the droplets' relative phase, but this is mainly due to shot-to-shot noise in the *in situ* position and the relative spacing of the droplets since we are not yet in the far-field regime. Future studies with fixed *in situ* conditions prior to the time of flight could bring insight into the phase coherence of an ensemble of droplets, even in the case of a high number of them [37]. Our measurements reported here have established the existence of a novel system forming droplets stabilized by quantum fluctuations. These results open prospects of forming pure liquid droplets of a quantum gas in free space characterized by a total absence of growth.

We acknowledge insightful discussions with L. Santos and D. Petrov as well as with H. P Büchler, A. Pelster,

G. Raithel, and F. Ferlaino. We thank T. Maier for experimental assistance at early stages. This work is supported by the German Research Foundation (DFG) within SFB/TRR21.

[1] I. Bloch, J. Dalibard, and W. Zwerger, Many-body physics with ultracold gases, Rev. Mod. Phys. **80**, 885 (2008).
[2] T. D. Lee, K. Huang, and C. N. Yang, Eigenvalues and eigenfunctions of a bose system of hard spheres and its low-temperature properties, Phys. Rev. **106**, 1135 (1957).
[3] G. E. Volovik, *The Universe in a Helium Droplet*, International Series of Monographs on Physics (Oxford University Press, Oxford, 2009).
[4] D. S. Petrov, Quantum Mechanical Stabilization of a Collapsing Bose-Bose Mixture, Phys. Rev. Lett. **115**, 155302 (2015).
[5] F. Dalfovo, A. Lastri, L. Pricaupenko, S. Stringari, and J. Treiner, Structural and dynamical properties of superfluid helium: A density-functional approach, Phys. Rev. B **52**, 1193 (1995).
[6] M. Bender, P.-H. Heenen, and P.-G. Reinhard, Self-consistent mean-field models for nuclear structure, Rev. Mod. Phys. **75**, 121 (2003).
[7] S. Komineas and N. R. Cooper, Vortex lattices in Bose-Einstein condensates with dipolar interactions beyond the weak-interaction limit, Phys. Rev. A **75**, 023623 (2007).
[8] K. Baumann, N. Q. Burdick, M. Lu, and B. L. Lev, Observation of low-field Fano-Feshbach resonances in ultracold gases of dysprosium, Phys. Rev. A **89**, 020701 (R) (2014).
[9] T. Maier, I. Ferrier-Barbut, H. Kadau, M. Schmitt, M. Wenzel, C. Wink, T. Pfau, K. Jachymski, and P. S. Julienne, Broad universal Feshbach resonances in the chaotic spectrum of dysprosium atoms, Phys. Rev. A **92**, 060702(R) (2015).
[10] Y. Tang, A. Sykes, N. Q. Burdick, J. L. Bohn, and B. L. Lev, *s*-wave scattering lengths of the strongly dipolar bosons ^{162}Dy and ^{164}Dy, Phys. Rev. A **92**, 022703 (2015).
[11] T. Maier, H. Kadau, M. Schmitt, M. Wenzel, I. Ferrier-Barbut, T. Pfau, A. Frisch, S. Baier, K. Aikawa, L. Chomaz, M. J. Mark, F. Ferlaino, C. Makrides, E. Tiesinga, A. Petrov, and S. Kotochigova, Emergence of Chaotic Scattering in Ultracold Er and Dy, Phys. Rev. X **5**, 041029 (2015).
[12] H. Kadau, M. Schmitt, M. Wenzel, C. Wink, T. Maier, I. Ferrier-Barbut, and T. Pfau, Observing the Rosensweig instability of a quantum ferrofluid, Nature (London) **530**, 194 (2016).
[13] P. Pedri and L. Santos, Two-Dimensional Bright Solitons in Dipolar Bose-Einstein Condensates, Phys. Rev. Lett. **95**, 200404 (2005).
[14] See Supplemental Material at http://link.aps.org/supplemental/10.1103/PhysRevLett.116.215301 for a detailed description of the different magnetic field and trapping lasers ramping procedures as well as a presentation of the theoretical models used throughout the Letter, which includes Refs. [15–19].
[15] K. Jachymski and P. S. Julienne, Analytical model of overlapping Feshbach resonances, Phys. Rev. A **88**, 052701 (2013).
[16] M. Fattori, G. Roati, B. Deissler, C. D'Errico, M. Zaccanti, M. Jona-Lasinio, L. Santos, M. Inguscio, and G. Modugno, Magnetic Dipolar Interaction in a Bose-Einstein Condensate Atomic Interferometer, Phys. Rev. Lett. **101**, 190405 (2008).
[17] B. Gao, General form of the quantum-defect theory for $-1/r^{\alpha}$ type of potentials with $\alpha > 2$, Phys. Rev. A **78**, 012702 (2008).
[18] Y. Wang and P. S. Julienne, Universal van der Waals physics for three cold atoms near Feshbach resonances, Nat. Phys. **10**, 768 (2014).
[19] Z. Shotan, O. Machtey, S. Kokkelmans, and L. Khaykovich, Three-Body Recombination at Vanishing Scattering Lengths in an Ultracold Bose Gas, Phys. Rev. Lett. **113**, 053202 (2014).
[20] T. Koch, T. Lahaye, J. Metz, B. Fröhlich, A. Griesmaier, and T. Pfau, Stabilization of a purely dipolar quantum gas against collapse, Nat. Phys. **4**, 218 (2008).
[21] K.-T. Xi and H. Saito, Droplet formation in a Bose-Einstein condensate with strong dipole-dipole interaction, Phys. Rev. A **93**, 011604 (2016).
[22] R. N. Bisset and P. B. Blakie, Crystallization of a dilute atomic dipolar condensate, Phys. Rev. A **92**, 061603(R) (2015).
[23] S. B. Papp, J. M. Pino, R. J. Wild, S. Ronen, C. E. Wieman, D. S. Jin, and E. A. Cornell, Bragg Spectroscopy of a Strongly Interacting ^{85}Rb Bose-Einstein Condensate, Phys. Rev. Lett. **101**, 135301 (2008).
[24] N. Navon, S. Piatecki, K. Günter, B. Rem, T. C. Nguyen, F. Chevy, W. Krauth, and C. Salomon, Dynamics and Thermodynamics of the Low-Temperature Strongly Interacting Bose Gas, Phys. Rev. Lett. **107**, 135301 (2011).
[25] R. Schützhold, M. Uhlmann, Y. Xu, and U. R. Fischer, Mean-field expansion in bose-einstein condensates with finite-range interactions, Int. J. Mod. Phys. B **20**, 3555 (2006).
[26] A. R. P. Lima and A. Pelster, Quantum fluctuations in dipolar Bose gases, Phys. Rev. A **84**, 041604(R) (2011).
[27] A. R. P. Lima and A. Pelster, Beyond mean-field low-lying excitations of dipolar Bose gases, Phys. Rev. A **86**, 063609 (2012).
[28] T. Lahaye, C. Menotti, L. Santos, M. Lewenstein, and T. Pfau, The physics of dipolar bosonic quantum gases, Rep. Prog. Phys. **72**, 126401 (2009).
[29] Since $f_{\mathrm{dip}}(\kappa)$ is a monotonically decreasing function of κ, at lower aspect ratios than 0.2, the mean-field dipolar contribution is larger and renders the droplets more unstable in the mean-field approximation.
[30] D. H. J. O'Dell, S. Giovanazzi, and C. Eberlein, Exact Hydrodynamics of a Trapped Dipolar Bose-Einstein Condensate, Phys. Rev. Lett. **92**, 250401 (2004).
[31] At our aspect ratios $f_{\mathrm{dip}}(\kappa)$ depends only weakly on κ as is visible in the Supplemental Material [14].
[32] S. Giovanazzi, P. Pedri, L. Santos, A. Griesmaier, M. Fattori, T. Koch, J. Stuhler, and T. Pfau, Expansion dynamics of a dipolar Bose-Einstein condensate, Phys. Rev. A **74**, 013621 (2006).

[33] T. Lahaye, T. Koch, B. Fröhlich, M. Fattori, J. Metz, A. Griesmaier, S. Giovanazzi, and T. Pfau, Strong dipolar effects in a quantum ferrofluid, Nature (London) **448**, 672 (2007).

[34] M. J. Holland, D. S. Jin, M. L. Chiofalo, and J. Cooper, Emergence of Interaction Effects in Bose-Einstein Condensation, Phys. Rev. Lett. **78**, 3801 (1997).

[35] Measurements of L_3 will be presented in a future publication.

[36] F. Wächtler and L. Santos, Quantum filaments in dipolar Bose-Einstein condensates, arXiv:1601.04501.

[37] Z. Hadzibabic, S. Stock, B. Battelier, V. Bretin, and J. Dalibard, Interference of an Array of Independent Bose-Einstein Condensates, Phys. Rev. Lett. **93**, 180403 (2004).

LETTER

doi:10.1038/nature20126

Self-bound droplets of a dilute magnetic quantum liquid

Matthias Schmitt[1], Matthias Wenzel[1], Fabian Böttcher[1], Igor Ferrier-Barbut[1] & Tilman Pfau[1]

Self-bound many-body systems are formed through a balance of attractive and repulsive forces and occur in many physical scenarios. Liquid droplets are an example of a self-bound system, formed by a balance of the mutual attractive and repulsive forces that derive from different components of the inter-particle potential. It has been suggested[1,2] that self-bound ensembles of ultracold atoms should exist for atom number densities that are 10^8 times lower than in a helium droplet, which is formed from a dense quantum liquid. However, such ensembles have been elusive up to now because they require forces other than the usual zero-range contact interaction, which is either attractive or repulsive but never both. On the basis of the recent finding that an unstable bosonic dipolar gas can be stabilized by a repulsive many-body term[3], it was predicted that three-dimensional self-bound quantum droplets of magnetic atoms should exist[4,5]. Here we report the observation of such droplets in a trap-free levitation field. We find that this dilute magnetic quantum liquid requires a minimum, critical number of atoms, below which the liquid evaporates into an expanding gas as a result of the quantum pressure of the individual constituents. Consequently, around this critical atom number we observe an interaction-driven phase transition between a gas and a self-bound liquid in the quantum degenerate regime with ultracold atoms. These droplets are the dilute counterpart of strongly correlated self-bound systems such as atomic nuclei[6] and helium droplets[7].

Liquid droplets of water or helium are formed by the mutual attractive and repulsive forces that are created by the different parts of the inter-particle potential (and are due to covalent or van der Waals attraction and to the electronic Pauli exclusion principle, respectively). Helium droplets in particular have been a focus of research, owing to their interesting quantum nature[8,9]. Droplets can serve as closed, isolated quantum systems with which to probe, for example, superfluidity of mesoscopic ensembles[10]. In the context of ultracold atoms, the observation of an ensemble of stable droplets[11] in a dilute magnetic quantum gas opened up the possibility of a three-dimensional self-bound state[4,5]. A trapped quantum droplet of magnetic atoms has recently also been observed using erbium atoms[12]. Here we demonstrate the observation of dilute, self-bound liquid droplets in a sample of ultracold bosonic dysprosium atoms, which have a strong long-range magnetic dipolar interaction and a tunable repulsive short-range contact interaction. The interplay between these two interactions can be tuned such that the overall mean field is weakly attractive, but so that the interactions also create quantum depletion and a corresponding many-body repulsion. This repulsion exactly counteracts the attraction when the density of the droplet reaches the stabilization density. We use the word 'liquid' here to describe a state of matter that is defined by the presence of self-bound droplets and by the stabilization of the self-binding forces as a result of repulsion beyond the simple mean-field level, which manifests itself as a nontrivial correlation function. For dilute liquids, these correlations can be very weak (as in the present case), contrary to dense liquids for which correlations are strong. At small atom numbers (around 1,000 atoms), the finite size of the wavefunction of the quantum droplet leads to a quantum pressure for each individual atom that results in an evaporation out of the self-binding potential. Therefore, these droplets are bound only above a critical atom number, which we investigate systematically.

We use ^{164}Dy, which has one of the strongest magnetic dipole moments in the periodic table with $\mu = 9.93\mu_B$, where μ_B is the Bohr magneton. These atoms also offer control on the short-range interaction by a magnetic field using Feshbach resonances[13–15]. Here we use a specific resonance at a field of $B_0 = 7.117(3)$ G with a width of $\Delta B = 51(15)$ mG. (Here and elsewhere, the errors in parentheses indicate one standard deviation.) This resonance allows the scattering length a to be tuned from that of a dipole-dominated sample to a contact-dominated sample, without strong losses (Fig. 1b). To quantify the relative influence of the short-range and dipole–dipole interactions, we describe the interaction strengths using the relative dipolar strength $\epsilon_{dd} = a_{dd}/a$, where $a_{dd} = \mu_0\mu^2 m/(12\pi\hbar^2) \approx 131a_0$ is the dipolar length, a_0 is the Bohr radius, $\hbar$ is the reduced Planck constant, μ_0 is the vacuum permeability and m is the atomic mass. To observe the self-bound state, we prepare an initially oblate Bose–Einstein condensate (BEC)[16] of ^{164}Dy with an atom number of $N = 6{,}000(500)$ at a temperature of $T = 20$ nK at large scattering length ($B_{BEC} = 7.089(5)$ G), for which the interaction is contact-dominated, and shape it using an additional optical trap into a prolate shape along the magnetic field direction. This reshaping is done in two stages. First, we ramp up a focused beam (with a wavelength of 532 nm, aligned in the z direction) within 50 ms. With this attractive potential, the radial trap frequencies are increased to change the aspect ratio of the trap $\lambda = \omega_z/\omega_\rho$ from $\lambda = (80\,\text{Hz})/(20.5\,\text{Hz}) = 3.9$ down to $\lambda = (80\,\text{Hz})/(61\,\text{Hz}) = 1.3$; here, ω_z (ω_ρ) is the trapping frequency along (perpendicular to) the magnetic field direction. At this point, owing to magnetostriction[17], the BEC becomes prolate with a cloud aspect ratio $\kappa = \sigma_z/\sigma_\rho$ of approximately 1.5 (with σ_z (σ_ρ) the physical size (at $1/e^2$) of the cloud in (perpendicular to) the field direction) and has a typical atom number that is estimated to be $N = 3{,}000(300)$. Note that not all of these atoms are found to be in the self-bound state. Second, we apply a magnetic field gradient to the atomic cloud that exactly compensates the gravitational force and thus results in levitation. In this configuration, the cloud undergoes a continuous crossover from the BEC state directly to the single-droplet ground state as the scattering length is reduced, bypassing a bistable region[4,18]. Over the next 50 ms we lower the field to various values between $B = 6.831(5)$ G and $B = 6.469(5)$ G (indicated by the hatched area in Fig. 1b) to decrease the scattering length and create a single droplet. We hold the atoms in this configuration for 10 ms before ramping the optical trap powers within 20 ms to approximately 5% of their initial values, keeping a constant trap aspect ratio. At this point, we suddenly turn off the trap and image the cloud using far-detuned phase-contrast polarization imaging after various levitation times up to $t_{levitate} = 90$ ms. This sequence is shown schematically in Fig. 1a. Being sensitive only to high densities, we observe that a thermal fraction of the atomic cloud expands very quickly, whereas a very small and dense cloud remains for very long times. We interpret this observation

[1]5. Physikalisches Institut and Center for Integrated Quantum Science and Technology, Universität Stuttgart, Pfaffenwaldring 57, 70550 Stuttgart, Germany.

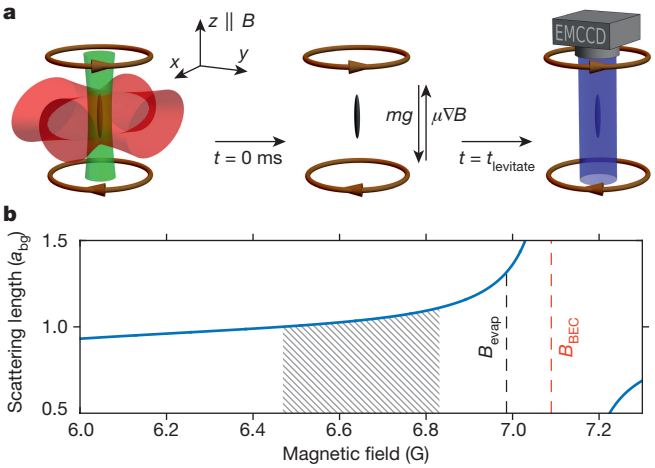

Figure 1 | Experimental sequence. a, A schematic of the experimental sequence. We start with an atomic ensemble in a crossed optical trap superimposed with a magnetic field gradient that is strong enough to compensate the gravitational force. We then turn off the trapping beams and levitate the droplet for various times $t_{levitate}$. Finally, we image the atoms using phase-contrast polarization imaging projected on an EMCCD (electron multiplying charge coupled device) camera. **b**, Scattering length as a function of magnetic field at the region of the Feshbach resonance in units of the positive background scattering length a_{bg}. The red dashed line indicates the field (B_{BEC}) at which we create a BEC. The hatched area describes the region in which the experiments were performed. The dashed black line shows the magnetic field (B_{evap}) used to intentionally evaporate the droplets to the gas phase.

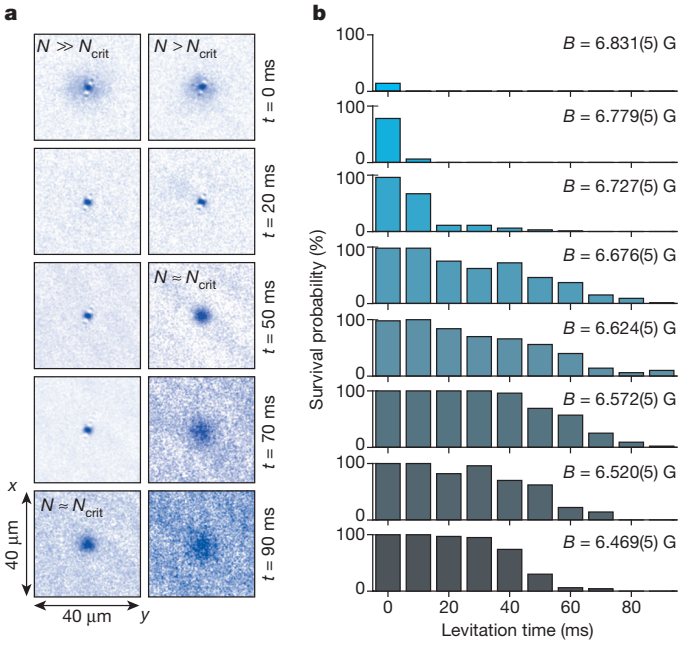

Figure 2 | Droplet survival probability. a, Image sequences of two droplets with different levitation times at the same magnetic field $B = 6.676(5)$ G. The images are not multiple images of the same droplet, but are selected from various images because the imaging process is destructive. All images are rescaled to the maximum optical density and have been re-centred. In the left-hand column, we start with an atom number that is much larger than the critical atom number for stable droplets and observe a single droplet up to $t_{levitate} = 70$ ms. Between $t = 70$ ms and $t = 90$ ms, the cloud reaches the critical atom number and evaporates back to a gas phase, observed as an expanding cloud. In the right-hand column, the droplet starts with an atom number that is much closer to the critical atom number, leading to an earlier evaporation, between 20 ms and 50 ms of levitation time. From this point, the cloud evaporates to the BEC phase and expands. **b**, Histogram of the survival probability of a single droplet as function of levitation time and magnetic field. At low scattering lengths ($B = 6.469(5)$ G), we always observe droplets for up to $t_{levitate} = 30$ ms, followed by a fast decay in survival probability that is explained by a fast decay in atom number as a result of three-body collisions. For increasing scattering length, we observe an increase in the lifetime of the droplets up to a magnetic field range of $B = 6.572(5)$–$6.676(5)$ G. At these conditions we observe a single droplet with a size below our resolution after a levitation time of $t_{levitate} = 90$ ms. Further increase of the scattering length leads to a fast decay of self-bound droplets even for short times ($t_{levitate} = 20$ ms), which we interpret as originating from an increase in the critical atom number to values close to our initial atom number. For the highest scattering length ($B = 6.831(5)$ G), we barely create droplets in the trap.

as a self-bound quantum droplet. We calculated the radial size of the quantum droplets to be approximately 300 nm, which is smaller than our imaging resolution of 1 μm such that we observe astigmatic diffraction (see Fig. 2a). At specific fields, we observe these droplets for times as long as $t_{levitate} = 90$ ms. At some time during the trap-free levitation, we observe that the droplets have expanded. We reason that this behaviour is due to the fact that droplets lose atoms as a result of three-body decay or residual excitations until they reach a critical atom number, below which they are no longer self-bound and evaporate back into a gas phase. In this context, the word 'evaporation' is used to denote the transition from a dilute self-bound liquid state to an expanding gas state. Given our shot-to-shot noise in the initial atom number, the critical atom number is reached at different times. This behaviour is represented in Fig. 2a.

As a first analysis, we count the images in which we observe a single droplet over 100 realizations and plot the survival probability for different magnetic fields (Fig. 2b). The levitation time is varied between $t_{levitate} = 0$ ms, which essentially represents a trapped cloud, and $t_{levitate} = 90$ ms. For low scattering length ($B = 6.469(5)$ G), we always create a single droplet, but its lifetime is short. As the scattering length increases, so does the lifetime. We find a maximal survival probability in the magnetic field range $B = 6.572(5)$–$6.676(5)$ G. For even higher scattering lengths, we find droplets only at 0 ms, and very few self-bound droplets. The calculated survival probabilities are in qualitative agreement with an increasing critical atom number and a decreasing rate of atom loss in the droplets with increasing scattering length. This behaviour has been observed[3] in a waveguide configuration and for a single trapped droplet[12], and is supported by calculations on a self-bound droplet[5,19]. However, the precise evolution depends on the spread in initial atom number and the fact that droplets evaporate at different atom numbers (see below).

To obtain a more quantitative analysis of the critical atom number of these droplets, we intentionally evaporate them after variable levitation times by increasing the magnetic field to $B_{evap} = 6.986(5)$ G (dashed black line in Fig. 1b). At this field, we observe that all droplets have been evaporated and interpret this to mean that the critical atom number at this field is higher than all relevant atom numbers observed here. After expansion, the atom number can be determined accurately without being limited by the finite resolution of the imaging optics. Here we observe that the number of atoms in the droplets decays to an essentially constant number—further indication of a critical atom number for self-bound droplets. This behaviour is demonstrated in Fig. 3a for a magnetic field of $B = 6.520(5)$ G, wherein each point is represented by a mean atom number that is calculated from 20 images, and the error denotes one standard deviation. A histogram of the atom number distribution for long levitation times ($t_{levitate} \geq 60$ ms) and for different magnetic fields is shown in Fig. 3b. We observe that the atom number distributions shift with scattering length, and conclude that the droplets lose atoms until they reach the critical atom number, at which point all of the atoms evaporate out of the droplets into the gas phase. We observe that at long times, when most droplets have evaporated, there is an asymmetric dispersion in atom number to higher values. We posit that this reflects the fact that not all droplets evaporate at exactly the

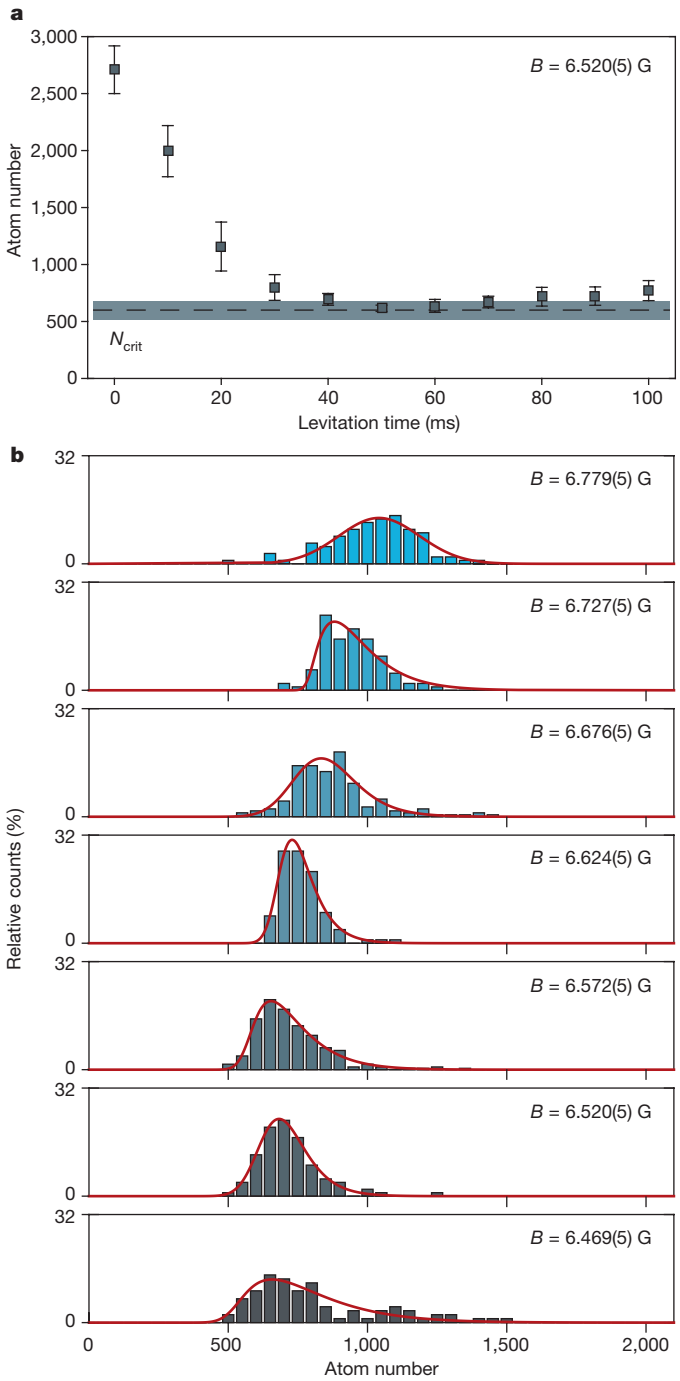

Figure 3 | Critical atom number. a, Decay in atom number as function of levitation time. Each point represents the mean atom number of 20 realizations; error bars denote the standard deviation. We observe a decay for short times to an essentially constant number for long times. The dashed line shows the critical atom number as determined by the best fit of our convoluted model (see text) to the data; the shaded area shows the error in this fit, represented by the quadratic mean of the widths of the convoluted distributions. For levitation times of less than 20 ms, the measured atom number overestimates the atom number in the self-bound droplet because it is hard to distinguish the droplet from the surrounding BEC in our experimental procedure. **b**, We analyse the atom number distribution for levitation times in the range $t_{\mathrm{levitate}} = 60$–$100$ ms because the atom number is mostly constant in this range. We bin the atom number to a window of 50 atoms and plot the relative counts as a function of atom number and magnetic field. The red curves represent fits of the convoluted functions to the observed histograms. The colours of the plotted histograms match those in Fig. 2b, and represent the magnetic field.

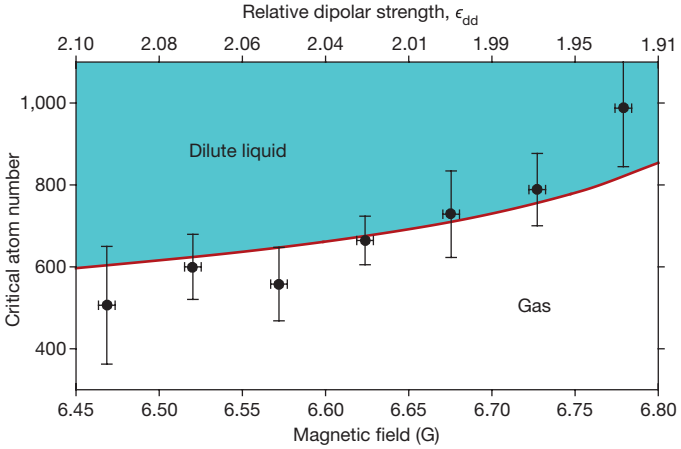

Figure 4 | Phase transition between dilute liquid and gas. The data points show the critical atom number as a function of the magnetic field, as determined from the fit values from Fig. 3b. The error in the atom number is given by the quadratic mean of the widths of the Gaussian and Maxwell–Boltzmann distributions; the error in magnetic field describes the resolution of our magnetic field coils. As the magnetic field decreases, so does the critical atom number N_{crit}. We identify the upper-left corner as the dilute liquid phase and the lower-right corner as the gas phase. The critical atom number describes the phase transition between dilute liquid and gas. The solid red line represents a full Gross–Pitaevskii simulation for different relative dipolar strengths ϵ_{dd}.

critical atom number, but that the evaporation for some droplets can occur with $N > N_{\mathrm{crit}}$, owing to the presence of residual (for example, thermal) excitations in the droplet. To extract a critical atom number we fit the histograms with a convolution of a Gaussian and a Maxwell–Boltzmann distribution (see Methods).

The best fits are shown in Fig. 3b as red curves. We plot our result of the critical atom number in Fig. 4 and compare it to full, extended Gross–Pitaevskii simulations (see Methods). The error is given by the quadratic mean of the widths of the Maxwell–Boltzmann and Gaussian distributions. This way of determining N_{crit} depends on the model used to determine the fit; other definitions could lead to slightly different values. Nevertheless, we see a clear change in the critical atom number with magnetic field, and with this we probe the phase transition line between the dilute liquid phase and the gas phase. To compare the results with the simulations, we calculate the relative dipolar strength for our magnetic field range. To do so, we include the Feshbach resonance at $B_{01} = 7.117(3)$ G with a width of $\Delta B_1 = 51(15)$ mG and a resonance at $B_{02} = 5.1(1)$ G with a width of $\Delta B_2 = 0.1(1)$ G. A best fit is obtained when we change the previously assumed local background scattering length[14] of $a_{\mathrm{bg}} = 92(8)a_0$ to $a_{\mathrm{bg}} = 62.5a_0$. This lower value seems, at first, to be incompatible with previous measurements at different fields[14]; however, the complexity of the scattering problem in dysprosium does not allow a theoretical prediction and the local a_{bg} might vary in other ranges of magnetic field. In addition, theoretical simulations of the Rosensweig instability[18,19] suggest that a background scattering length of less than $92a_0$ is necessary to agree with experimentally observed timescales[11]. In our measurements, the strong dependence of N_{crit} on scattering length provides a very high sensitivity. Changing the background scattering length from $92a_0$ to $62.5a_0$ reduces N_{crit} by almost a factor of ten. This method therefore enables a very precise measurement of the scattering length. However, at this level of precision, we must question the approximations made in our model, such as the first-order Born approximation for the dipolar scattering and the local density approximation. Consequently, the value of a_{bg} quoted here is model-dependent, and could be subject to future corrections. An independent measurement of a, via the methods of ref. 12 for instance, would make N_{crit} measurements a very sensitive benchmark for many-body theories.

By removing the need for any trapping potential, our observation of the self-bound regime offers access to truly isolated, dissipative quantum systems in which the effective cancellation of the mean field enables quantum correlations to be studied in detail. The gas-to-liquid transition and, in particular, the nucleation dynamics of the droplets will be sensitive probes of the interplay between interactions and quantum correlations.

Online Content Methods, along with any additional Extended Data display items and Source Data, are available in the online version of the paper; references unique to these sections appear only in the online paper.

Received 25 July; accepted 29 September 2016.

1. Petrov, D. S. Quantum mechanical stabilization of a collapsing Bose–Bose mixture. *Phys. Rev. Lett.* **115,** 155302 (2015).
2. Bulgac, A. Dilute quantum droplets. *Phys. Rev. Lett.* **89,** 050402 (2002).
3. Ferrier-Barbut, I., Kadau, H., Schmitt, M., Wenzel, M. & Pfau, T. Observation of quantum droplets in a strongly dipolar Bose gas. *Phys. Rev. Lett.* **116,** 215301 (2016).
4. Wächtler, F. & Santos, L. Ground-state properties and elementary excitations of quantum droplets in dipolar Bose–Einstein condensates. *Phys. Rev. A* **94,** 043618 (2016).
5. Baillie, D., Wilson, R. M., Bisset, R. N. & Blakie, P. B. Self-bound dipolar droplet: a localized matter wave in free space. *Phys. Rev. A* **94,** 021602(R) (2016).
6. Bender, M., Heenen, P.-H. & Reinhard, P.-G. Self-consistent mean-field models for nuclear structure. *Rev. Mod. Phys.* **75,** 121–180 (2003).
7. Dalfovo, F. & Stringari, S. Helium nanodroplets and trapped Bose–Einstein condensates as prototypes of finite quantum fluids. *J. Chem. Phys.* **115,** 10078–10089 (2001).
8. Volovik, G. *The Universe in a Helium Droplet* 27–31 (Oxford Univ. Press, 2009).
9. Toennies, J. P. & Vilesov, A. F. Superfluid helium droplets: a uniquely cold nanomatrix for molecules and molecular complexes. *Angew. Chem. Int. Ed.* **43,** 2622–2648 (2004).
10. Gomez, L. F. *et al.* Shapes and vorticities of superfluid helium nanodroplets. *Science* **345,** 906–909 (2014).
11. Kadau, H. *et al.* Observing the Rosensweig instability of a quantum ferrofluid. *Nature* **530,** 194–197 (2016).
12. Chomaz, L. *et al.* Quantum-fluctuation-driven crossover from a dilute Bose–Einstein condensate to a macro-droplet in a dipolar quantum fluid. Preprint at https://arxiv.org/abs/1607.06613 (2016).
13. Chin, C., Grimm, R., Julienne, P. & Tiesinga, E. Feshbach resonances in ultracold gases. *Rev. Mod. Phys.* **82,** 1225–1286 (2010).
14. Tang, Y., Sykes, A., Burdick, N. Q., Bohn, J. L. & Lev, B. L. *s*-wave scattering lengths of the strongly dipolar bosons ^{162}Dy and ^{164}Dy. *Phys. Rev. A* **92,** 022703 (2015).
15. Maier, T. *et al.* Emergence of chaotic scattering in ultracold Er and Dy. *Phys. Rev. X* **5,** 041029 (2015).
16. Lu, M., Burdick, N. Q., Youn, S. H. & Lev, B. L. Strongly dipolar Bose–Einstein condensate of dysprosium. *Phys. Rev. Lett.* **107,** 190401 (2011).
17. Lahaye, T., Menotti, C., Santos, L., Lewenstein, M. & Pfau, T. The physics of dipolar bosonic quantum gases. *Rep. Prog. Phys.* **72,** 126401 (2009).
18. Bisset, R. N., Wilson, R. M., Baillie, D. & Blakie, P. B. Ground-state phase diagram of a dipolar condensate with quantum fluctuations. *Phys. Rev. A* **94,** 033619 (2016).
19. Wächtler, F. & Santos, L. Quantum filaments in dipolar Bose–Einstein condensates. *Phys. Rev. A* **93,** 061603 (2016).

Acknowledgements We thank H. P. Büchler, L. Santos, F. Ferlaino, W. Ketterle, H. Sadeghpour, M. Zwierlein and V. Vuletić for discussions. This work is supported by the German Research Foundation (DFG) within SFB/TRR21 as well as FOR 2247. I.F.-B. acknowledges support from the EU within Horizon2020 Marie Skłodowska Curie IF (703419 DipInQuantum).

Author Contributions All authors discussed the results, made critical contributions to the work and contributed to the writing of the manuscript.

Author Information Reprints and permissions information is available at www.nature.com/reprints. The authors declare no competing financial interests. Readers are welcome to comment on the online version of the paper. Correspondence and requests for materials should be addressed to M.S. (m.schmitt@physik.uni-stuttgart.de) or T.P. (t.pfau@physik.uni-stuttgart.de).

Reviewer Information *Nature* thanks B. Blakie, R. Hulet and the other anonymous reviewer(s) for their contribution to the peer review of this work.

METHODS

Convolution model. To extract the critical atom number from the data in Fig. 3 we fit the histograms with a phenomenological model (represented as red lines). This model consists of the convolution of a Gaussian and a Maxwell–Boltzmann distribution. The symmetric Gaussian distribution represents broadening effects that result from statistical errors including detection noise. The asymmetric Maxwell–Boltzmann distribution is used to model the possibility of a droplet fully evaporating at atom numbers higher than the critical atom number, as a result of the presence of collective excitations in the droplets. From the fit we extract the critical atom number and two widths, one from each distribution in the convolution. We represent the quadratic mean of these widths as error bars in Fig. 4.

Extended Gross–Pitaevskii simulation. To compare our results to current theory[4,5], we perform simulations of the effective Gross–Pitaevskii equation

$$i\hbar\partial_t\psi = \Bigg[-\frac{\hbar^2\nabla^2}{2m} + V_{\mathrm{ext}} + g|\psi|^2 + \int V_{\mathrm{dd}}(\boldsymbol{r}-\boldsymbol{r}')|\psi(\boldsymbol{r}')|^2\,\mathrm{d}\boldsymbol{r}' + \frac{32g\sqrt{a^3}}{3\sqrt{\pi}}\left(1+\frac{3}{2}\epsilon_{\mathrm{dd}}^2\right)|\psi|^3 - i\frac{\hbar}{2}L_3|\psi|^4\Bigg]\psi(\boldsymbol{r}) \quad (1)$$

using a simple interaction potential, and taking into account quantum fluctuations within a local density approximation[20,21] and three-body losses. Here

$$V_{\mathrm{dd}}(\boldsymbol{r}) = \frac{\mu_0\mu^2}{4\pi}\frac{1-3\cos^2(\vartheta)}{|\boldsymbol{r}|^3}$$

describes the dipole–dipole interaction potential, with ϑ denoting the angle between the polarization direction of the dipoles and their relative orientation. The main assumptions of this model are therefore the validity of the local density approximation and of the interaction potential, which results from the first-order Born approximation. The magnetic moment and scattering length are $\mu = 9.93\mu_{\mathrm{B}}$ and $a = 60a_0$–$80a_0$, respectively. The latter defines $g = 4\pi a\hbar^2/m$ and is chosen such that we are in agreement with the critical atom numbers we observe in the experiment. The loss parameter $L_3 = 1.25\times10^{-41}\,\mathrm{m}^6\,\mathrm{s}^{-1}$ is estimated from measurements on a thermal cloud and is assumed to be constant over the small range of scattering lengths. The validity of the local density approximation is supported by quantum Monte Carlo simulations[22] and recent measurements with erbium atoms[12].

To obtain the data in Fig. 4, we choose $V_{\mathrm{ext}} = 0$ and initially prepare $N_0 > N_{\mathrm{crit}}$ atoms with a Gaussian density distribution ($\sigma_r = 250\,\mathrm{nm}$, $\sigma_z = 1{,}500\,\mathrm{nm}$). The ground state is reached by imaginary time evolution of equation (1) using a split-step Fourier method. Following this preparation of the self-bound droplet with N_0 atoms, we simulate the dynamics via real-time evolution. Because the atom number $N < N_0$ decays, owing to three-body losses, the density and the effective two-body attraction are also reduced. At $N = N_{\mathrm{crit}}$, the contributions by the effective two-body attraction and the quantum pressure are the same in magnitude, and the droplet evaporates quickly. This evaporation process manifests itself as a decrease in peak density of at least one order of magnitude. Three-body losses are highly suppressed then, such that the atom number stays almost constant for an evaporated droplet.

Data availability. The data that support the findings of this study are available from the corresponding author upon reasonable request.

20. Lima, A. R. P. & Pelster, A. Quantum fluctuations in dipolar Bose gases. *Phys. Rev. A* **84,** 041604 (2011).
21. Lima, A. R. P. & Pelster, A. Beyond mean-field low-lying excitations of dipolar Bose gases. *Phys. Rev. A* **86,** 063609 (2012).
22. Saito, H. Path-integral Monte Carlo study on a droplet of a dipolar Bose–Einstein condensate stabilized by quantum fluctuation. *J. Phys. Soc. Jpn* **85,** 053001 (2016).

Scissors Mode of Dipolar Quantum Droplets of Dysprosium Atoms

Igor Ferrier-Barbut,[1,*] Matthias Wenzel,[1] Fabian Böttcher,[1] Tim Langen,[1]
Mathieu Isoard,[2,†] Sandro Stringari,[2] and Tilman Pfau[1]
[1]5. Physikalisches Institut and Center for Integrated Quantum Science and Technology IQST, Universität Stuttgart, Pfaffenwaldring 57, 70550 Stuttgart, Germany
[2]INO-CNR BEC Center and Dipartimento di Fisica, Università di Trento, 38123 Povo, Italy

(Received 19 December 2017; published 18 April 2018)

We report on the observation of the scissors mode of a single dipolar quantum droplet. The existence of this mode is due to the breaking of the rotational symmetry by the dipole-dipole interaction, which is fixed along an external homogeneous magnetic field. By modulating the orientation of this magnetic field, we introduce a new spectroscopic technique for studying dipolar quantum droplets. This provides a precise probe for interactions in the system, allowing us to extract a background scattering length for ^{164}Dy of $69(4)a_0$. Our results establish an analogy between quantum droplets and atomic nuclei, where the existence of the scissors mode is also only due to internal interactions. They further open the possibility to explore physics beyond the available theoretical models for strongly dipolar quantum gases.

DOI: 10.1103/PhysRevLett.120.160402

The recent observation of quantum droplets in dipolar Bose-Einstein condensates (dBEC) [1–3] and in BEC mixtures [4–6] opens the opportunity to bridge the gap between dense quantum liquids, such as atomic nuclei and helium, and very dilute ultracold atomic samples. This link was reinforced by the observation of the self-bound character of quantum droplets [5–7]. Prior to this, several phenomena shared by dense quantum liquids and dilute superfluids were observed. In particular, the so-called scissors mode first observed in nuclei [8–10] was later predicted and observed in Bose-Einstein condensates in anisotropic external potentials [11,12]. In nuclei, this mode corresponds to the out-of-phase rotation of the neutrons and protons, and in BECs it is an angular oscillation around the anisotropy axis [13]. Its existence is a marker of the breaking of a rotational symmetry. A stark difference, however, between BECs and nuclei is that in the latter, the scissors mode arises only due to internal interactions. In contact-interacting BECs, this mode exists only in an anisotropic external potential; it vanishes in cylindrically symmetric traps.

Quantum droplets are liquidlike objects, bound by a mean-field attraction and stabilized by beyond mean-field effects [2,4]. Their collective modes are a revealing probe for their internal properties [3,14,15]. The scissors mode was theoretically explored in the context of dBEC in Ref. [16]. Here, we demonstrate that the anisotropy of the dipole-dipole interaction (DDI), set by the external homogeneous magnetic field, leads to a well-defined scissors mode in dipolar quantum droplets even in cylindrically symmetric trapping geometries. We parametrically excite this mode, and the high frequencies observed reveal the very strong intrinsic anisotropy of dipolar quantum droplets. In addition, it is known that this mode is well defined only for low excitation amplitude, while it is nonlinearly coupled to other low-frequency modes for large excitation angles [13]. We observe clear signatures of this nonlinear mode coupling and use such coupling to excite a low-frequency mode. Altogether, these measurements represent a strong test of internal interactions in the droplets; we thus extract the value of the s-wave background scattering length of ^{164}Dy with good precision. We put this in perspective with previous measurements, highlighting the two- and many-body physics at play in dipolar quantum droplets of dysprosium.

Theory.—The scissors mode, corresponding to an angular oscillation, is naturally excited by the z component of the angular momentum operator $\hat{L}_z = \sum_{k=1}^{N}(x_k p_k^y - y_k p_k^x)$. In the experiment, this corresponds to a rotation of the external magnetic field axis around $\hat{z}$. We consider here dipoles oriented along the y direction [see Fig. 1(a)], thereby breaking rotational invariance in the xy plane, even in the presence of a cylindrically symmetric trap. Employing linear response theory, one can derive a rigorous upper bound to the frequency of the scissors mode in the form [13]

$$\hbar\omega_{\mathrm{sc}} = \sqrt{\frac{m_1}{m_{-1}}}, \tag{1}$$

where $m_1 = \hbar^2 \int d\omega \omega S_{L_z}(\omega)$ is the energy-weighted moment of the dynamical structure factor $S_{L_z}(\omega)$, relative to the angular momentum operator, while $m_{-1} = \int d\omega/\omega S_{L_z}(\omega)$ is the inverse energy-weighted moment. Both moments m_1 and m_{-1} encapsulate important physical information on the scissors mode. The m_1 moment can, in

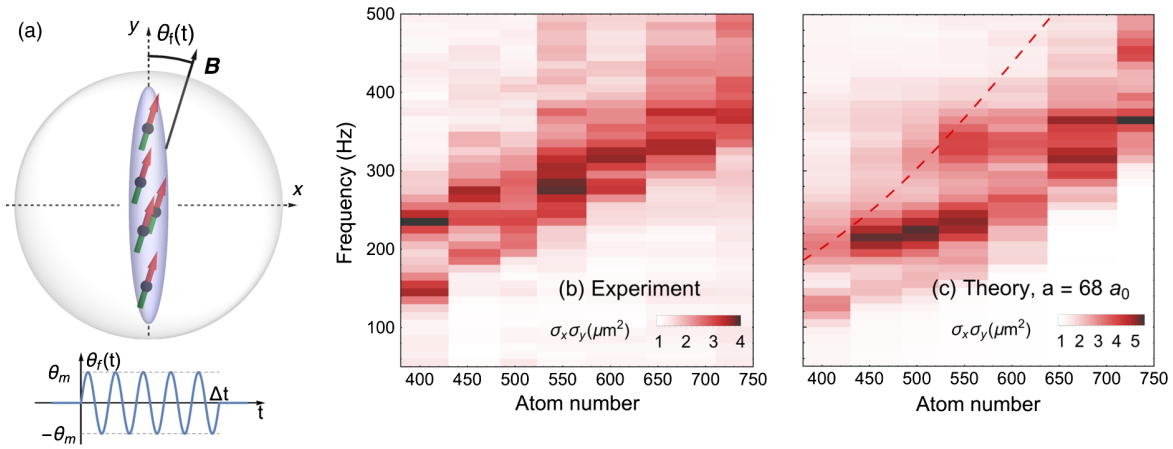

FIG. 1. (a) Experimental method: The quantum droplet is held in a cylindrically symmetric trap (around z); the orientation of the field is modulated around its mean value along y for $\Delta t = 20$ ms at variable frequency. The amplitude θ_m follows $\theta_m(f) = 12°/\sqrt{f/100\ \mathrm{Hz}}$. (b) Experimental response measured as a growth in the visible size of the droplet $\sigma_x \times \sigma_y$ as a function of atom number and modulation frequency. (c) The theory shows the same value extracted from solutions of the equations of motion within the Gaussian ansatz using the best-fit value of $a = 68a_0$. It takes into account the finite excitation time as well as departure from the linear response regime. The shot-to-shot fluctuations in atom number are simulated, and finite resolution is also implemented in the theory calculation of $\sigma_x \times \sigma_y$. Note the different scales for theory and experiments; the ~20% difference in droplet size could be due to imaging miscalibration. The dashed line shows the theoretical scissors mode frequency in linear response theory; see Ref. [17].

fact, be expressed in terms of a double commutator involving the Hamiltonian of the system as

$$m_1(\hat{L}_z) = \frac{1}{2}\langle[\hat{L}_z,[\hat{H},\hat{L}_z]]\rangle \tag{2}$$

and can be regarded as an effective restoring force parameter for the scissors oscillation. Here $\langle . \rangle$ is the average taken on the equilibrium configuration of the system. The nonvanishing of the commutator $[\hat{H},\hat{L}_z]$ is the consequence of the breaking of rotational invariance. This can be due to the presence of an anisotropic trapping potential, and/or to the presence of the dipolar interaction. In the case we are interested in, of isotropic harmonic trapping ($\omega_x = \omega_y \equiv \omega_\perp$) (or in the absence of trapping), only the dipolar interaction contributes to the commutator, and the m_1 sum rule takes the useful form (see Supplemental Material [17])

$$m_1 = \frac{\hbar^2}{2}(\langle V^x_{\mathrm{dd}}\rangle - \langle V^y_{\mathrm{dd}}\rangle), \tag{3}$$

where $\langle V^\alpha_{\mathrm{dd}}\rangle = \int d\boldsymbol{r}d\boldsymbol{r}' n(\boldsymbol{r}) V^\alpha_{\mathrm{dd}}(\boldsymbol{r}-\boldsymbol{r}') n(\boldsymbol{r}')$, and $V^\alpha_{\mathrm{dd}}(\boldsymbol{r}) = (\mu_0\mu^2/4\pi r^3)[1-3(\alpha^2/r^2)]$, $\alpha = x,\ y,\ z$. Equation (3) emphasizes the crucial role played by the dipolar interaction, which causes an asymmetry between the ground-state expectation values $\langle V^x_{\mathrm{dd}}\rangle$ and $\langle V^y_{\mathrm{dd}}\rangle$. For ^{164}Dy $\mu \approx 10\mu_B$, with μ_B the Bohr magneton, this defines the dipolar length $a_{\mathrm{dd}} = (\mu_0\mu^2 m/12\pi\hbar^2)$, compared to the s-wave scattering length a via $\varepsilon_{\mathrm{dd}} = a_{\mathrm{dd}}/a$.

Differently from m_1, the inverse energy-weighted moment m_{-1} cannot be written in terms of commutators, but it can be usefully identified in terms of the moment of inertia Θ of the system. Actually, the moment m_{-1} corresponds, apart from a factor $1/2$, to the static response of the system to an angular momentum perturbation of the form $-\omega\hat{L}_z$. The moment of inertia, which provides the mass parameter of the scissors oscillation, is very sensitive to superfluidity, and for a Bose-Einstein condensate at zero temperature, is given by the expression [13]

$$\Theta = 2m_{-1} = m\frac{(\langle y^2\rangle - \langle x^2\rangle)^2}{\langle y^2\rangle + \langle x^2\rangle}, \tag{4}$$

which follows from the irrotationality constraint characterizing the superfluid velocity. For an axisymmetric configuration, the moment of inertia of a superfluid then identically vanishes.

All the average quantities characterizing the moments m_1 and m_{-1} can be evaluated using the Gaussian ansatz $\psi(\boldsymbol{r}) = (\sqrt{N}/\pi^{3/4}\bar{\sigma}^{3/2})e^{\sum_\alpha -(\alpha^2/2\sigma_\alpha^2)}$ for the order parameter relative to the ground state, with $\alpha \in \{x,y,z\}$ and $\bar{\sigma}^3 = \sigma_x\sigma_y\sigma_z$. The square radii, entering the expression for the moment of inertia, are given by $\langle r_i^2\rangle = \sigma_i^2/2$. The values $\langle V^x_{\mathrm{dd}}\rangle$ and $\langle V^y_{\mathrm{dd}}\rangle$, entering the m_1 sum rule, can also be calculated using the Gaussian ansatz, and in the general case of anisotropic trapping we recover the results for dipolar BECs obtained in Ref. [16]. The expression for the resulting scissors mode frequency $\hbar\omega_{\mathrm{sc}} = \sqrt{m_1/m_{-1}}$ is reported as Eq. (S13) in Ref. [17]. It is worth noticing that the calculated equilibrium sizes σ_i, obtained through a variational procedure applied to the energy of the system, strongly depend on the scattering length a [14,20], which

gives an implicit dependence of the scissors frequency on a. We have checked that a time-dependent simulation, based on extended Gross-Pitaevskii (eGPE) theory, agrees in the linear limit with the sum rule value for the scissors frequency calculated using the Gaussian ansatz. The basic ingredients underlying the dynamics of the scissors mode are indeed well captured by the sum rule approach. Actually, our result takes into account both the breaking of rotational symmetry caused by the dipolar interaction [see Eq. (3)] and the superfluid expression (4) for the moment of inertia, which, however, does not differ significantly from the classical rigid value $m(\langle x^2\rangle + \langle y^2\rangle)$ due to the large anisotropy of the dipolar droplet characterizing the present experimental conditions. The sum rule approach provides a reliable estimate of the scissors frequency in the linear regime. Experiments, however, involve relatively large amplitudes of the oscillation, and for a systematic quantitative comparison it is useful to develop a time-dependent extension of the variational approach. It is based on the Lagrangian formalism, where the Gaussian ansatz is generalized to include a phase playing the role of a velocity potential, as already employed for dipolar BECs in Ref. [21] and in Ref. [14] for quantum droplets, now with an additional parameter accounting for the orientation θ of the droplet in the xy plane. The new calculation, which corresponds to solving the equations of motion for the four degrees of freedom $\sigma_{x,y,z}$ and θ, accounts for the excitation of the scissors mode as well as that of additional low-frequency modes of quadrupole and compression nature, which play an important role in the nonlinear limit, as we will discuss below.

Experiments.—We perform experiments on dipolar quantum droplets in an optical dipole trap, in which we obtain lifetimes of several hundreds of milliseconds. The trapping configuration was presented in Ref. [22]. Here the trap has fixed frequencies of $f_x = f_y = 40(1)$ Hz, $f_z = 950$ Hz ($\hat{z}$ being along gravity), and is thus isotropic in the xy plane, as assumed by the theory presented above. The magnetic field is always oriented in this plane, initially along $\hat{y}$. In such geometry, quantum droplets can exist for smaller atom numbers than in free space and for very small atom numbers outside the range of our experiments; similarly to Ref. [23], they transform into solitons [24,25], which differ from quantum droplets by being stable even without beyond-mean-field corrections; see Ref. [17]. To extract their properties, we fit column-integrated images with a Gaussian distribution $\bar{n} = (N/\pi\sigma_x\sigma_y)\exp[-(x^2/\sigma_x^2) - (y^2/\sigma_y^2)]$. We obtain a typical size along $\hat{y}$ of $\sigma_y \sim 1.5$ μm, while the extent along $\hat{x}$ is smaller than our resolution [17]. We create single droplets containing a few hundred atoms. Their density being initially high, the atom number decays fast from $N \approx 750$ down to $N \approx 400$ via three-body losses. The systematic uncertainty on the number of condensed atoms within the droplet is $\delta N/N = 0.25$ [17]. The absolute value of the magnetic field is fixed to be $B_0 = 800$ mG, far from any Feshbach resonance [26], so that the scattering length takes the low-field background value a_{bg}.

In the first set of experiments, we parametrically excite the scissors mode by adding an oscillating magnetic field along $\hat{x}$, exemplified in Fig. 1(a). The x field follows $B_x(t) = B_{x0}\sin(2\pi f t)$, with a variable frequency f and a maximum amplitude of $B_{x0} \leq 200$ mG. The angle of the field with respect to the y axis θ_f is then $\theta_f(t) \simeq B_x(t)/B_0 = \theta_m \sin(2\pi f t)$. The modulation time is $\Delta t = 20$ ms, chosen so that atom numbers variations are small, $\Delta N/N \leq 10\%$, during this time. Since Δt is kept fixed, to keep a constant pulse "energy" we decrease the modulation amplitude with a $1/\sqrt{f}$ scaling: $\theta_m(f) = \theta_0/\sqrt{f/100\ \mathrm{Hz}}$. We first perform our experiments with $\theta_0 = 12°$.

When the field direction is modulated, we observe a clear excitation of the scissors mode. We show in Ref. [17] that this is not due to the very small modulation of the absolute field ($[(\delta|B|)/B_0] \leq 4 \times 10^{-2}$). The excitation is seen as an increase in the observed size of the droplet: $\sigma_x \times \sigma_y$. Since the atom number varies with time, we can investigate the variation of the response with atom number. We observe a clear dependence, shown in Fig. 1(b). The maximum response frequency clearly increases with atom number. We note that several features are also visible in Fig. 1(b). In particular, a splitting into two lines is observable at low atom numbers. These characteristics signal that the observed response contains more than a simple parametric excitation of the scissors mode in the linear response regime. The rather large anisotropy of dipolar quantum droplets even in symmetric traps leads to a well-defined scissors mode. However, as we impose values of the excitation angle close to the deformation $(\sigma_y^2 - \sigma_x^2)/(\sigma_x^2 + \sigma_y^2)$ of the atomic cloud, we expect to approach the regime where the scissors mode is not well defined as it couples to other low-lying modes [11].

To confirm that the line splitting for the lowest atom numbers is due to hybridization of the scissors mode, we perform experiments at a fixed atom number $N = 390(100)$, but for varying amplitude. This is represented in Fig. 2(b)—for low amplitude we obtain a much lower response, requiring much more data averaging to reach a sufficient signal-to-noise ratio. But we do observe that only one peak appears at lower amplitude, confirming that departure from the linear regime occurs for the amplitudes used in Fig. 1(b). In order to capture these effects, which come from a coupling between the different lowest-lying modes of the system, we compare the experimental results with the predictions of the variational time-dependent model introduced in the *Theory* section of this Letter and discussed in details in Ref. [17]. With this theoretical approach, we can implement the exact experimental field modulation and reproduce very well the line splitting as seen in Fig. 2(a). In addition, we can also obtain a good agreement between theory and experiments for the

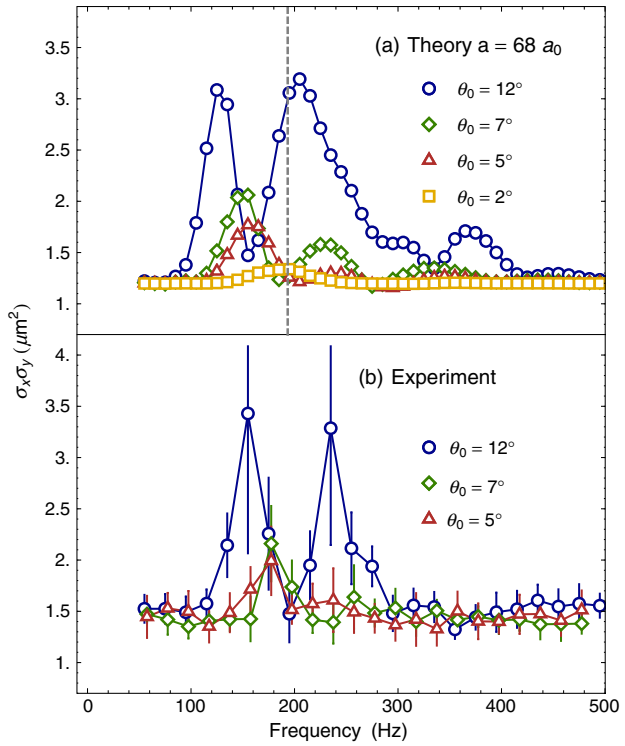

FIG. 2. Variation of the response with the angle modulation amplitude. Data and theory in Fig. 1 correspond to $\theta_0 = 12°$. (a) Theory: We take $a = 68a_0$, as it gives the best fit over the whole range of atom numbers in Fig. 1; this explains the slight horizontal disagreement with experiment. For increasing excitation amplitude, the response increases, and a line splitting is observed due to departure from the linear response regime. The dashed line shows the linear repsonse prediction. (b) Experiment, with atom number 390(100): The same increase in response and line splitting is observed. We surmise that the small peaks at high frequency absent in the experiment are due to the simplifying assumptions of our model.

range of atom numbers probed in Fig 1(b), with the scattering length as a single adjustable parameter. The result is shown in Fig. 1(c). In this plot, the scissors mode frequency is shown as a dashed line, showing that the departure from linear response causes a significant shift of the signal. Finally, this allows us to conclude on the scattering length for which our observations at different atom numbers and $\theta_0 = 12°$ are best reproduced: $a = 68(5)a_0$, where the main contribution to the error is coming from the systematic uncertainty in the atom number [17]. When on the other hand we use only the low-amplitude data $\theta_0 = 5°$ at $N = 390$ shown in Fig. 2, we obtain $a = 67(6)a_0$, in agreement.

The nonlinear coupling between the scissors and other low-lying modes provides us with a new tool to excite the latter. In the last part of this Letter, we use this to study the properties of the lowest mode. The mode coupling arises at large angles between the field and the droplet. To probe this regime, we perform a 90° rotation of the field at constant $B_0 = 800$ mG in a time $t \simeq 3$ ms. Systematic imaging errors prevent the direct observation of angle oscillations. Nevertheless, we observe that the droplet quickly rotates by 90°. Via this field orientation quench, we obtain clear evidence for the excitation of a collective mode, seen as a time oscillation of the droplet length. These oscillations are strongly damped, and we are able to observe them up to times of about 20 ms [17]. We infer that these oscillations correspond to an excitation of the lowest-frequency collective mode of the system, observed in Ref. [3]. It consists essentially of a compression of the long axis of the droplet. Performing simulations of the equations of motion, we find that nonlinearities must be taken into account. We therefore compare our experiments to numerical solutions of the equations of motion as above, applying our exact experimental field sequence.

We vary the z trapping frequency f_z and record the variation in the observed frequency of oscillation over the first 10 to 20 ms. The experimental data are shown in Fig. 3, where we observe very little shift. We compare our measurements to theory and obtain relatively good agreement, though the increase in frequency predicted by theory is not clear in the experimental data. The best agreement is obtained for $a = 70.5(6.0)a_0$. This value is compatible with the scattering length extracted from the scissors mode parametric excitation.

The scattering length values extracted here allow us to conclude on the interactions present in Dy ultracold samples at $B = 800$ mG so that $a = a_{\mathrm{bg}}$. The error-weighted mean experimental value from the two measurements is $a_{\mathrm{bg}} = 69(4)a_0$. Values obtained in noncondensed samples [27–29] are consistently higher than that reported in quantum droplets [7], though with large error bars. This

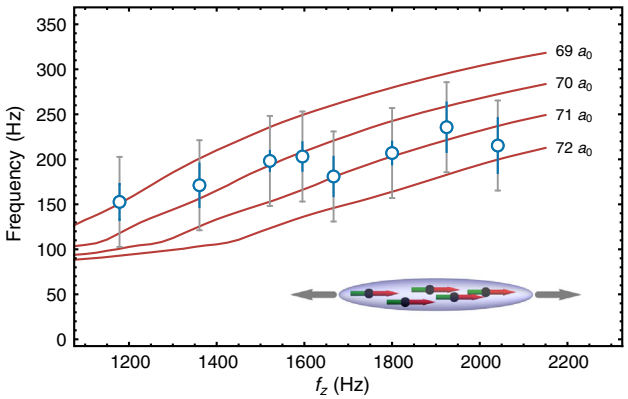

FIG. 3. Long axis oscillation frequency following a 90° field angle quench. Experiments are performed with an atom number of 690 (150). The error bar in blue shows the result of a squared sum of the fit standard error and the fitted decay time. The grey error bars show a 100 Hz interval corresponding to the short observation time. The red lines are theory calculations using the equations of motion for different scattering lengths (indicated on the figure).

might stem from the effect theoretically predicted in Ref. [30] of an effective dipole-dipole interaction dependent on collisional energy. Systematic measurements, for instance using the lattice method of Ref. [3], could shed further light into the two-body interactions, which can no longer be described by a simple addition of the DDI potential and the effective contact interaction potential [31,32]. An interesting direction to further explore is to try to compare precise measurements of collective mode frequencies on one side and critical atom number in self-bound droplets on the other side. Indeed, these precise spectroscopic probes should hold a signature of departure from the eGPE description of the system, a breakdown of the local density approximation should be expected, and the critical atom number might depend on details of the potential beyond the s-wave scattering length, as was shown for Bose mixtures in Ref. [33]. Quantum Monte Carlo works like Refs. [34–36] will need to include two-body interaction potentials faithful to the real Dy-Dy potential.

In conclusion, our work sheds new light on dipolar quantum droplets, demonstrating a macroscopic collective mode shared with atomic nuclei. In both systems, this mode is due to internal interactions, though for the present case of dipolar quantum droplets, the rotational symmetry is broken by the external homogeneous magnetic field, while it is spontaneously broken in nuclei. We showed that the method developed here is a powerful probe for interactions in dipolar quantum droplets, and its systematic application should lead to the observation of physics beyond the current theoretical level.

The Stuttgart group would like to acknowledge discussions with John Bohn. S. S. thanks Russell Bisset for useful comments and acknowledges funding from the Provincia Autonoma di Trento and the QUIC grant of the European Horizon2020 FET program. This work is supported by the German Research Foundation (DFG) within FOR2247. I. F. B. and T. L. acknowledge support from the EU within Horizon2020 Marie Skłodowska Curie IF (Grants No. 703419 DipInQuantum and No. 746525 coolDips, respectively). T. L. acknowledges support from the Alexander von Humboldt Foundation through a Feodor Lynen Fellowship.

*i.ferrier-barbut@physik.uni-stuttgart.de
†Present address: LPTMS, CNRS, Univ. Paris-Sud, Université Paris-Saclay, 91405 Orsay, France.

[1] H. Kadau, M. Schmitt, M. Wenzel, C. Wink, T. Maier, I. Ferrier-Barbut, and T. Pfau, Observing the Rosensweig instability of a quantum ferrofluid, Nature (London) **530**, 194 (2016).
[2] I. Ferrier-Barbut, H. Kadau, M. Schmitt, M. Wenzel, and T. Pfau, Observation of Quantum Droplets in a Strongly Dipolar Bose Gas, Phys. Rev. Lett. **116**, 215301 (2016).
[3] L. Chomaz, S. Baier, D. Petter, M. J. Mark, F. Wächtler, L. Santos, and F. Ferlaino, Quantum-Fluctuation-Driven Crossover from a Dilute Bose-Einstein Condensate to a Macrodroplet in a Dipolar Quantum Fluid, Phys. Rev. X **6**, 041039 (2016).
[4] D. S. Petrov, Quantum Mechanical Stabilization of a Collapsing Bose-Bose Mixture, Phys. Rev. Lett. **115**, 155302 (2015).
[5] C. R. Cabrera, L. Tanzi, J. Sanz, B. Naylor, P. Thomas, P. Cheiney, and L. Tarruell, Quantum liquid droplets in a mixture of Bose-Einstein condensates, Science **359**, 301 (2018).
[6] G. Semeghini, G. Ferioli, L. Masi, C. Mazzinghi, L. Wolswijk, F. Minardi, M. Modugno, G. Modugno, M. Inguscio, and M. Fattori, Self-bound quantum droplets in atomic mixtures, arXiv:1710.10890.
[7] M. Schmitt, M. Wenzel, F. Böttcher, I. Ferrier-Barbut, and T. Pfau, Self-bound droplets of a dilute magnetic quantum liquid, Nature (London) **539**, 259 (2016).
[8] N. Lo Iudice and F. Palumbo, New Isovector Collective Modes in Deformed Nuclei, Phys. Rev. Lett. **41**, 1532 (1978).
[9] E. Lipparini and S. Stringari, Isovector M1 rotational states in deformed nuclei, Phys. Lett. **130B**, 139 (1983).
[10] J. Enders, H. Kaiser, P. von Neumann-Cosel, C. Rangacharyulu, and A. Richter, Comprehensive analysis of the scissors mode in heavy even-even nuclei, Phys. Rev. C **59**, R1851 (1999).
[11] D. Guéry-Odelin and S. Stringari, Scissors Mode and Superfluidity of a Trapped Bose-Einstein Condensed Gas, Phys. Rev. Lett. **83**, 4452 (1999).
[12] O. M. Maragò, S. A. Hopkins, J. Arlt, E. Hodby, G. Hechenblaikner, and C. J. Foot, Observation of the Scissors Mode and Evidence for Superfluidity of a Trapped Bose-Einstein Condensed Gas, Phys. Rev. Lett. **84**, 2056 (2000).
[13] L. Pitaevskii and S. Stringari, *Bose-Einstein Condensation and Superfluidity*, Vol. 164 (Oxford University Press, New York, 2016).
[14] F. Wächtler and L. Santos, Ground-state properties and elementary excitations of quantum droplets in dipolar Bose-Einstein condensates, Phys. Rev. A **94**, 043618 (2016).
[15] D. Baillie, R. M. Wilson, and P. B. Blakie, Collective Excitations of Self-Bound Droplets of a Dipolar Quantum Fluid, Phys. Rev. Lett. **119**, 255302 (2017).
[16] R. M. W. van Bijnen, N. G. Parker, S. J. J. M. F. Kokkelmans, A. M. Martin, and D. H. J. O'Dell, Collective excitation frequencies and stationary states of trapped dipolar Bose-Einstein condensates in the Thomas-Fermi regime, Phys. Rev. A **82**, 033612 (2010).
[17] See Supplemental Material at http://link.aps.org/supplemental/10.1103/PhysRevLett.120.160402 for the theoretical derivation of the scissors mode frequency as well as details of the experimental procedure and data analysis, which includes Refs. [18,19].
[18] K. Glaum and A. Pelster, Bose-Einstein condensation temperature of dipolar gas in anisotropic harmonic trap, Phys. Rev. A **76**, 023604 (2007).
[19] S. Giovanazzi, P. Pedri, L. Santos, A. Griesmaier, M. Fattori, T. Koch, J. Stuhler, and T. Pfau, Expansion dynamics of a dipolar Bose-Einstein condensate, Phys. Rev. A **74**, 013621 (2006).
[20] R. N. Bisset, R. M. Wilson, D. Baillie, and P. B. Blakie, Ground-state phase diagram of a dipolar condensate with quantum fluctuations, Phys. Rev. A **94**, 033619 (2016).

[21] S. Yi and L. You, Trapped condensates of atoms with dipole interactions, Phys. Rev. A **63**, 053607 (2001).
[22] M. Wenzel, F. Böttcher, T. Langen, I. Ferrier-Barbut, and T. Pfau, Striped states in a many-body system of tilted dipoles, Phys. Rev. A **96**, 053630 (2017).
[23] P. Cheiney, C. R. Cabrera, J. Sanz, B. Naylor, L. Tanzi, and L. Tarruell, Bright Soliton to Quantum Droplet Transition in a Mixture of Bose-Einstein Condensates, Phys. Rev. Lett. **120**, 135301 (2018).
[24] I. Tikhonenkov, B. A. Malomed, and A. Vardi, Anisotropic Solitons in Dipolar Bose-Einstein Condensates, Phys. Rev. Lett. **100**, 090406 (2008).
[25] P. Köberle, D. Zajec, G. Wunner, and B. A. Malomed, Creating two-dimensional bright solitons in dipolar Bose-Einstein condensates, Phys. Rev. A **85**, 023630 (2012).
[26] K. Baumann, N. Q. Burdick, M. Lu, and B. L. Lev, Observation of low-field Fano-Feshbach resonances in ultracold gases of dysprosium, Phys. Rev. A **89**, 020701 (2014).
[27] Y. Tang, A. Sykes, N. Q. Burdick, J. L. Bohn, and B. L. Lev, *s*-wave scattering lengths of the strongly dipolar bosons ^{162}Dy and ^{164}Dy, Phys. Rev. A **92**, 022703 (2015).
[28] T. Maier, I. Ferrier-Barbut, H. Kadau, M. Schmitt, M. Wenzel, C. Wink, T. Pfau, K. Jachymski, and P. S. Julienne, Broad universal Feshbach resonances in the chaotic spectrum of dysprosium atoms, Phys. Rev. A **92**, 060702 (2015).
[29] Y. Tang, A. G. Sykes, N. Q. Burdick, J. M. DiSciacca, D. S. Petrov, and B. L. Lev, Anisotropic Expansion of a Thermal Dipolar Bose Gas, Phys. Rev. Lett. **117**, 155301 (2016).
[30] R. Ołdziejewski and K. Jachymski, Properties of strongly dipolar Bose gases beyond the Born approximation Phys. Rev. A **94**, 063638 (2016); Erratum, **95**, 049901 (2017).
[31] D. C. E. Bortolotti, S. Ronen, J. L. Bohn, and D. Blume, Scattering Length Instability in Dipolar Bose-Einstein Condensates, Phys. Rev. Lett. **97**, 160402 (2006).
[32] R. Ołdziejewski and K. Jachymski, Properties of strongly dipolar Bose gases beyond the Born approximation, Phys. Rev. A **94**, 063638 (2016).
[33] V. Cikojević, K. Dželalija, P. Stipanović, L. Vranješ Markić, and J. Boronat, Ultradilute quantum liquid drops, Phys. Rev. B **97**, 140502(R) (2018).
[34] H. Saito, Path-integral Monte Carlo study on a droplet of a dipolar Bose-Einstein condensate stabilized by quantum fluctuation, J. Phys. Soc. Jpn. **85**, 053001 (2016).
[35] A. Macia, J. Sánchez-Baena, J. Boronat, and F. Mazzanti, Droplets of Trapped Quantum Dipolar Bosons, Phys. Rev. Lett. **117**, 205301 (2016).
[36] F. Cinti, A. Cappellaro, L. Salasnich, and T. Macrì, Superfluid Filaments of Dipolar Bosons in Free Space, Phys. Rev. Lett. **119**, 215302 (2017).

Igor Ferrier-Barbut is a researcher at the Institut d'Optique and CNRS in Palaiseau, France.

Ultradilute Quantum Droplets

A new class of quantum mechanical liquids is stabilized by an elegant mechanism that allows them to exist despite being orders of magnitude thinner than air.

Igor Ferrier-Barbut

In his PhD thesis from 1873, Johannes van der Waals devised a theoretical framework to describe the gas and liquid phases of a molecular ensemble and the phase transition from one to the other. That work resulted in the celebrated equation of state bearing his name. To this day, the van der Waals theory is still the prevailing picture in most physicists' minds to explain the emergence of the liquid state. It asserts that the liquid state arises at high densities from an equilibrium between attractive interatomic forces and short-range repulsion. Now, a new type of liquid has emerged in ultracold, extremely dilute atomic systems for which the van der Waals model does not predict a liquid phase.

Using the tools of laser cooling and trapping, experimenters can reach the ultracold regime to create atomic quantum gases.[1] Quantum interference effects between atoms are an important part of the statistical descriptions of those systems. However, if a monatomic ensemble is simply cooled, any chemical species will form a liquid instead of a gas due to van der Waals forces and the system will never reach the quantum regime. So to see quantum effects, the classical liquid state must be avoided. That requires extremely low densities that keep the distances between atoms much larger than the range of attractive forces that would bind the liquid. But keeping the atoms far apart traps them in a dilute, metastable state. A whole new mechanism is needed for atoms in such dilute conditions to form a liquid phase.

Mean-field quantum gases

Atoms in the quantum regime must be described as waves rather than classical point-like objects. They come in two flavors, bosons and fermions. That characterization dictates particles' collective behavior: Bosons interfere constructively, whereas fermions do so destructively. In the materials used to make ultradilute liquids, constructive bosonic interference leads to the accumulation at very low temperature of all the atoms into the same quantum state with zero momentum. That collective

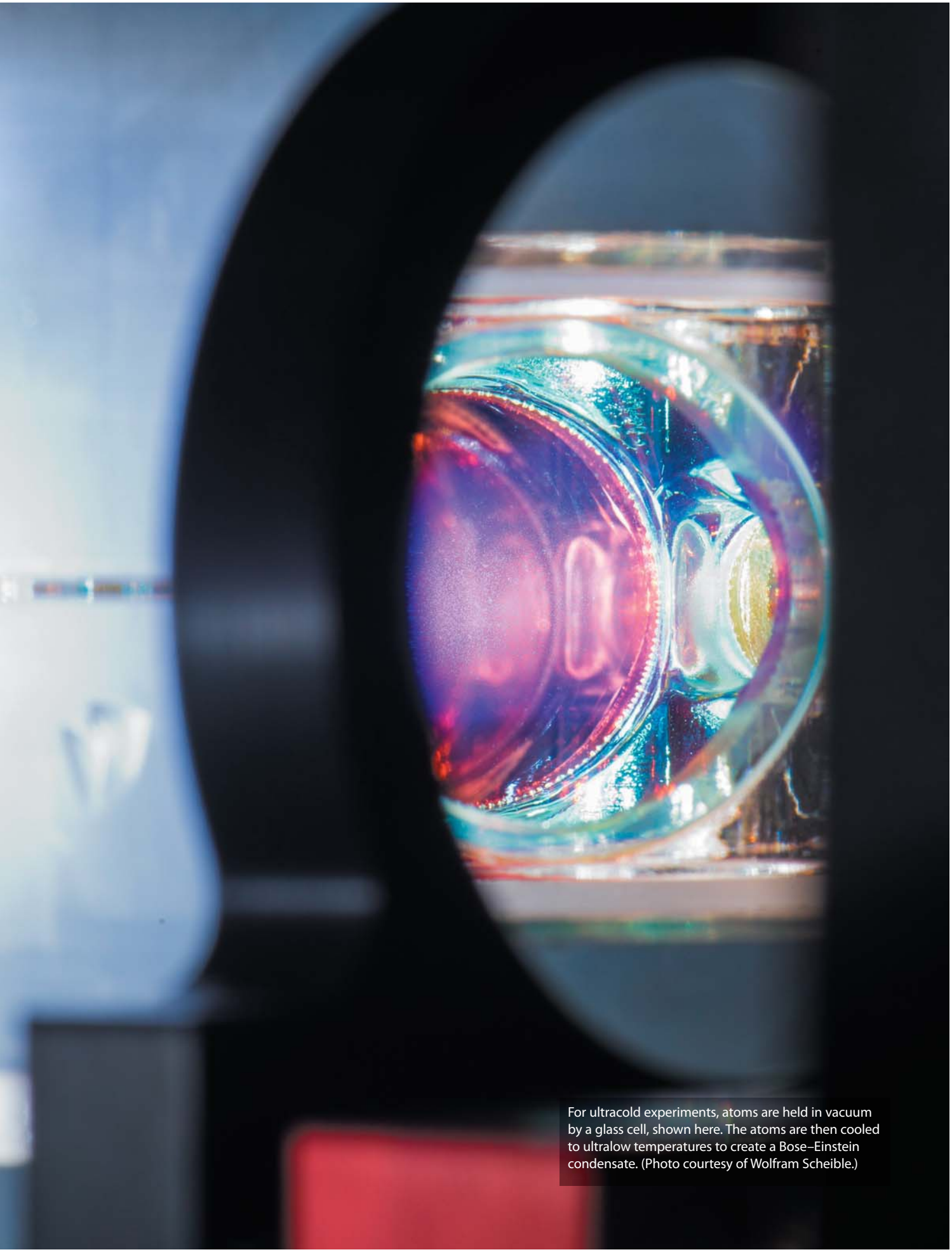

For ultracold experiments, atoms are held in vacuum by a glass cell, shown here. The atoms are then cooled to ultralow temperatures to create a Bose–Einstein condensate. (Photo courtesy of Wolfram Scheible.)

state is known as a Bose–Einstein condensate (BEC) and is now routinely produced experimentally (see, for example, the article by Keith Burnett, Mark Edwards, and Charles Clark, PHYSICS TODAY, December 1999, page 37).

Bose–Einstein condensation is a pure quantum interference effect that requires no interaction between atoms. Interatomic forces do still affect that state, but rather than the familiar attractive potential with repulsive core, interactions take a much simpler form in ultracold and ultradilute conditions. Forming a BEC requires the interparticle distance l to be much larger than the typical interaction range r_0 to prevent the material from forming a classical liquid. Additionally, the thermal de Broglie wavelength λ_{dB}, which describes the typical atomic wavelength, needs to be larger than l. Together those conditions require that λ_{dB} be much larger than r_0. In other words, the atomic waves cannot resolve the details of the interaction potential (see figure 1). As a result, the particles behave as if they were interacting through a zero-range contact potential that can be written as $V(r) = g\,\delta(r)$, where $\delta(r)$ is the Dirac delta function, g is a coupling constant, and r is the interatomic separation distance.

Despite the conceptual simplicity of the interaction, calculating the ground state of N bosons interacting through a contact potential is difficult and requires approximations. First is the mean-field approximation, which assumes that atoms all still occupy only one state, as they would in the absence of interactions; the interactions only modify the state with respect to the single-particle case. The ground-state energy E of an ensemble with uniform density n in a volume V is then simply $E/V = 1/2\,gn^2$. That equation says that the BEC can exist only in the gas phase: If g is positive, meaning that the particles are repulsive, then the energy of the system is lowest when n is minimized—in practice, that means the system always expands, which is why external trapping potentials are needed to confine BECs. On the other hand, if g is negative and the particles are attractive, the energy is minimized when n is maximized, so the ensemble collapses on itself. Both situations have been observed experimentally, but neither forms a liquid.

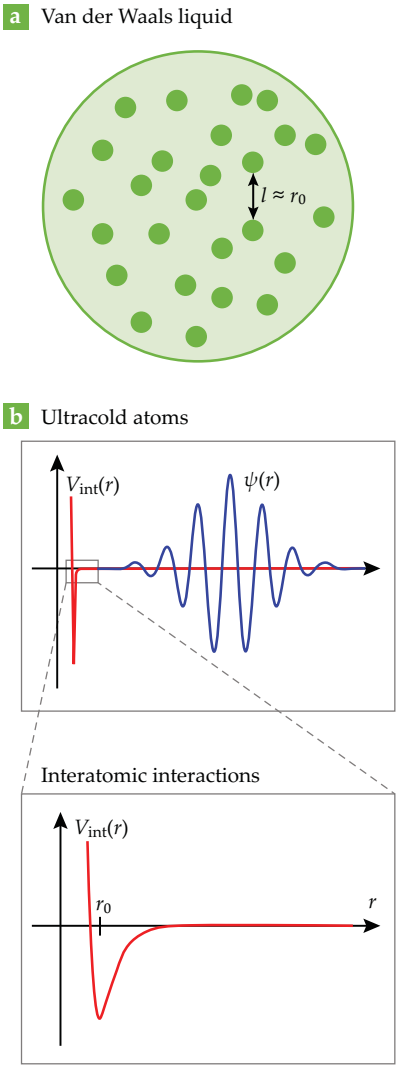

FIGURE 1. (a) IN A VAN DER WAALS LIQUID, the nearest-neighbor interatomic distance l is on the order of the typical distance r_0 over which the interaction potential varies. **(b)** In the ultracold regime, two interacting atoms are described as matter waves $\psi(r)$. Their wavelengths are too large to resolve the details of the effective interaction potential $V_{int}(r)$ that only extends a radial distance r_0 from the atom. The effective interaction therefore has zero range, and van der Waals liquids cannot be found in ultracold conditions.

A game-changing correction

As usual, corrections to a quantum ensemble's energy go beyond the mean-field approximation. The first of those corrections was calculated in the 1950s. At the time, the goal was to develop a theoretical description of superfluid helium. (For more information on superfluid helium droplets, see the article by Peter Toennies, Andrej Vilesov, and Birgitta Whaley, PHYSICS TODAY, February 2001, page 31.) The He–He interaction potential is far too complex to analytically solve in the many-body limit, so a zero-range potential was used as an academic exercise. The first exact calculation of the next leading-order term in the energy came from Tsung-Dao Lee, Kerson Huang, and Cheng-Ning Yang in 1957 and is thus termed the LHY correction.[2] At that level of approximation, the ground state is composed of a large fraction of atoms still in the zero-momentum condensed state and also of a small noncondensed fraction, known as the quantum depletion, in higher momentum states. The interpretation of the LHY correction is that it accounts for the fact that the collective modes of the BEC are not fully at rest, even in the ground state, but undergo zero-point fluctuations as dictated by Heisenberg's uncertainty principle.

Accounting for the zero-point energy in the ground state leads to a modified energy, $E/V = 1/2\,gn^2 + \alpha_{LHY}(gn)^{5/2}$, where α_{LHY} depends only on the atomic mass and Planck's constant. The new expression recovers the mean-field term from before, along with an extra term from accounting for the quantum mechanical nature of the fluid. The correction becomes more important at higher densities,[3] as shown in figure 2a. The beyond-mean-field theory at the LHY level is in excellent agreement with experiments that have observed the quantum depletion and measured the LHY energy correction.[4,5] However, since the correction depends only on g and is repulsive, just like the mean-field term, the energy minimization works the same way and the atomic ensemble remains a gas.

The crucial ingredient for qualitatively altering the nature of the BEC was first laid out in 2015 in an imaginative theoretical proposal by Dmitry Petrov at CNRS in Orsay, France, and was incidentally experimentally observed shortly afterward by a group headed by Tilman Pfau at the University of Stuttgart in Germany.[6,7] The two papers used different systems but with the same idealized situation: Imagine a bosonic system described by two separate interactions rather than one, with coupling constants g and g'. The energy is just the sum of the two contributions, so if the interactions both have the same sign, no qualitative change in behavior occurs.

An interesting situation arises when the two interactions are competing, meaning one is attractive (negative) and the other re-

pulsive (positive). The mean-field energy becomes $E/V = 1/2\,\delta g n^2$ where $\delta g = g - g'$. Assuming g and g' are of the same order of magnitude, the mean-field energy is reduced but the qualitative behavior of the system does not change. Because of that reduction, however, the beyond-mean-field corrections are not necessarily negligible. The total energy is now given by $E_{tot}/V = 1/2\,\delta g n^2 + \alpha'_{LHY}(gn)^{5/2}$, where α'_{LHY} depends on the ratio g'/g. As long as g and g' are individually not small, the LHY correction remains relatively large even as the mean-field term shrinks. The presence of two interactions can create collective high-energy excitations that have a large zero-point energy, which allows the LHY correction to be largely repulsive even as the mean-field term remains attractive.

Importantly, the first term in the expression for E_{tot}/V depends on δg, whereas the second depends on g and g'/g. When g and g' are of the same order and $g' > g$, the mean-field term is attractive ($\delta g < 0$) and the LHY correction is repulsive (g, $\alpha'_{LHY} > 0$). The resulting energy, shown in figure 2b, reaches a minimum at a finite density by balancing the weakened mean-field attraction at low n and the beyond-mean-field repulsion at high n. That competition enables the formation of a self-bound liquid.

A liquid and a gas differ essentially by their density.[8] In this article, we define a gas by its expansion to fill the whole available volume; a liquid does not fill the whole volume, but instead forms a self-bound droplet with a fixed density. The peak density of a droplet in infinite volume can be thought of as the order parameter for the liquid–gas phase transition. It takes a nonzero value in the liquid phase but vanishes for a gas.

Making an ultradilute droplet

The question is, what experimental system is ruled by two different interactions? In general, only one type of contact interaction results from the details of the short-range forces. Petrov's proposal to overcome that was to mix two types of bosons in which like atoms repel each other with one coupling constant, g_l, and unlike atoms attract each other with a coupling constant g_u. Using two different species allows the system to be effectively described by two different interactions, both coming from short-range forces.

Petrov showed that when the previously described conditions for g and g' (here g_l and g_u) were met, the mixture would form a liquid. Remarkably, the liquid would still be extremely dilute, so the interatomic distance l remains much larger than the interaction range r_0. Another consequence of the low density is that the quantum depletion remains weak, so the LHY-level approximation remains valid. The existence of such a liquid is not explained by a van der Waals–like mechanism but instead stems from a many-body effect that is a consequence of the quantum mechanical nature of the bosonic ensemble. Petrov's proposal identified several concrete atomic mixtures in which such intraspecies repulsion and interspecies attraction could be found, which suggested that a liquid BEC could be realized in contemporary experiments.

Instead of two species, the Stuttgart experiments were performed on a single species of atoms with two different interactions. The experiments used dysprosium atoms, which have a large magnetic moment. As a result, they are subject not only to a repulsive contact interaction but also to an anisotropic dipole–dipole interaction. The dipole interaction is longer-ranged than the contact interaction[9] and characterized by a coupling constant g_d that, in the experiments, was slightly larger than the contact coupling g. When the atoms are mostly distributed head-to-tail, the attractive dipole interaction leads to the same competition between attractive and repulsive interactions as in the two-species system.

The mean-field energy at the center of a droplet again reads $E/V \approx 1/2\,\delta g n^2$, although the equality is no longer exact because the effective dipolar interaction is slightly altered when the dipoles are not exactly head-to-tail, and it predicts collapse because $\delta g < 0$. However, in experiments the bosonic system formed stable, long-lived droplets—as before, once beyond-mean-field effects are accounted for, the ensemble forms a liquid.[10,11] Following the observation of liquid droplets with dysprosium,

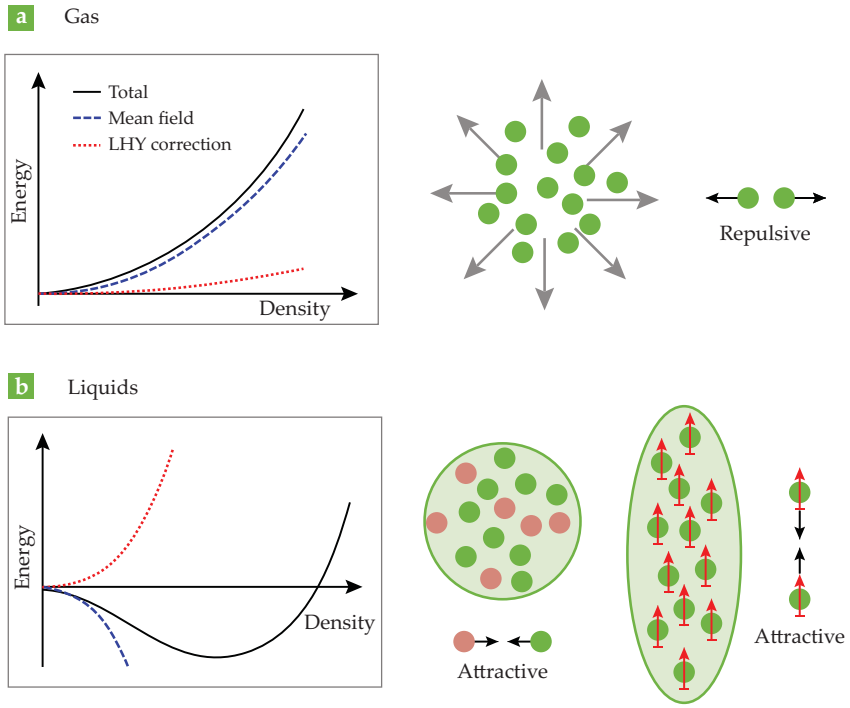

FIGURE 2. (a) A TYPICAL SINGLE-SPECIES BOSE–EINSTEIN CONDENSATE has repulsive short-range interactions. The sum of the mean-field energy and the Lee-Huang-Yang (LHY) correction is positive and therefore repulsive, so the atoms are not bound and form a gas. **(b)** Bose–Einstein condensates of atomic mixtures or magnetic atoms can have both attractive and repulsive interactions. When the mean-field energy and the LHY correction have opposite signs, the total energy can develop a minimum at finite density, which causes the atoms to form self-bound liquid droplets.

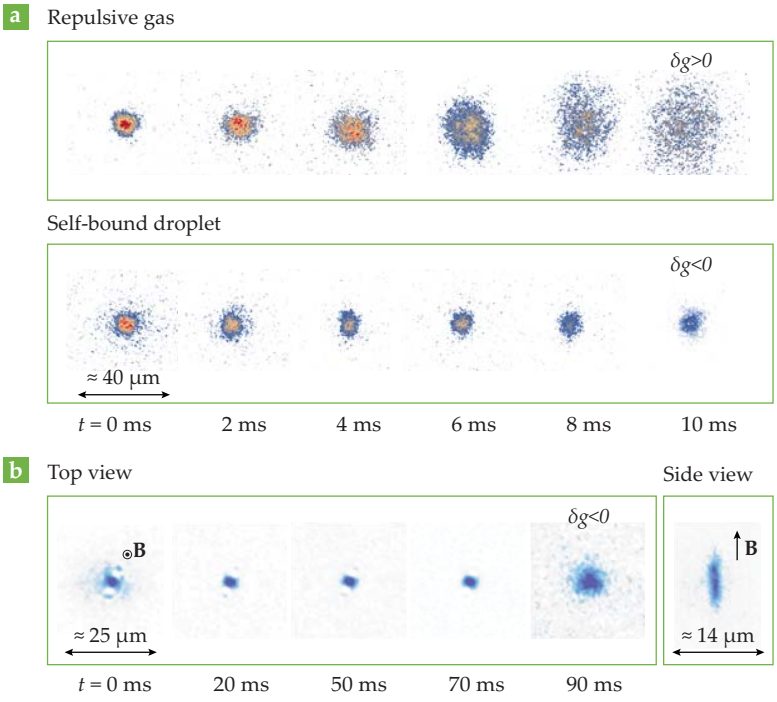

FIGURE 3. SELF-BOUND DROPLETS in the absence of an external trapping potential can be imaged experimentally. The densities of two such systems are shown here. **(a)** When the mean-field energy of a Bose–Bose mixture is repulsive (top row), it results in a gas phase, and the droplet expands over time. When the mean-field energy is attractive (bottom row), the size of the self-bound droplet remains constant over time, although its density, shown in false color, decays due to three-body losses. (Adapted from ref. 13.) **(b)** A droplet of dipolar magnetic atoms stays confined until the atom number decays below the critical atom number, at which point it starts expanding as a gas. The side view of the droplet clearly shows its elongation along the magnetic field **B**. (Adapted from ref. 14.)

experiments at the University of Innsbruck, Austria, under the direction of Francesca Ferlaino showed the same stabilization with erbium atoms,[12] which, like dysprosium, have a large magnetic moment. The experiments confirmed that the stabilization mechanism is general to atoms that possess competing short-range repulsion and longer-range dipole interactions.

Many experimental groups can produce bosonic atomic mixtures with a variety of elements and isotopes. The mixture that won the race for the first observation of a two-component liquid phase was a blend of two internal states of the same isotope of potassium. By creating the proper mixture of internal states in the right magnetic field, two teams, one led by Leticia Tarruell at the Institute of Photonic Sciences in Barcelona, Spain, and the other by Marco Fattori at the University of Florence, Italy, both observed the ultradilute quantum liquid phase.[13] They confirmed their findings by removing all external trapping potentials, thus placing the BEC in an infinite volume. If the condensate were still a quantum gas, it would have expanded until the density was too thin to be measurable. Instead, the researchers saw self-bound droplets that did not expand in free space and could easily be observed for long times.[13]

The experimental results shown in figure 3 for Bose mixtures and magnetic atoms[14] are visual proof of the gas–liquid phase transition. The theoretical prediction and later observation of quantum liquids marked a paradigm shift because they showed that the LHY correction, which was thought to be a small quantitative shift due to weak quantum fluctuations in a many-body system, can stabilize a liquid phase. That phase would be impossible under mean-field conditions. The diluteness of those liquids is remarkable, with typical densities being about four orders of magnitude lower than air and about eight orders of magnitude lower than liquid helium at room pressure.

Oscillating and disappearing droplets

Ultradilute liquids also exhibit another feature rooted in their quantum mechanical nature. Their simplified energy description captures the liquid and gas phases, but it completely ignores finite-size and surface effects by assuming a uniform density n. In any real liquid droplet, the density is not uniform; it increases from zero at the droplet's edge to a peak value at its center. For matter waves such as BECs, such density gradients cost kinetic energy, as dictated by the Schrödinger equation. In droplets of dilute quantum liquids, kinetic energy acts as a surface tension, contributing an additional energy that depends on the density gradient at the surface. The consequence can be dramatic, because if the surface tension shifts the total energy from negative to positive, then the self-bound solution no longer exists and the ground state is a gas. Quantum liquids thus have another very peculiar feature: Kinetic energy, accounting for single-particle quantum fluctuations, can drive a liquid-to-gas transition.

Another way to think about the effective surface tension is that the density distribution created by all the atoms in a droplet acts as a trapping potential on each individual atom because of the effectively attractive interaction. If the trapping potential is strong enough to hold a bound state, then it supports a self-bound liquid solution. If not, then the ensemble forms a gas. A third possibility is that the liquid exists in a metastable state, but for low enough atom number, the trapping becomes too shallow and only the gas exists. The depth of the effective potential is determined by the number of atoms, N, and the difference between the two interaction strengths, δg. For larger values of N and more negative δg, the trapping volume is larger and the attraction is stronger, so the effective potential becomes more binding. A liquid–gas phase diagram can therefore be drawn as a function of system size and interaction strength,[6,15] as shown in figure 4. The critical atom number N_c that marks the gas–liquid transition varies as $|\delta g/g|^{-2/5}$, so the minimal atom number to sustain a self-bound droplet grows dramatically as δg approaches zero.

The structure of the phase diagram has been confirmed experimentally[13,14] using a mechanism that experimenters usually try to avoid: three-body losses. The number of atoms in a liquid drop decreases as a result of collisions that recombine two atoms into one molecule. To respect conservation of energy and momentum, such a recombination can only happen if three atoms are involved in the collision, so the loss rate grows strongly with density. When a liquid droplet is created, losses

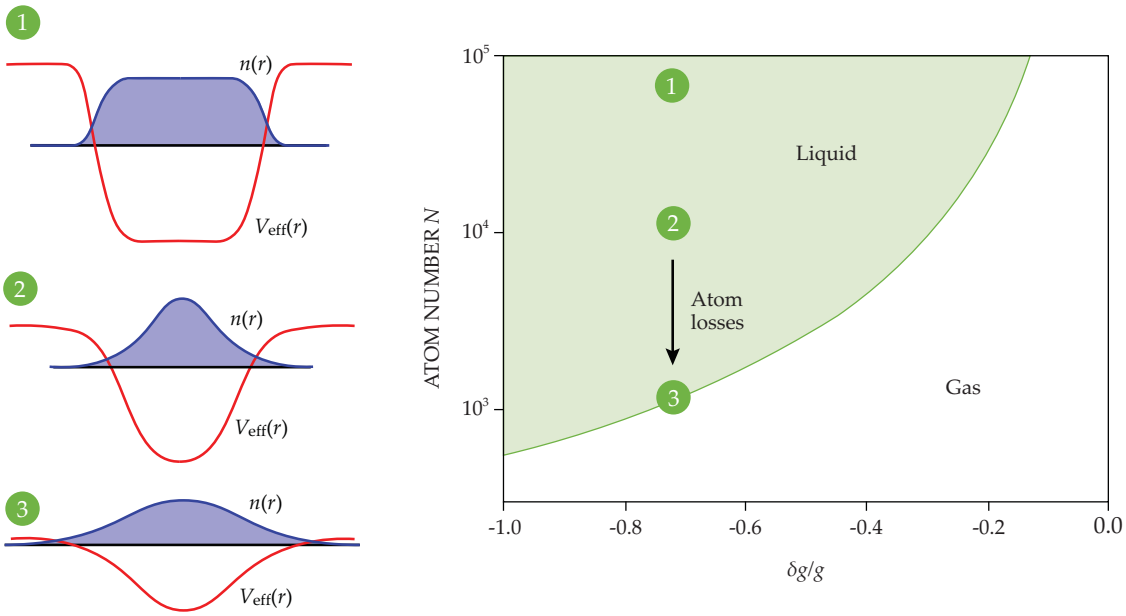

FIGURE 4. THE PHASE DIAGRAM FOR AN ULTRADILUTE DROPLET depends on the atom number N, the contact coupling g, and the difference between the mean-field and beyond-mean-field coupling constants δg. At high N (point 1 in the phase diagram), the density $n(r)$ of a droplet has a flat-top profile, which creates a deep self-binding potential $V_{\text{eff}}(r)$ and a liquid droplet. Experiments obtain lower N (point 2), and the density does not reach the flat top, but the self-trapping remains relatively deep. Atom losses deplete the droplet over time until the self-bound state barely exists (point 3). When N decreases further, the droplet crosses the phase boundary and becomes a gas.

typically limit its lifetime to between a few and tens of milliseconds. During that time, the atom number decays until it reaches the liquid–gas phase transition. At that point the self-bound liquid turns into a gas, the atoms expand in space, and the density immediately drops, as in the final frame of figure 3b (90 ms).

Once the liquid transitions to a gas, the three-body losses stop, and the number of atoms stays constant. Experimenters can therefore readily identify the critical atom number N_c for the liquid–gas transition at a given δg. They can also adjust the attraction strength using so-called Feshbach resonances, which vary the coupling constant g for contact interactions by means of a magnetic field. By varying the coupling constant and measuring the critical atom number, researchers mapped the phase diagram for the different experimental quantum liquids.

Although the two-component and dipolar liquids share the same stabilization mechanism, each also has its own characteristics. Quantum liquids of dipolar atoms are anisotropic: For the dipolar interaction to be attractive, the atoms need to be aligned. As a result, droplets are elongated along the dipole direction, as can be seen experimentally in figure 3. The shape of the dipolar droplets results from a competition between dipolar interactions trying to align the atoms and a surface tension that favors a round droplet. In atomic mixtures, the density ratio between the two species is locked to a value fixed by the precise short-range interactions. However, one species can end up in overabundance, which causes a gas halo of untrapped majority atoms to form around the droplet.

The elongation of dipolar droplets and the fixed density ratio for mixtures lead to specific, collective oscillation modes, illustrated in figure 5. Dipolar quantum droplets feature a scissor-like oscillation that corresponds to an angular oscillation of the droplet around the dipole's axis.[16] Quantum mixture droplets, on the other hand, exhibit excitations in which the two components move either in or out of phase relative to each other. Accurately mapping their spectrum of collective excitations should yield precious information about their precise equation of state beyond the current description.

The future of ultradilute liquids

The discovery of physically realizable ultradilute liquids highlights the strengths of ultracold atom experiments. Using exquisite control of the constituents of a many-body system and the interactions that characterize it, such experimental setups can expose the key mechanism that underpins the many-body state. The family of ultradilute quantum liquids will likely continue to grow because the same stabilization mechanism can be found in other systems.[17] Theoretical proposals have already been laid out for mixtures of other constituents, such as bosons and fermions.

Exploring the possibility of making such liquids in lower dimensions is also of great interest because quantum fluctuations are enhanced, so any attractive potential allows for a self-bound liquid solution. Additionally, quantum droplets are localized matter waves in three dimensions, so they bear similarities to matter-wave solitons, which can be fully accounted for within mean-field theory and have been observed solely in lower dimensions. In strongly confined systems, competition between solitons and quantum droplets can lead to a crossover or abrupt transition between the two states.[18] Localized matter waves could also be useful for performing interferometry, and the prospect of using quantum droplets experimentally to avoid trapping potentials remains to be investigated. (For an experimental example of matter-wave interferometry, see PHYSICS TODAY, April 2015, page 12.)

The exploration of the properties of ultradilute quantum liquids is in its infancy. The quantum depletion and LHY correction are, in theory, accompanied by quantum entanglement, and observing the presence of entanglement in the liquid phase

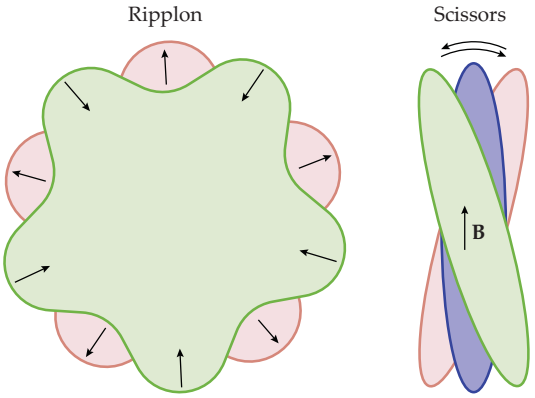

FIGURE 5. ISODENSITY CUTS OF QUANTUM DROPLETS at different times show their collective oscillation modes. Ripplons are typical for normal liquid droplets. They arise from surface tension, which creates a restoring force when the droplet is deformed, and are expected to exist in mixture droplets.[6] The scissors mode is a signature of the breaking of rotational invariance in dipolar droplets. It consists of an angular oscillation of the elongated droplet around the direction of the magnetic field **B** and has been observed in dysprosium droplets.[16]

would be remarkable. The thermodynamics of such systems is also unknown—it is not yet clear whether or how thermal equilibrium is reached within a droplet.

While the theoretical descriptions of ultradilute liquids have progressed and approximations that include the LHY correction allow for an analytical expression for their energy, many-body theories still lack a precise description of such liquids. However, in some existing experimental systems the usually dominant mean-field energy is masked, so beyond-mean-field effects that include interactions can be effectively magnified and measured. Corrections beyond the LHY description of the bosonic ensemble remain unobserved, but ultradilute quantum liquids finally provide a new testing ground for theories of quantum many-body interactions.

REFERENCES

1. I. Bloch, J. Dalibard, W. Zwerger, *Rev. Mod. Phys.* **80**, 885 (2008).
2. T. D. Lee, K. Huang, C. N. Yang, *Phys. Rev.* **106**, 1135 (1957).
3. A. J. Leggett, *New J. Phys.* **5**, 103 (2003).
4. R. Chang et al., *Phys. Rev. Lett.* **117**, 235303 (2016); R. Lopes et al., *Phys. Rev. Lett.* **119**, 190404 (2017).
5. N. Navon et al., *Phys. Rev. Lett.* **107**, 135301 (2011).
6. D. S. Petrov, *Phys. Rev. Lett.* **115**, 155302 (2015).
7. H. Kadau et al., *Nature* **530**, 194 (2016).
8. J. Barker, D. Henderson, *Rev. Mod. Phys.* **48**, 587 (1976).
9. T. Lahaye et al., *Rep. Prog. Phys.* **72**, 126401 (2009).
10. A. R. P. Lima, A. Pelster, *Phys. Rev. A* **84**, 041604 (2011).
11. I. Ferrier-Barbut et al., *Phys. Rev. Lett.* **116**, 215301 (2016).
12. L. Chomaz et al., *Phys. Rev. X* **6**, 041039 (2016).
13. C. R. Cabrera et al., *Science* **359**, 301 (2018); G. Semeghini et al., *Phys. Rev. Lett.* **120**, 235301 (2018).
14. M. Schmitt et al., *Nature* **539**, 259 (2016).
15. F. Wächtler, L. Santos, *Phys. Rev. A* **94**, 043618 (2016); D. Baillie et al., *Phys. Rev. A* **94**, 021602 (2016).
16. I. Ferrier-Barbut et al., *Phys. Rev. Lett.* **120**, 160402 (2018).
17. D. S. Petrov, G. E. Astrakharchik, *Phys. Rev. Lett.* **117**, 100401 (2016); D. Edler et al., *Phys. Rev. Lett.* **119**, 050403 (2017); D. Rakshit et al., https://arxiv.org/abs/1801.00346.
18. P. Cheiney et al., *Phys. Rev. Lett.* **120**, 135301 (2018).

PT

2 Collective light-atom interactions with two-level atomic dipoles

2.1 Introduction

I joined the Quantum Optics group at LCF in October 2018. My first two/three years have been mostly devoted to experimental work in the existing Rb setup ("Cyclopix"), as well as co-managing the team together with Antoine and mentoring graduate students and postdocs working on this thematics. The results we have obtained since my arrival on this setup on collective light scattering will be the subject of the first part of this section.

Then, I worked to develop a new experimental line of research within the group, which was made possible by an ANR JCJC grant followed by an ERC Starting grant. Since 2021 we have built a working experimental setup, whose early results and outlook will be the topic of the second part of this section. As of today, I share my time between supervising the Dy and Rb teams, with more time implication on Dy and sharing duties with Antoine on Rb.

Our study of collective scattering of light by atomic ensembles is motivated first by the fact that it is a fundamental, challenging many-body problem in itself. The system is simply composed of an ensemble of atoms in free space, driven by a resonant field. But solving its dynamics is extremely challenging, because it is a many-body system composed of two-level atoms interacting with each other via their dipole radiation (resonant dipole-dipole interaction), and with collective dissipation (spontaneous emission) to the environment [Kiffner et al., 2010]. Theoretical predictions require de develop specific approximations [Gross & Haroche, 1982, Allen & Eberly, 1975], and thus call for experimental tests. Furthemore, with the advent of quantum technologies based on atomic systems and in particular atomic arrays, novel light-matter interfaces are proposed and realized [Facchinetti et al., 2016, Asenjo-Garcia et al., 2017, Bekenstein et al., 2020, Moreno-Cardoner et al., 2021, Rui et al., 2020], with several motivations. One might for instance be interested in stabilizing correlations (or entanglement) in an atomic array using its collective coupling to light, or conversely to use the atomic ensemble as a nonlinear medium to produce non-classical states of light. Our activity centers on operating dedicated setups to study at a fundamental level the collective coupling of atomic ensembles to resonant light and make progress towards controlled interfaces. First, I present below experiments performed on the Rb setup, the results on the Dy setup are presented in section 2.3.

2.2 Experiments on the Rb setup : Collective spontaneous emission of laser-driven dense atomic clouds

The Rb setup has been used to explore collective light scattering by small atomic clouds trapped in an optical tweezer for a number of years [Pellegrino et al., 2014, Jenkins et al., 2016, Jennewein et al., 2016, Jennewein et al., 2016]. The particularity of this setup is to produce clouds with external dimensions close to or smaller than the wavelength of the D2 transition of Rb at $\lambda_0 = 780\,\mathrm{nm}$. When a transition between two levels ($|g\rangle$ and $|e\rangle$) with wavelength λ_0 is excited, the response to light is collective. This has allowed the group to study the collective interaction of an atomic cloud with resonant light in a regime where *the interatomic distance is comparable to or shorter than this wavelength*. Such studies are complementary to those in magneto-optical traps (MOT), where the interatomic distance is much larger while the number of atoms is also orders of magnitude larger so that the optical depth is very high [Guerin et al., 2017].

Light-scattering studies in cold atomic clouds have particularly focused recently on collective

spontaneous emission, reviving somehow a field that was born seventy years ago with Dicke superradiance [Dicke, 1954, Gross & Haroche, 1982, Allen & Eberly, 1975]. Recent experiments in MOTs [Guerin et al., 2016, Araújo et al., 2016, Roof et al., 2016] have renewed interest in studying the modification of spontaneous emission time by collective effects, either superradiance or subradiance. In the LCF group, we have worked largely on understanding and harnessing collective spontaneous emission in dense clouds, opening in particular the regime where *many* excitations are stored by the medium so that the quantum two-level structure of the atoms must be accounted for : The fact that the atoms are saturable plays a major role and they cannot be considered as classical dipoles. These studies have been possible on the setup thanks to an increase in the number of atoms trapped in the tweezers. This is due to experimental improvements which I briefly review first.

2.2.1 Experimental upgrades

The Rb setup was upgraded from its initial version in 2017. In this first version, it was the first setup to trap single atoms with the use of an aspheric lens in vacuum to focus the trap light and collect fluorescence, as opposed to a microsope objective [Sortais et al., 2007]. In the 2017 upgrade, the two in-vacuum lenses were changed. A second pair of lenses was added, perpendicular to the first one [Brossard, 2020], see scheme in figure 3. This offered a second direction of observation to probe the atomic cloud perpendicularly to the trapping laser. The loading of the optical tweezer with dense clouds was then performed by shining it directly on the MOT. Thanks to a telescope made of two tunable lenses, the tweezer beam waist was tuneable between about 1.5 µm and 4 µm. With this, a few hundred atoms could be loaded in the tweezer.

When I arrived, we improved upon these performances by implementing a stage of gray molasses [Boiron et al., 1995, Esslinger et al., 1996], after the MOT and during the tweezer loading. Gray molasses performed on the D1 line [Fernandes et al., 2012, Grier et al., 2013] are especially useful to load optical dipole traps. Indeed, they rely on placing atoms in *dark states* (hence the name). Since the atoms are in the dark states most of the time, they scatter much less light, and undergo less light-induced collisions. Thus, grey molasses allow to cool down to sub-Doppler temperature in dense samples [Sievers et al., 2015]. They permit to fill more atoms into a dipole trap of small volume and finite trap depth with respect to usual bright molasses. We added D1 gray molasses for ^{87}Rb on the setup, by using beams co-propagating with the MOT beams and with opposite polarization [Glicenstein, 2022]. With this upgrade, the experiment was then able to produce atomic clouds with a few thousand atoms in the tweezers. The density profile of the clouds follows a cigar-shaped thermal Gaussian profile with cylindrical symmetry about the tweezer axis, with a radial $1/e^2$ size of roughly 500 nm and an axial size of the order of 10 µm [Glicenstein et al., 2021]. This large increase in atom number in the tweezer unlocked the study of the collective spontaneous emission. We have indeed observed that collective effects start to arise above a threshold of roughly 1000 atoms [Ferioli et al., 2021a, Ferioli et al., 2021b], which we reached thanks to the addition of grey molasses.

In parallel, we added the possibility to retro-reflect the optical tweezer beam, after it went through the two aspheric lenses in vacuum. For this we placed a mirror at the focal point of a lens, to ensure that the retro-reflected beam had the same profile as the incoming one. The tweezer then forms an optical lattice. The lattice has a spacing between the sites of $\lambda_{\text{trap}}/2 = 470\,\text{nm}$ (the trap wavelength is $\lambda_{\text{trap}} = 940\,\text{nm}$). Due to collisional blockade as in a single atom tweezer [Schlosser et al., 2001], at most one atom can be loaded in each site with optical molasses. We thus obtained a *randomly loaded* chain of atoms with 50 % loading, thus with an average

interatomic distance of $\lambda_{trap} = 1.2\,\lambda_0$. We performed experiments on how collective scattering can shift the atomic line in such a chain, which I discuss below before turning to experiments on clouds [2].

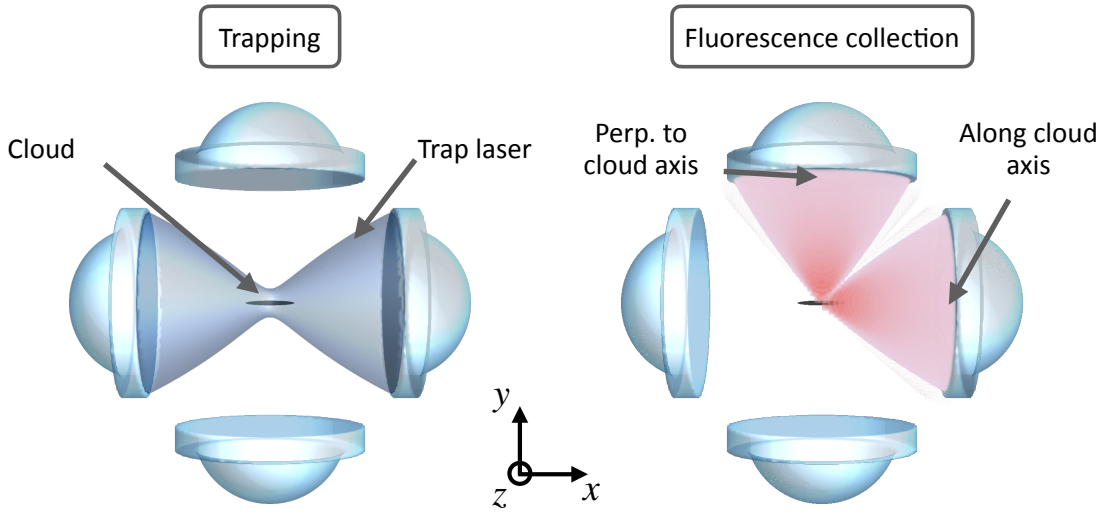

Figure 3 – **Representation of the experiment (not to scale)**. Four aspheric lenses offer optical access to trap (shown on the left) and observe (right) the atomic cloud. Left : The trap laser at 940 nm (blue) is focused between two lenses, and allows to trap the atomic cloud. Right : We have the possibility in the experiment to collect the cloud fluorescence either along the trap axis (x) or perpendicular to it (y). In different experiments discussed in this work, the driving laser propagates either along x or along $z+y$. A magnetic field along $z+y$ of up to 100 G is added to isolate a two-level transition with σ^+ polarization.

2.2.2 Collective shift of a randomly loaded atomic chain

The experiments presented here are published in [Glicenstein et al., 2020], and were inspired by the theoretical proposal of ref. [Sutherland & Robicheaux, 2016]. These experiments are mainly the work of Antoine Glicenstein whose PhD thesis (2018-2022) I supervised, together with Antoine Browaeys.

The system we studied is a chain of single atoms randomly placed in about 200 sites of the optical lattice discussed above with spacing 470 nm. The atoms were excited by resonant light on the D2 transition and we measured fluorescence spectra, that is the amount of fluorescence emitted by the atoms detected on a camera, *in steady state* as a function of the excitation light frequency. Thanks to the second pair of aspheric lenses (vertical pair in figure 3), we could measure *position-resolved* spectra.

2. Note that grey molasses being blue detuned, one might have hoped to obtain near-unity filling of single atoms in the chain as reported in [Brown et al., 2019]. However we did not observe an enhancement of the loading above 50 %. This might be due to several factors, like a too low molasses density or too large trap volume and more research is necessary to arrive at reliable, stable performances.

An important feature of this one-dimensional system is revealed when it is excited by a drive beam propagating along its axis : In this case the dipole radiation of atoms excited by the drive interfere constructively in the forward direction (there is no constructive interference in the backwards direction, see discussion in [Glicenstein et al., 2020]). As a consequence, there is a buildup of the N-atom scattered field E_N along the chain, and atoms down the line see a total field that is the interference of the drive E_D and the scattered field $E_\mathrm{T} = E_\mathrm{D} + E_N$. Depending on the drive detuning, the dipole radiation is either in-phase (red detuning) and leads to an enhanced field, $|E_{textT}| > |E_\mathrm{D}|$, or out-of-phase (blue detuning), and leads to a reduced field, $|E_\mathrm{T}| < |E_\mathrm{D}|$. Altogether this creates a red shift of the detected peak of fluorescence along the chain. We indeed observed a shift of the resonance of the atoms by an amount of about $0.3\,\Gamma_0$ and $0.2\,\Gamma_0$ averaged over the chain, with $\Gamma_0 = \simeq (2\pi)\,6\,\mathrm{MHz}$ the D2 linewidth of ^{87}Rb.

This showed that the spatial distribution (here the 1D character) can enhance and allow to control collective light scattering. But to obtain shifts larger than Γ_0, one must necessarily reduce the interatomic distance. This is one motivation to produce structured single atom arrays for light scattering presented in section 2.3 of this manuscript.

2.2.3 Subradiance in dense clouds

After investigating 1D chains, we turned our attention to dense clouds, and in particular collective spontaneous emission. These studies were carried out by Antoine Glicenstein and Giovanni Ferioli who had joined the group as a postdoc in 2020, under my and Antoine Browaeys's supervision.

While superradiance had been extensively tested in experiments, its counterpart, subradiance, was scarcely studied. It is indeed more of an experimental challenge to detect subradiant emission since by definition the photon emission rate is weakened with respect to that of independent atoms. In atomic systems, following first experimental hints in vapours [Pavolini et al., 1985], a few studies measured subradiant decay in two ions [DeVoe & Brewer, 1996] or two-atom molecules [Takasu et al., 2012, McGuyer et al., 2015], and it was observed in MOTs only very recently in [Guerin et al., 2016]. Motivations to study subradiance are numerous. For example there are proposals to use subradiance for light storage [Facchinetti et al., 2016, Asenjo-Garcia et al., 2017]. And from a fundamental physics point of view, the description of subradiance *in the quantum regime* still represents a theoretical challenge because it requires to deal with the entire Hilbert space of an N-atom system [Asenjo-Garcia et al., 2017, Zhang & Mølmer, 2019].

With these motivations in mind, we set out to observe subradiance in the dense clouds trapped in our optical tweezers. We were interested in exploring the consequences of two aspects in particular : the small dimensions ($\sim \lambda_0$) of the clouds and the *saturated* (or quantum) regime reached for a drive intensity $I > I_\mathrm{sat}$. In order to observe subradiance in dense clouds we performed the following protocol : Once the clouds were prepared, they were released in free space to suppress the inhomogenous broadening due to the trap light shift. We then immediately applied a driving pulse by a near-resonant laser beam propagating perpendicularly to the cloud axis. The driving pulse had constant intensity and lasted hundreds of nano seconds so that the steady state was reached. We varied the intensity I between the linear classical regime of much less than one photon absorbed per atom $I \ll I_\mathrm{sat}$ to the quantum regime $I \gg I_\mathrm{sat}$. Details can be found in the publication [Ferioli et al., 2021a]. We observed subradiance *during the decay* of the cloud fluorescence after the switch-off of the pulse. It was clearly observable as a slowing down of the fluorescence decay, following an initial fast drop, figure 4. This early dynamics is induced by the emission of photons from collective excitations that have a short lifetime i.e. superradiant, which we will discuss later. Subradiance was then

observed with a characteristic decay time of a few times the single atom lifetime $\tau_0 = 1/\Gamma_0 \simeq 26\,\text{ns}$.

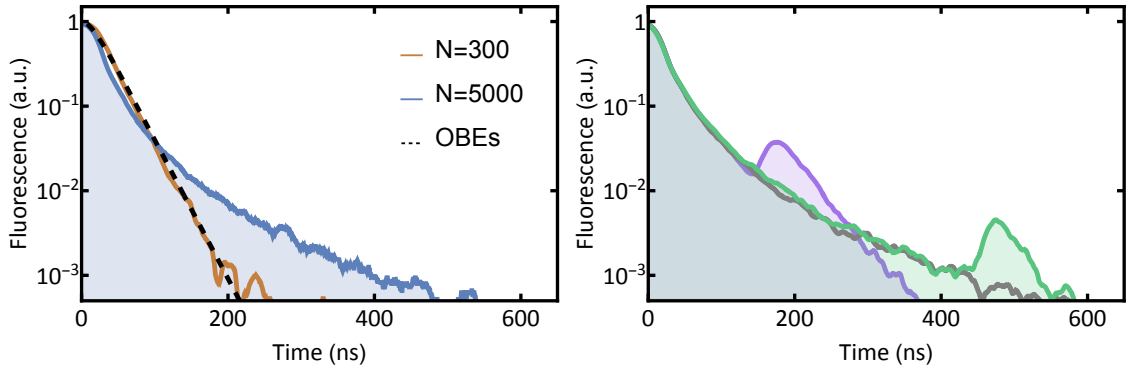

Figure 4 – **Subradiance.** Left : Decay of fluorescence along the cloud axis once the driving light is switched off. In the low atom number regime ($N = 300$), the fluorescence decays precisely following the optical Bloch equations (dashed), with a decay time given by the single atom lifetime. In the high atom number regime ($N = 500$), an initial fast decay is followed by a decay *slower* than the single atom lifetime : subradiance. Right : example of release of the light stored in subradiant excitations. The purple and green curves show the fluorescence decay after driving is switched off, but when the trap is turned back on during the decay (at $t \simeq 150\,\text{ns}$ and $t \simeq 450\,\text{ns}$), inducing inhomogeneous broadening that suppresses subradiance inducing the release of the excitations stored in subradiance as a short light pulse. Data adapted from [Ferioli et al., 2021a].

Our observation of subradiance in dense clouds in [Ferioli et al., 2021a] differed from observations in dilute MOTs [Guerin et al., 2016, Das et al., 2020, Cipris et al., 2021] in the fact that if one calculates the photon mean-free path in our clouds, it is shorter than the interatomic distance. Indeed the cloud radial section is on the same order as the atom photon cross-section $3\lambda_0^2/2\pi$. As a consequence a description in terms of collective excitations shared by the entire ensemble is appropriate. And a description based on photons travelling through the cloud and scattering off individual atoms [Asselie et al., 2022] is not relevant to our experiments. By repeating experiments for different cloud shapes, densities and atom numbers, we found that the subradiant decay time was not proportional to optical depth as is the case for MOTs [Guerin et al., 2016], but to the atom number N. In fact, as we will see later, the parameter that dictates the decay time in our cloud should not exactly be N but the *cooperativity* : $C = \mu \times N$, which is defined later-on in this manuscript. In the experiments reported in [Ferioli et al., 2021a], μ was nearly constant which explains why the decay time appeared proportional to N. Qualitatively, the fact that we found a cooperativity that is not the optical depth is intrinsically linked to the fact that the clouds have a radius smaller than the wavelength. Indeed along the cloud axis, all atoms absorb or emit a photon collectively since the cloud cross-section is on the order of the photon absorbtion cross-section. We will come back to these features when discussing superradiance.

Once we had established subradiance in our clouds, we addressed a first question : How does subradiance behave in the quantum regime ? To address it, we measured the subradiant decay at varying drive intensity, that is at a variable saturation of the medium. We reported one important finding : the decay time of excitations with subradiant decay was observed to be constant, even as we varied the number of these excitations by an order of magnitude. This indicates that many

excitations can be present in the atomic medium without influencing each-other's lifetime. This was compatible with theoretical predictions for the construction of subradiance with multiple excitations in atomic ensembles. Several works predicted that multiple-excitations subradiant states are formed as a fermionic superposition of single excitations that do not influence each other's lifetime [Asenjo-Garcia et al., 2017, Albrecht et al., 2019, Henriet et al., 2019, Zhang & Mølmer, 2019]. It leaves a very interesting prospect of measuring in-situ in a single shot how the positions of excited atoms are correlated which will allow to witness directly the fermionic superposition [Henriet et al., 2019]. The new Dy setup has the capability of single-shot readout of the state of individual atoms and should be in a position to perform this type of measurement.

The second question we tackled is : Can one control subradiance in real time ? To answer it, we performed a proof-of-principle experiment to show that one can control subradiance and release excitations on demand. For this we made use of the trapping laser. Indeed, the trap induces a strong, position-dependent light shift, the transition frequency of each atom is different depending on its position (inhomogeneous broadening). Hence, with the trapping laser on, the atoms are not resonant with one another, they cannot exchange excitations (their detuning with each other is larger than the strength of their coupling). As a consequence, atoms decay independently, at the single atom rate. By turning on the tweezer at a time of our choice during the subradiant decay, we then observed (figure 4, right) a pulse of light made of photons that were stored as subradiant excitations and suddenly released as the atoms turned independent. This was a proof of principle, but in the future, by controlling the spatial ordering of atoms in a 2D plane and addressing them individually, we wish with the new Dy setup to be able to directly create subradiant excitations in the medium and to retrieve single photons in a given spatial mode for instance. See for instance [Fayard et al., 2023] where we propose such a protocol in 1D.

These experiments on subradiance of dense atomic ensembles have thus revealed both the complexity and also the promises held by this quantum many-body system. These aspects motivated the new research project on Dy that I review last in the manuscript. Before this we turn to experiments on the counterpart of subradiance : superradiance.

2.2.4 Superradiance in dense, driven clouds

The rest of the work presented below is mainly the result of Giovanni Ferioli's postdoc who was the leading force on the setup. He worked together with Antoine Glicenstein, and with some recent input from Sara Pancaldi who has joined the team in October 2022 as a graduate student.

By no means is superradiance a recent topic in atomic physics. The theoretical paper of Dicke [Dicke, 1954] is considered to have given birth to the field, and many observations have followed, reviewed in part in [Allen & Eberly, 1975, Gross & Haroche, 1982]. Nevertheless, the experimental progresses of cold atom platforms have unlocked new opportunities to explore new phenomena beyond the work of pioneers. As an example, one objective is to realize a steady-state superradiant laser as was proposed in [Meiser et al., 2009]. The promise is to use superradiance to produce a steady-state laser in cavity whose frequency is determined by the atomic transition but insensitive to the cavity mirror noise. This noise is a limiting factor in lasers used to interrogate the atomic transition in state of-the-art optical clocks. Several experiments are approaching this regime [Bohnet et al., 2012, Norcia & Thompson, 2016, Laske et al., 2019, Schäffer et al., 2020], but more progress is needed. This motivates the understanding of superradiance *in steady-state, in the presence of a drive*.

It is this problem that we have been tackling in particular : the fate of superradiance in clouds of two-level atoms in free space, *in the presence of a driving field*. To understand the appearance of Dicke superradiance in our clouds, it helps to calculate what we term their *cooperativity* [Tanji-Suzuki et al., 2011]. In simple words, it is the ratio of coherent emission rate of the cloud in a diffraction mode to the incoherent emission rate in all directions (4π solid angle),

$$C = N \times \mu = P_{\text{coh}}/P_{\text{incoh}}. \tag{7}$$

The coherent diffraction mode is the mode in which the fields radiated by the atomic dipoles interfere constructively such that the atoms emit cooperatively. Constructive interferences will depend on the relative phase of the atoms inside the cloud, which dictates in which direction they occur. The parameter μ then scales approximately like $\mu \sim \Delta\Omega/4\pi$ where $\Delta\Omega$ is the solid angle in which constructive interference can occur. For instance, in the Dicke case for a cloud with all dimensions $\ll \lambda_0$, then all dipoles are phased identically when excited by a laser and $\Delta\Omega = 4\pi$ and $\mu = 1$, $C = N$. Our clouds have a very elongated shape, with radial diameter about λ_0 and a long axis (x) extent $> 15\,\lambda_0$. When one does the math [Allen & Eberly, 1975, Sutherland & Robicheaux, 2017], one finds that in our clouds the cooperativity can be larger than one if and only if atoms are phased such that their radiations interfere constructively *along the cloud*. For instance a spin wave of the type $\Pi_{\otimes n}(\alpha\ |g\rangle_n + \beta \exp(-i\, k_0 \boldsymbol{u}_x \cdot \boldsymbol{r}_n)\ |e\rangle_n)$ will emit coherently along the cloud axis x, just as phased antennae do. If phase coherence is present with the right wavevector, then one can have $\mu N > 1$ and cooperative emission dominates. Note that in large clouds with radius larger than λ_0, one can show that $N\mu = b_0$ where b_0 the optical depth of the cloud, and in the limit $\beta \ll 1$ one recovers classical dipoles that can describe "single-photon" as superradiance observed in MOTs [Araújo et al., 2016, Roof et al., 2016].

On our experiment, we were interested in the quantum regime of many excitations in the ensemble. In this regime, we tackled two cases : one where the phase coherence emerged *spontaneously*, due to Dicke superradiance which I review first, and one where the driving laser directly creates the phase relation.

Let us start with the first case, in which the laser that drives the atoms has a wave-vector $\boldsymbol{k}_{\text{las}} \perp \boldsymbol{u}_x$. If we ignore any collective effect, the phase of each atomic dipole is induced only by the driving laser : it takes the value $\boldsymbol{k}_{\text{las}} \cdot \boldsymbol{r}_n$ for atom n. With this phase relation between dipoles, no constructive interference should take place along the cloud ($\boldsymbol{u}_x$). As a consequence, if cooperative emission is observed along the cloud, it can only be due to phase coherence between the atomic dipoles appearing spontaneously from collective effects. We know since Dicke that dipoles can phase-correlate during their collective spontaneous emission, and this is what we set out to observe experimentally in driven clouds.

We probed this situation by driving the cloud along $\boldsymbol{u}_z + \boldsymbol{u}_y$, i.e. *perpendicularly* to its axis. First, to verify that Dicke superradiance was indeed taking place in the cloud, we performed population inversion by applying a short pulse of light of about 12 ns. This π-pulse created an excitation fraction of about 85 %. We measured the atomic emission along the cloud by collecting the radiated light in a single mode fiber coupled avalanche photodiode. Upon switching off the pulse, we observed different behaviours depending on atom number, shown in figure 5. At low N, the intensity emitted by the cloud decayed exponentially, with an emission directly proportional to atom number. Above a threshold of about 1000 atoms, we observed that the emission rate along the cloud was initially *increasing*, before reaching a maximum that scaled more than linearly in N, approaching N^2. The characteristic time of this light pulse decreased with atom number. These observations

are in agreement with what is expected for Dicke superradiance in our samples. It demonstrated that our clouds indeed are superradiant and that superradiance takes place only in a diffraction mode centered *along the cloud axis* (we observed no superradiance perpendicular to the cloud axis).

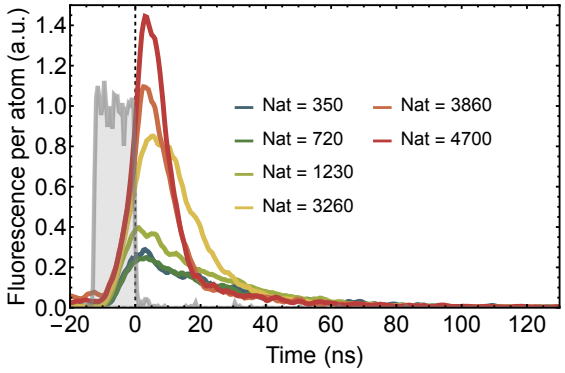

Figure 5 – **Dicke superradiance.** Fluorescence per atom measured along the cloud axis, after the population is inverted for various atom numbers. The population is inverted by a short pulse of driving light (shown in gray), whose timing is set so that it corresponds to a π pulse. The fluorescence per atom is seen to increase above a threshold atom number $N \simeq 1000$; above this threshold, intensity is enhanced and a short pulse of light as predicted by Dicke superradiance is observed. Data adapted from [Ferioli et al., 2021b].

Once we had established this occurence of superradiance in a diffraction mode, we could perform experiments *in the driven regime*. In particular we tested how our observations of dynamics under driving differed from the behaviour of a single atom. For a single atom, the detected photon emission is directly proportional to the excited state population $\rho_{ee} = \langle \hat{e} \rangle$, which undergoes Rabi oscillations under driving. On the experiment we were able to drive the system with intensities up to about $200\, I_{\text{sat}}$ corresponding to a Rabi frequency of $\Omega \lesssim 10\,\Gamma_0$. Thus if collective effects were absent one would observe damped Rabi oscillations, solution to the optical Bloch equations. What we observed instead is that the fluorescence emitted along the superradiant axis does not follow predictions from the optical Bloch equations. We observed an enhanced emission rate during the Rabi flops when ρ_{ee} was large. In essence, despite the fact that the cloud was driven with wavevector $\boldsymbol{k}_{\text{las}} \perp \boldsymbol{u}_x$, some superradiance took place along $\pm\boldsymbol{u}_x$ during the Rabi flops when population was inverted, as shown in figure 6, right. The intensity is given by $I_N = \langle \hat{I}_N \rangle = \langle \hat{E}_N^- \hat{E}_N^+ \rangle$, with $\hat{E}_N^-$ the field emitted by the N atoms. Using the expression of the far-field in the direction $\boldsymbol{u}$: $\hat{E}_N^-(\boldsymbol{u}) \propto \sum_n \hat{\sigma}_n^+ e^{-ik_0 \boldsymbol{u}\cdot\boldsymbol{r}_n}$, one obtains that the far-field intensity along $\boldsymbol{u}_x$ follows :

$$I_N(\boldsymbol{u}_x) = I_1(\boldsymbol{u}_x) \left[\sum_n \langle \hat{e}_n \rangle + \sum_{m \neq n} e^{ik_0(x_m - x_n)} \langle \hat{\sigma}_n^+ \hat{\sigma}_m^- \rangle \right], \tag{8}$$

with $I_1(\boldsymbol{u}_x)$ the emission pattern of a single atom (dipole radiation). So from this expression one sees that measuring an intensity dynamics that differs from that of the population ($\rho_{ee,\,n} = \langle \hat{e}_n \rangle$) means that *correlations* increase the intensity. This is due to the second term in eq. (8) that expresses interferences in the atomic dipole radiations. On the other hand, figure 6, left, shows that the fluorescence emitted perpendicularly to the cloud axis (but not along the excitation laser) was unchanged with respect to the single atom case. Using our cloud dimensions, one can show that when collecting light perpendicularly from the cloud, the contribution from correlations (second

term in (8)) is completely negligible and one should observe only population. Our observations showed that the dynamics of population is only weakly modified with respect to the single atom case.

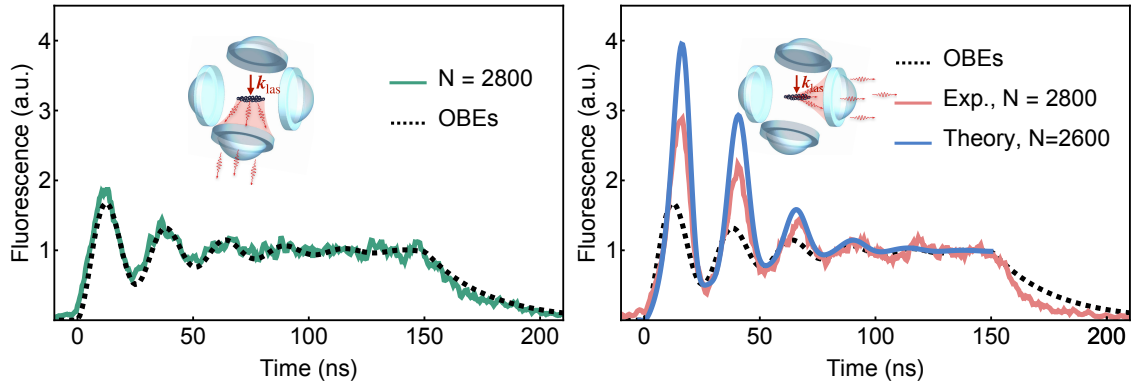

Figure 6 – **Driven superradiance.** Left : Fluorescence collected perpendicular to the cloud axis which measures atomic population (see text), while the cloud is continuously driven starting from $t = 0$. The dynamics of atomic population is in agreement with the prediction of optical Bxloch equations (dashed) showing that collective effects do not modify strongly atomic population. Right : Fluorescence along the cloud axis. A clear enhancement of fluorescence is observed during the Rabi flops witnessing the growth of atomic correlations, due to Dicke superradiance when population is inverted during Rabi oscillations. The blue solid line shows the result of second-order cumulant expansion theory without any adjustable parameter. Data adapted from [Ferioli et al., 2021b].

Quantitative predictions of the measured intensity are very challenging to obtain since they require accounting for the full density matrix of the atomic degrees of freedom of thousands of 2-level atoms. That is of course beyond reach, and approximations need to be made. We collaborated with Francis Robicheaux and Tyler Sutherland who had developed useful approximations to numerically solve the master equations with the right number of atoms and the exact spatial distribution. The code developed by Francis uses the cumulant approximation, which is an expansion in terms of order of correlations [Robicheaux & Suresh, 2021, Plankensteiner et al., 2022]. One truncates the expansion at a given order by assuming that the *cumulant* as defined in [Kubo, 1962] is zero at that order. They found the following : If one assumes at the lowest order that the second cumulant $\langle\hat{\sigma}_n^+\hat{\sigma}_m^-\rangle_c = \langle\hat{\sigma}_n^+\hat{\sigma}_m^-\rangle - \langle\hat{\sigma}_n^+\rangle\langle\hat{\sigma}_m^-\rangle$ is equal to zero for any two-atom correlator (mean-field approximation [3]), the experimental data cannot be reproduced. To reproduce our observations (figure 6) and in particular the enhancement of intensity during Rabi flops, they had to account for beyond mean-field correlations $\langle\hat{\sigma}_n^+\hat{\sigma}_m^-\rangle \neq \langle\hat{\sigma}_n^+\rangle\langle\hat{\sigma}_m^-\rangle$ by going to the next cumulant order. At this order, for any three operators $\hat{A}$, $\hat{B}$, $\hat{C}$ one performs the replacement [4]

$$\langle\hat{A}\hat{B}\hat{C}\rangle \rightarrow \langle\hat{A}\hat{B}\rangle\langle\hat{C}\rangle + \langle\hat{A}\hat{C}\rangle\langle\hat{B}\rangle + \langle\hat{C}\hat{B}\rangle\langle\hat{A}\rangle - 2\langle\hat{A}\rangle\langle\hat{B}\rangle\langle\hat{C}\rangle, \tag{9}$$

[Ferioli et al., 2021b]. The good agreement with our observations without any adjustable parameter demonstrated remarkably that collective spontaneous emission (here superradiance) is able to establish correlations in a driven system beyond what a classical separable density matrix can

3. This is the so-called mean-field approximation $\langle\hat{\sigma}_n^+\hat{\sigma}_m^-\rangle \rightarrow \langle\hat{\sigma}_n^+\rangle\langle\hat{\sigma}_m^-\rangle$ obtained also by imposing that the density matrix is a product of the individual atomic ones i.e. $\rho_N = \Pi_{\otimes n}\rho_n$.

4. The third cumulant is $\langle\hat{A}\hat{B}\hat{C}\rangle_c = \langle\hat{A}\hat{B}\hat{C}\rangle - (\langle\hat{A}\hat{B}\rangle\langle\hat{C}\rangle + \langle\hat{A}\hat{C}\rangle\langle\hat{B}\rangle + \langle\hat{C}\hat{B}\rangle\langle\hat{A}\rangle - 2\langle\hat{A}\rangle\langle\hat{B}\rangle\langle\hat{C}\rangle)$ [Kubo, 1962].

encompass. These correlations were witnessed as an increase in intensity during early Rabi oscillations. Once the oscillations are damped and we reach steady-state, we observed a flat intensity, which is hard to compare quantitatively with theory. In section **??** I will show that one can witness the presence of correlations in the steady state by performing photon correlation measurements on the field radiated by the atomic clouds.

But first, I will concentrate on a different situation which emerges when the laser prepares directly the right wavevector for superradiance : $\boldsymbol{k}_{\text{las}} \parallel \boldsymbol{u}_x$. In this case, the atoms are directly driven with correlations that enhance the intensity. Superradiance readily counteracts driving and the steady state is the result of a direct competition between the two.

When the driving laser propagates along the cloud ($\boldsymbol{u}_x$), the Rabi frequency for atom n reads $\Omega_n = \Omega_0 e^{-ik_0 x_n}$, which is precisely the same phase as the one induced by superradiance that enhances intensity in eq. (8). It thus sounds like a good approximation to assume that all atomic dipoles $\hat{\sigma}_n^-$ have a fixed phase $e^{-ik_0 x_n}$. This approximation simplifies a lot the description. It is put on firm ground in [Gross & Haroche, 1982]. There it is shown that if one further assumes that only a spin wave is excited, that is : $\langle \hat{\sigma}_n^- \rangle = e^{-ik_0 x_n} \langle \hat{\sigma}^- \rangle$, then one obtains equations for the time evolution of atomic operators that are remarkably simple (see also [Ferioli et al., 2023]). They are the same as the ones that are obtained in the Dicke case (all atoms exactly on top of each other), but with a *reduced atom number* $N \to \tilde{N} = \mu N$ with μ defined in (7).

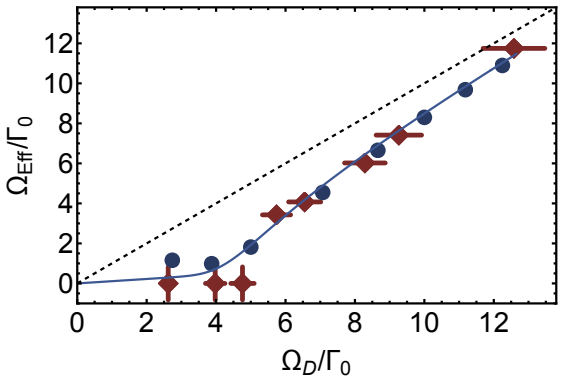

Figure 7 – **Agreement with the Dicke case.** The figure shows the experimentally observed frequency of oscillations of the atomic population (Ω_{eff}, red diamonds), as a function of the Rabi frequency of the drive (Ω_{D} measured at very low atom number). The blue curve (analytical solution) and dots (numerical simulations) show the predictions of what we call here the Dicke model. Figure from [Ferioli et al., 2023].

In [Ferioli et al., 2023], we reported observations of the dynamics and steady state of the excited state population and intensity emitted by the cloud in the conditions of driving along the cloud. We found a stunning agreement with the predictions of the Dicke case with a reduced atom number for nearly all observables, both in the dynamics and in the steady state. We found in particular that the competition between driving and superradiance leads to a transition between two very different states. At low driving (low Rabi frequency), a little bit of population inversion is directly counteracted by superradiance. The result is what we called a *magnetised* state, where all atoms have a dipole in phase with the driving field and proportional to it, and no Rabi oscillations are observed. However, the atomic dipoles cannot become arbitrarily large. As a consequence, increasing

the Rabi frequency of the drive, one reaches a threshold above which damped Rabi oscillations are observed again. This is visible in figure 7, which shows the observed frequency of Rabi oscillations as a function of the Rabi frequency of the drive, displaying a clear threshold above which Rabi oscillations occur. Above the threshold, the steady-state atomic population saturates. In this saturated phase, we observed that the intensity scales as N^2 exactly as predicted by the Dicke model. This observation of *steady state* superradiance is to the best of our knowledge a first in free space. It could allow to make a parallel with superradiant lasers [Norcia & Thompson, 2016, Laske et al., 2019, Schäffer et al., 2020], where steady state superradiance is expected to be used as a resource for metrology. It might be that in the far future, cavity-less steady state superradiance is useable for metrology.

Despite the stunning agreement with the Dicke model, several things are yet to be understood. The mapping with the Dicke model relies on strong assumptions (atomic dipoles with fixed phase, excitation of only a spin-wave), and an understanding of our observations based on a model more faithful to our experimental conditions is still lacking. Investigations are ongoing in the theoretical teams of our colleagues Darrick Chang and Ana-Maria Rey to determine the origin of the agreement. In particular a mean-field description in terms of the Maxwell-Bloch equations should give good predictions of our observations, but a full agreement with our results is yet missing. More extended investigations could reveal the presence of non-trivial correlations.

2.2.5 Photon correlations

The experiments on light scattering that I discussed so far in this manuscript were concerned with measurements of the intensity emanating from the clouds. The emitted light can however be further characterized using a fundamental tool of quantum optics : the measurement of intensity correlations, or second-order coherence [Kimble et al., 1977, Diedrich & Walther, 1987, Loudon, 2000]. The second-order correlation function in steady-state is defined as :

$$g^{(2)}(\tau) = \frac{\langle \hat{E}^-(t)\hat{E}^-(t+\tau)\hat{E}^+(t+\tau)\hat{E}^+(t)\rangle}{\langle \hat{I}(t)\rangle^2}, \tag{10}$$

where $\hat{E}^-(t)$ is the field emitted at time t in steady state and $\hat{I}(t) = \hat{E}^-(t)\hat{E}^+(t)$ the intensity. $g^{(2)}(\tau)$ is proportional to the probability for a photon to be emitted a time $t+\tau$ if one was emitted at t. Experimentally, we measured it by using a fibered beam-splitter and split the light collected from the cloud into two avalanche photo-diodes, realizing the Hanbury-Brown and Twiss configuration [5]. The second-order correlation function is then calculated from the photon arrival times recorded on a time-tagger [Ferioli et al., 2024].

In quantum optics, $g^{(2)}(\tau)$ is used for instance to distinguish between classical quantum light [Loudon, 2000], to characterise single-photon emitters [Gazzano et al., 2013, Aharonovich et al., 2016], or to measure star radii [Hanbury Brown & Twiss, 1956]. Here we are interested in the field radiated by the N atoms. Writing $g_N^{(2)}(\tau)$ in terms of atomic dipoles as in (8) leads to the following :

$$g_N^{(2)}(\tau) \propto \sum_{ijkl} \langle \hat{\sigma}_i^+(t)\hat{\sigma}_j^+(t+\tau)\hat{\sigma}_k^-(t+\tau)\hat{\sigma}_l^-(t)\rangle \, e^{-ik_0\boldsymbol{u}\cdot(\boldsymbol{r}_i-\boldsymbol{r}_j+\boldsymbol{r}_k-\boldsymbol{r}_l)}, \tag{11}$$

where $\boldsymbol{u}$ is the observation direction. This expression shows that $g_N^{(2)}(\tau)$ gives access to correlation

5. This allows to overcome the dead-time of an APD and to detect two photons at the same time.

functions of four atomic operators. In particular, it can directly reveal whether the field (or atomic medium) obeys Gaussian statistics or not. Gaussian statistics are characterized by the fact that all moments of a distribution can be expressed as a function of the first two moments. Expressed in terms of correlation functions, this means that all cumulants [Kubo, 1962] above two are equal to zero : everything depends only on the mean and second-order correlations of operators $\langle \hat{A} \rangle$, $\langle \hat{A}\hat{B} \rangle$. For instance, the approximation of equation (9) used to describe the dynamics of intensity emitted our clouds assumed Gaussian statistics, and was in fair agreement with our data. When measuring $g_N^{(2)}(\tau)$ however, we found that Gaussian statistics cannot explain the experimental data.

To test Gaussian statistics, we used the following fact : if the field obeys Gaussian statistics *and* the average value of the field cancels $\langle \hat{E}_N^- \rangle = 0$, then one should recover the so-called Siegert relation which reads [Siegert, 1943, Lemieux & Durian, 1999, Loudon, 2000, Steck, 2007] :

$$g_N^{(2)}(\tau) = 1 + |g_N^{(1)}(\tau)|^2, \tag{12}$$

where the N-atom first-order coherence function is $g_N^{(1)}(\tau) = \langle \hat{E}_N^-(t)\hat{E}_N^+(t+\tau)\rangle / \langle I_N(t)\rangle$. The Siegert relation has been tested in cold atom platforms [Bali et al., 1996, Grover et al., 2015] and in particular in dilute clouds by measuring both $g^{(1)}(\tau)$ and $g^{(2)}(\tau)$ [Ferreira et al., 2020]. It is typically known to be verified by "chaotic" light emanating from many phase-uncorrelated sources [Carmichael et al., 1978, Loudon, 2000].

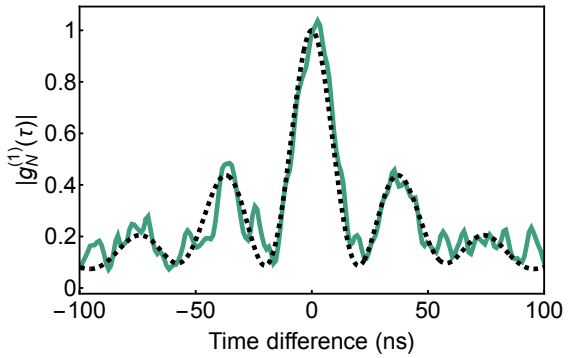

Figure 8 – **First-order coherence** $|g_N^{(1)}(\tau)|$**.** Data measured for a cloud of $N \simeq 2000$ atoms on the experiment (green solid line). The dashed line shows the prediction for a single atom [Steck, 2007], showing good agreement. This demonstrates that no collective effect are observed in first-order coherence, and that the average field cancels : $|\langle \hat{E}_N^- \rangle|^2 / \langle \hat{I}_N \rangle = g_N^{(1)}(\tau \to \infty) = 0$. Data adapted from [Ferioli et al., 2024].

In the experiments of [Ferioli et al., 2024], the cloud was driven perpendicularly to its long axis : $\boldsymbol{k}_{\text{las}} \perp \boldsymbol{u}_x$, again with intensity up to $200\, I_{\text{sat}}$ corresponding to a Rabi frequency up to $10\,\Gamma_0$. We measured both $g_N^{(1)}(\tau)$ and $g_N^{(2)}(\tau)$ from our N atom clouds. These were measured in steady state, after Rabi oscillations discussed above have damped out and intensity is constant in time. To measure $g_N^{(1)}(\tau)$, we used the heterodyne technique described in [Hong et al., 2006], and that was used recently to measure the Mollow triplet in cold atoms [Ortiz-Gutiérrez et al., 2019]. It relies on adding a coherent field to the signal, but detuned from it by a frequency δ, and measuring $g^{(2)}(\tau)$ of this sum. $g^{(2)}(\tau)$ has then several components in frequency, and one component at frequency δ is proportional to $g^{(1)}(\tau)$. With this technique, we found that $g_N^{(1)}(\tau)$ is fully compatible with the prediction for a *single* atom : no collective effects are visible in the first-order coherence function,

figure 8. In addition, for long time one has $g_N^{(1)}(\tau) \to |\langle \hat{E}_N^- \rangle|^2 / \langle \hat{I}_N \rangle$. In the experiment we found that at long times ($\tau \Gamma_0 \gg 1$) $g_N^{(1)}(\tau) \to 0$. This demonstrated that in our clouds, the collective average field cancels $\langle \hat{E}_N^- \rangle = 0$. When we measured $g_N^{(2)}(\tau)$, we observed that the Siegert relation (12) was verified for the field radiated perpendicularly to the cloud (figure 9 left). Along the cloud axis on the contrary, we found a behaviour that did not match expectations for independent atoms : We found that the Siegert relation was violated, and that $g_N^{(2)}(\tau)$ was smaller than the expectation of Siegert, figure 9 right. In particular we found $g_N^{(2)}(0) = 1.65(5)$ and $g_N^{(2)}(\tau) < 1$ at $\Omega\tau \simeq \pi$. Eq. (12) predicts $g_N^{(2)}(0) = 2$ and $g_N^{(2)}(\tau) > 1$ for any τ, in contradictions with the experiment. This finding together with $\langle \hat{E}_N^- \rangle = 0$ implied that the field does not obey Gaussian statistics. It can be easily shown that if the field does not obey Gaussian statistics, it necessarily implies that the atomic medium that radiated the field does not either.

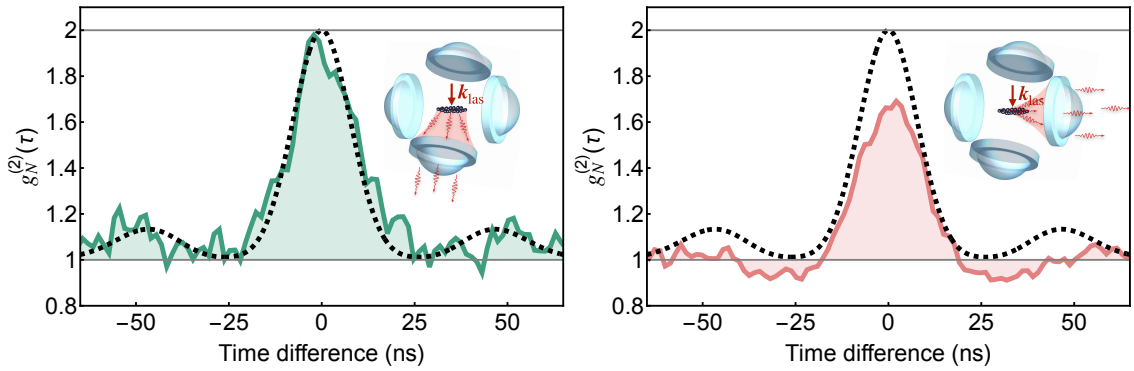

Figure 9 – **Second-order coherence $g_N^{(2)}(\tau)$.** Data measured on a cloud of $N \simeq 2000$ atoms. Left : light collected perpendicular to the cloud axis, showing excellent agreement with the Siegert relation $g_N^{(2)}(\tau) = 1 + |g_N^{(1)}(\tau)|^2$, dashed line. Right : light collected along the cloud axis. We observe clearly a reduction with respect to the Siegert prediction. This data together with that of figure 8 allows us to conclude that the statistics of the light emitted along the cloud axis is non-Gaussian. This also implies that the density matrix of the atomic cloud is non-Gaussian. Data adapted from [Ferioli et al., 2024].

We thus found that the collective, driven dissipative dynamics of a collection of atoms in free space can lead to a steady-state that is non-Gaussian, and therefore hosts non-trivial correlations. This was only very recently proposed for related systems [Stitely et al., 2023, Mink & Fleischhauer, 2023]. Thus far, no theoretical prediction exists for our system. This is particularly the case since we have shown that high-order correlations must be accounted for. Using the cumulant expansion truncated at higher order is likely not going to be possible. This is first because the number of equations grows exponentially with the truncation order, second because the cumulant expansion truncation causes linear equations to become non-linear, which can induce non-physical predictions at high orders. Another numerical tool that was introduced is to use the so-called discrete truncated Wigner approximation (DTWA) which is reviewed for light scattering in [Mink & Fleischhauer, 2023]. One might on the other hand rely on effective models, that do not keep the full physical complexity of the system but can give insight into the physical mechanisms at play. It will be interesting in the future to derive a physical model that is solvable, but keeps the right order of approximation to describe our data.

2.2.6 Prospects

To conclude on this part, I present a few prospects for future research in our group on this platform. The experiments that I described above were performed on the Rb machine first built in 2005, in its 2017 upgraded version. In the summer of 2023 it was decided to switch-off completely this machine. Its advamcing age made it more and more challenging to do state-of-the-art physics and also meant that several devices started to fail simply due to aging, making it hard to keep it running. The decision was made to rebuild a new setup, based on a 2D MOT and a glass cell with external objectives. This was also motivated by the availability of funding as part of the Pasquans 2 program, and also from an EIC pathfinder project PANDA in collaboration with colleagues from ICFO, LKB, and Pasqal. I give below some perspectives for explorations on this new machine, once it is running.

Motivated by our previous works, there are interesting tracks we wish to pursue. First, we showed in [Ferioli et al., 2024] that when the cloud is driven perpendicularly to its long axis $\boldsymbol{k}_{\text{las}} \perp \boldsymbol{u}_x$, the steady-state is non-Gaussian. On the other hand in the situation $\boldsymbol{k}_{\text{las}} \parallel \boldsymbol{u}_x$, it remains debated whether a mean-field (hence Gaussian) approximation describes fully our data. In that latter case, we measured $g_N^{(2)}(\tau)$ finding clearly a disagreement with the Siegert relation. However to establish non-Gaussian statistics requires also to show that $\langle \hat{E}_N^- \rangle = 0$. It would be very interesting to measure it, in order to know if the data discussed in [Ferioli et al., 2023] is indeed all at the mean-field level or not. In general an interesting question about driven-dissipative many-body system is whether the experimental steady-state that we observe where all observables cease to evolve is really the actual steady-state calculated theoretically. Generically, for a drive much stronger than atom-atom interactions, one expects that the driving field overcomes that radiated by surrounding atoms, so that the density matrix is a simple mixed density matrix $\rho_N = [(|e\rangle\langle e| + |g\rangle\langle g|)/2]^{\otimes N}$. Interestingly, our measurements are incompatible with this density matrix, and our results do not seem to depend on the drive strength when $\Omega > \Gamma_0$. The relevant questions are : How high a Rabi frequency is necessary to reach this theoretical steady-state and how long does it take to reach it ? Indeed, there are hints that there could be fast dynamics, followed by a much slower one [Ostermann et al., 2023, Mink & Fleischhauer, 2023]. The density matrix during this intermediate stage could be less trivial than the steady-state one.

Second, while we have demonstrated in our experiments that the Wigner function of the field and the atomic sample are non-Gaussian (in one case), we have not actually measured the Wigner function. Measuring the field quadratures in a homodyne setup would allow to measure the field Wigner function. Open questions are : what is the Wigner function, and is it negative ? Indeed, non-Gaussian quantum states (Wigner negative) are a vital resource for quantum computing with photons [Walschaers, 2021], and it is an important direction of research to learn how to generate them efficiently. It is worth pursuing an effort in our platform to determine if quantum non-Gaussian states can be generated. This is one goal of the PANDA project we are pursuing together with Pasqal, ICFO and LKB. From a many-body perspective, the many-body state is quite hard to calculate. It is known that when the system features Dicke symmetry, it is squeezed when approaching the Dicke transition from a small driving strength [Hannukainen & Larson, 2018, Buonaiuto et al., 2021, Somech & Shahmoon, 2022]. Whether this squeezing survives when the Dicke symmetry is broken such as is the case in our experiment is still an open question. Measuring squeezing in the medium requires to have access to several projections of the spin. It is relatively challenging to perform these rotations on our clouds faster than collective decay and it might require some dedicated upgrades on the driving laser control. One could also think of a way to perform this spin squeezing on an atomic species with richer transition spectrum, such as Dy, and it might be a

possibility to explore on our new setup.

Finally, when studying subradiance, we have been interested in the preparation of subradiant states, with the highest possible efficiency. Using our general pumping scheme, [Ferioli et al., 2021a], we were preparing the system incoherently, with about 10% of the excitations in the medium found to be stored in subradiant states. We found that these states were populated in part directly by the driving laser (but inefficiently), in part by repeated cycles through superradiant states that partially decayed to subradiant ones in a mechanism akin to optical pumping [Glicenstein et al., 2022]. This confirmed similar observations in dilute clouds by our colleagues in Nice [Cipris et al., 2021]. In general, preparing subradiant excitations is attracting growing interest, since they have been identified as possible quantum memories [Ballantine & Ruostekoski, 2021, Rubies-Bigorda et al., 2022, Fayard et al., 2023]. One interesting perspective is to try to tune the wave-vector of the excitation that we create. Indeed if one creates an excitation with wave-vector k larger than $k_0 = \omega_0/c$, then it should not be able to decay in vacuum, see also discussion in arrays below. Remarkable experiments by [He et al., 2020] in the group of Saijun Wu at Fudan university have demonstrated a way to engineer the wave-vector of the excitations using multiple pulses on an auxiliary transition. It would for sure be interesting to test wether in a dense gas this could lead to an efficient preparation of a few subradiant excitations.

2.3 The new Dy platform

The new experimental activity on Dy was started with the hiring of Damien Bloch as a M2 intern and then PhD student in 2021. He was joined for one year by Samuel Cohen, a Master intern from Princeton, now doing a PhD in Stanford. In 2022, Britton Hofer joined the team as M2 intern and then graduate student. The results that are presented below are the product of their hard work, under my supervision with input from Antoine.

The building of a new platform with a new atomic species was part of the research project on which I was recruited at CNRS. After two years of discovering the topic of light scattering, I was able to mature a project and the characteristics that we wanted for this new setup, I present them below. It has allowed our group to open a new research direction, and develop new techniques.

In this new setup, we wanted to apply the techniques of quantum simulation with arrays of single atoms in tweezer arrays developed by the group [Nogrette et al., 2014, Labuhn et al., 2016, Barredo et al., 2016] to the problem of collective light-matter interactions in dense atomic ensembles. In particular, the tweezers platform allows to fully control the sample geometry and to measure in a single shot the internal state of each atom. In the case of light scattering, one typically does not access directly the internal state, but only the radiated light. However, the theory of light scattering in free-space atomic ensembles requires to calculate the atomic state, and then the field is calculated as a result of the atomic state. It thus is desirable to obtain single-shot readout of the atomic state in light-scattering samples. One challenge in adapting the tweezers platform to this task is that the typical interparticle distance that one obtains is on the order of 1.5 µm at the shortest. However for light scattering in ordered arrays, the distance required to reach a strong light-array coupling is tyically $\lambda_0/2 \lesssim 400\,\text{nm}$. These considerations set the requirements for the new setup that we wished to build : A single atom tweeezer platform with access to the internal dynamics of individual atoms, and short spacings to reach strong couplings.

To meet these requirements, one needs an atomic structure that allows to drive a two-level transition, and to project the atomic state faster than the dynamics on the two-level transition.

This is met with a structure with a narrow(ish) two-level transition, possibly with long wavelength, and a broad transition, which can serve as a projector of the atomic state by scattering photons from the ground state at a high rate. Furthermore, to reduce the atomic spacing, it is desirable to be able to trap with a blue wavelength, affording a small diffraction-limited tweezer size, or a short spacing for an optical lattice. Hence a structure where a V-shaped subset can be isolated, with one arm being a broad, blue transition, and the other arm a narrow, red or infrared transition. Such structure can be found in several species that were already laser-cooled : in particular two-electron atoms Sr, Yb, and lanthanides Er, Dy. Sr and Yb could have been an interesting choice, but finding long wavelength transitions requires to excite atoms to metastable states, which increases the complexity of the experimental setup. Lanthanides offer interesting V-shaped structures from the ground state. Besides, single lanthanide atoms had never been trapped in optical tweezer arrays, this suggested that interesting atomic physics studies were open to achieve this goal. Thus, with in mind to develop an original direction of research, we decided for a lanthanide species, and given my experience, we picked Dy, whose atomic structure is shown in figure 10. I present below the experimental setup, detailed in [Bloch et al., 2024].

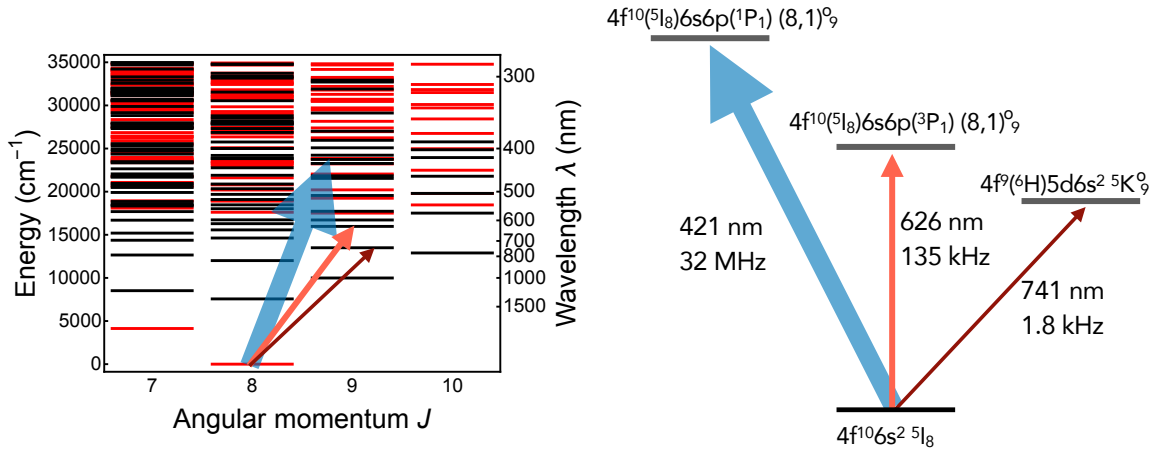

Figure 10 – **Dysprosium levels and transitions.** Left : Level diagram of Dy, showing the high number of transitions available (black/red : even/odd parity). The three transitions relevant to our experiments are shown as arrows and represented on the right. Right : details of the atomic states used and the transitions characteristics. The 626 nm tranisition is used for cooling and imaging in the optical tweezers, the 421 nm one is used for the 2D MOT and fast internal-state readout. The 741 nm one will be used soon for sideband cooling and light scattering.

2.3.1 The machine

To trap and image single atoms, the combination of a glass cell and a microscope objective has emerged as a versatile solution offering high optical access and compactness [Endres et al., 2016, Norcia et al., 2018, Cooper et al., 2018, Saskin et al., 2019]. We decided that such platform is a good choice for lanthanide atoms to perform single atom trapping and imaging in tweezers. It also allowed the group to learn new techniques that we did not have in-house. One experimental challenge faced in adapting these setups to lanthanides such as Er or Dy is that any surface in line of sight of the atomic oven will be coated by the high atomic flux due to their very high melting point. This prevents placing a glass surface or glass cell along the oven atomic jet. In order to

directly load a glass cell, the solution we implemented is a 2D MOT of Dy that we developed, collaborating in particular with Lauriane Chomaz at Heidelberg University. It serves as a continuous source of cold Dy atoms pushed towards the glass cell. This alleviates the need for optical transport and so ensures high experiment repetition rates ($> 1\,\mathrm{Hz}$).

For the first laser cooling stages, we use the broad blue transition of Dy between the ground state manifold ($4f^{10}6s^2\ {}^5I_8$) and the excited state $4f^{10}({}^5I_8)6s6p({}^1P_1^o)\ (8,1)_9^o$. Its wavelength is $\lambda = 421\,\mathrm{nm}$ and its linewidth is $\Gamma_{421} = 2\pi \times 32\,\mathrm{MHz}$. We also make use of the narrower intercombination line at $\lambda = 626\,\mathrm{nm}$ with excited state $4f^{10}({}^5I_8)6s6p({}^3P_1^o)\ (8,1)_9^o$ with linewidth $\Gamma_{626} = 2\pi \times 135\,\mathrm{kHz}$. This transition allows us to realise a 3D MOT and to image the atoms in the optical tweezers. The optical tweezers themselves are realised with far-detuned light at 532 nm, focused by a microscope objective with numerical aperture 0.5.

2.3.2 Dy polarizability at 532 nm and Dy atoms in magic optical tweezers

To image multi-electron atoms in optical tweezers, one typically has the choice between a broad ($\Gamma \sim (2\pi)\,30\,\mathrm{MHz}$) and a narrow transition ($\Gamma < (2\pi)\,1\,\mathrm{MHz}$). Due to the high Doppler temperature, imaging on the broad transition requires either very deep traps (few mK) or simultaneous cooling on the narrow transition. On the other hand the narrow line solution is slower due to a lower scattering rate but allows for shallow traps and produces much lower temperatures. In Dy we had the choice between one broad (421 nm, 32.5 MHz) and two narrow transitions (626 nm, 135 kHz or 741 nm, 1.8 kHz).

On our setup, we have tried to image single Dy atoms on the blue transition, without success. Large losses induced by the imaging light seemed to make it impossible to image faithfully single atoms. We then focused on imaging with the intercombination transition. One important aspect of imaging on a transition with linewidth on the order of 100 kHz (such as the intercombination line of Yb [Saskin et al., 2019, Ma et al., 2022]) is that it requires magic trapping : an identical light shift for the ground and excited state of the transition. Naively, there is little chance that 532 nm would be a magic wavelength. But in fact lanthanides possess a very anisotropic coupling to light, in the form of strong vector and tensor polarizabilities, giving hope to find a magic trapping by tuning the trap light polarization [Lepers et al., 2014, Kao et al., 2017, Becher et al., 2018]. Indeed it was shown for instance by [Chalopin et al., 2018] that at 1070 nm, one can employ the tensor polarizability to tune the light shift of the excited state to make it equal to that of the ground state.

To measure all the different polarizablities of the ground and excited state and look for a magic condition at 532 nm, we had to pay particular attention to avoid large systematic errors, that can arise if one miscalibrates the trap intensity. Indeed, the polarizability is extracted by measuring the trap depth or trapping frequencies, assuming the trap beam intensity is known. An error on the actual laser waist at the position of the atoms can lead to a large miscalibration of the intensity, and thus a wrong value of the polarizability. To suppress this source of error, we performed measurements both of the trap depth (U_0) and radial trap frequency (ω_r), and we use the fact that the ratio U_0/ω_r does not depend on the trap waist. To obtain the trap depth, we accelerated tweezers up to a given velocity v_g before stopping them abruptly. If $mv_g^2/2 > U_0$, the atoms leave the trap, if not they stay (see figure 11 left). We could thus obtain a precise value of the polarizability. We found a scalar polarizability in the ground state that disagrees with theoretical expectations from Maxence Lepers's calculations [Li et al., 2016]. This disagreement remains to be understood. The other polarizabilities (vector, tensor and in the excited state) agree with theory. A fortunate consequence of our data disagreeing with theory is that we concluded that there exists a polarization for which the transition between $m_J = -8$ in the ground state and $m_J = -9$ in the excited state

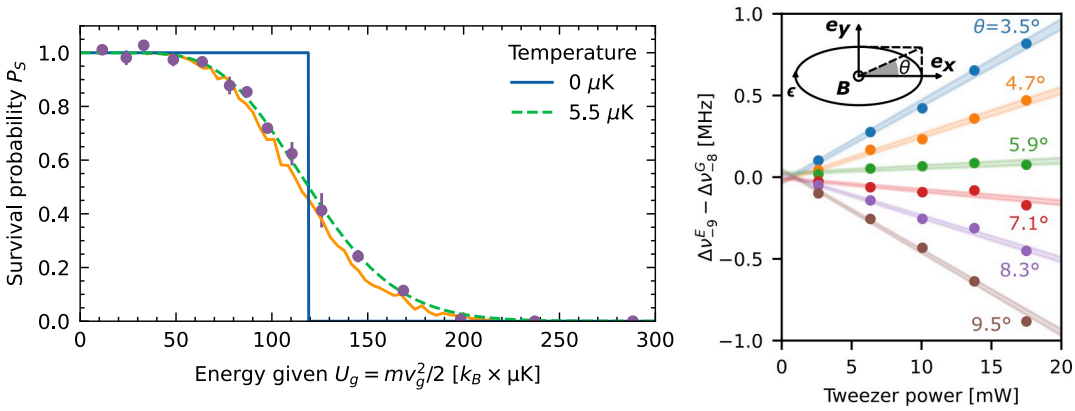

Figure 11 – **Dy polarizability measurements**. Left : Measurement of the trap depth. A tweezer is accelerated to a velocity v_g before it is stopped. We then measure the probability for the atom to remain in the trap, at different kinetic energy $mv_g^2/2$. If the kinetic energy overcomes the trap depth, the atom is expelled from the trap, otherwise, it is re-imaged. The atomic temperature in the trap smoothens the data (circles). The theory for 5.5 μK (dashed green : analytical, orange solid : numerical) is in excellent agreement with our measurements, allowing to extract a trap depth of 120 μK. Right : Light shift for different polarizations of the trap. The data show the shift in frequency between $|g\rangle$ and $|e\rangle$ in a tweezer, as a function of power in the tweezer beam. By changing the ellipticity parameter θ, we are able to find a *magic condition* ($\theta^* \simeq 6°$) for which the transition frequency is independent of tweezer power. Figure from [Bloch et al., 2024]

is magic. To obtain this, we employed the vector polarization in the excited state which is relatively large, and we found that for an elliptical polarization, the transition is magic (figure 11 right).

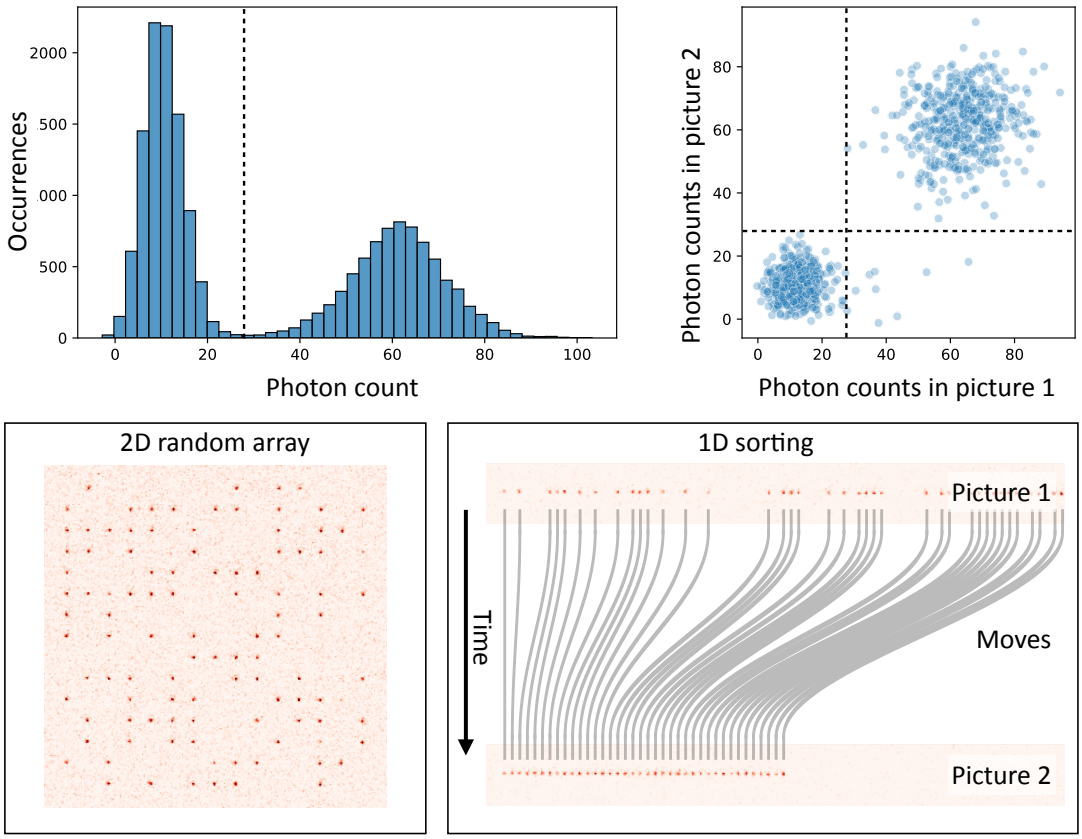

Figure 12 – **Dysprosium single atom imaging.** Top left : Histogram of the number of detected photons for 1 trap, showing a bi-modal distribution with a peak corresponding to background fluorescence in the absence of an atom, and the second peak corresponding to an atom being present. Top right : photon counts when imaging twice subsequently a trap. The threshold (dashed line) allows to diagnose the presence or absence of an atom in the trap. In some cases, the photon count in a first picture is above the threshold, corresponding to an atom being present in the trap, but in a subsequent picture, the count is below the threshold, indicating that the atom has left the trap or is in a metastable state that is not imaged. Bottom left : Fluorescence image in a 15x15 array of traps, randomly loaded with Dy atoms. The inter-trap spacing is about 4 µm. Bottom right : Sorting an ordered 1D chain (picture 2) starting from a randomly loaded chain (picture 1) by moving the traps containing atoms to fill the gaps. The traps are moved in 500 µs, using the method of [Endres et al., 2016].

Thanks to this, we are able now to image single atoms of Dy on the 626 nm transition, which we reported in [Bloch et al., 2023]. This imaging has a fidelity higher than 99 % and losses induced by imaging are as low as 2 %, see figure 12. We have observed that these imaging-induced losses are in large part ($\approx$ 1.3 %) due to decay to metastable state(s) in which the atoms are trapped and decay back to the ground state after hundreds of milliseconds. We ascribe the remaining (0.7 %) to losses to untrapped state(s) from which the atoms are lost. We have shown that the metastable

states are populated by a two-photon event : one photon at 626 nm is absorbed, and while in the excited state, the atoms absorbs a trap photon at 532 nm. The precise transition responsible for this second step is not yet determined. There exists numerous dipole-allowed transitions from the excited state, in particular very broad transitions in the blue. It is likely that such losses make it impossible to image with blue light : the blue transition excites to a higher-lying excited state in a region where more transitions exist, and the trap is much deeper which increases the rate of further excitation. In general, to reduce these losses it seems a better choice to use tweezers with a long wavelength, so that less transitions lie close. But since we reach losses down to 2 %, our 532 nm tweezers performed satisfyingly and we proceeded with further steps on the experiment.

2.3.3 Prospects

Our first goal, obtaining single Dy atoms in optical tweezers, was achieved. It was a first for lanthanides. With a 2D acousto-optic deflector, we can create 2D arrays of traps. We are also able to create a 1D chain by sorting a randomly loaded one, as was demonstrated in [Endres et al., 2016]. Thanks to the relatively small wavelength of the traps, we can create a chain with a spacing down to $1.5 \times \lambda_0 \approx 940\,\text{nm}$, with $\lambda_0 = 626\,\text{nm}$. At these distances, collective effects should already occur [Sutherland & Robicheaux, 2016]. We can thus in the coming months perform first studies on the intercombination transition.

Another goal of the platform is to be able to readout the atomic state in a single shot. For this we rely on the broad blue transition. It offers a high scattering rate, with a linewidth 240 times larger than the intercombination line. Thus it can scatter photons very fast in a time where the dynamics on the narrow line is frozen. Naively, to readout the atomic state on a narrow transition, one would *image* on the blue transition. But for Dy, we have observed that imaging in-trap on the blue is not an option. Besides, given the finite numerical any imaging system, a large number of photons is lost (typically 80 - 90 %) when imaging, requiring the atoms to scatter a large number of photons (typically at least 200).

However, one needs less blue photons to perform a measurement. In the experiment, we rely on *depumping* the atoms out of the ground state. The narrow transition is driven between $|g\rangle = |J = 8, m_J = -8\rangle$ and $|e\rangle = |J' = 9, m'_J = -9\rangle$. It is the same transition as is used for imaging. To measure the atomic state, a pulse of blue light with π-polarization is applied. In this case, simulations of the optical Bloch equations for the $J = 8$ to $J' = 9$ system show that in about 150 ns, atoms can be optically pumped out of $|g\rangle$ to other Zeeman states $|J, m_J\rangle$ with m_J close to 0. These states have a different transition frequency, and when we take an image at 626 nm, atoms in these states are not imaged. If an atom is in $|e\rangle$, it is shelved from the blue light [Nagourney et al., 1986, Sauter et al., 1986]) and hence remains in $|e\rangle$. After the blue pulse, it will decay back to $|g\rangle$, and will be imaged in a subsequent image. Thus this image measures in a single shot the $|e\rangle$ excitations. By performing this sequence on the experiment, we indeed find that about $> 95\,\%$ of the $|g\rangle$ atoms are not re-imaged after an 150 ns. On the other hand, more than 90 % of $|e\rangle$ atoms are re-imaged. Thus with this technique, we have obtained single-shot state readout, with a fidelity of about 90 %, a second major goal of this platform.

Next, we have two milestones ahead of us. First, we wish to address a second narrow transition, the one from the ground state to the excited state $4f^9(^6H^0)5d6s^2(^3P_1^o)\ 5K_9^o$, at $\lambda = 741\,\text{nm}$ with linewidth $\Gamma = (2\pi)\,1.8\,\text{kHz}$. The first advantage of this transition is that it has a longer wavelength, hence allowing for stronger collective effects at a given distance d, since those scale as λ/d. Its second advantage is that it will allow for a very high-fidelity state readout as the lifetime of the

excited state is $\sim 88\,\mu s$. Furthermore, this narrow linewidth should place us in the resolved-sideband regime $\Gamma/\omega_{trap} \ll 1$, and we might perform sideband cooling to the ground state [Diedrich et al., 1989]. In the lab, we just received the laser and a high-finesse, ultrastable cavity for its frequency lock. The experimental work to lock the laser on the cavity and find the first excitation signal on the atoms is ongoing. Eventually, we plan on performing light-scattering studies on this transition. For this, atoms have to be held in a magic trapping optical potential, in the Lamb-Dicke regime so that Doppler broadening is suppressed by Dicke narrowing [Ludlow et al., 2015]. We will thus have to identify magic trapping conditions, that can function at interatomic distances down to about 300 nm to be below half the wavelength.

Such low distances are reachable only in an optical lattice and not in a tweezer array. The following milestone of the experiment will thus be to transfer atoms from optical tweezers to an accordion lattice [Mitra et al., 2016, Ville et al., 2017] whose spacing ($d = \lambda_{lattice}/(2\sin\theta)$, with θ the half-angle between the two interfering beams) can be changed from $\sim 1.5\,\mu m$ to catch atoms from the tweezers down to a distance smaller than $\lambda_0/2$ with $\lambda_0 = 741\,nm$, in the interesting regime for light scattering. An optical lattice with fixed polarization can be obtained only with purely linearly polarized beams. This requires to find a wavelength for which magic trapping occurs only relying on the scalar and tensor polarizabiilities [Chalopin et al., 2018] (the vector contribution cancels for linear polarization). In this prospect, we obtained from Maxence Lepers calculations of the polarizability of the ground and excited state (of the 741 nm transition) for trap wavelengths below 500 nm, and there might be several opportunities. One particularly interesting region lies around $\lambda_{lattice} = 440\,nm$ where in principle magic trapping could be found. This is quite promising since upgrading the microscope objective to an NA of 0.7 ($\sin\theta \leqslant 0.7$) would yield $d \gtrsim 320\,nm$, within the interesting range. This implies also adding a blue trapping laser on the experiment, which we plan to do in the coming year.

Realizing these milestones on the experiment will represent a large amount of work. Once they are reached, we will study collective dissipation in ordered arrays. With an atomic spacing below λ_0, there is already very interesting physics to explore in collective light scattering by an array [Bettles et al., 2016b, Shahmoon et al., 2017, Rui et al., 2020]. In a 1D ordered chain, if we can create excitations with a wavelength $\lambda_{exc} < \lambda_0$ they will not be able to decay in vacuum perpendicularly to the chain ($k_{exc} = 2\pi/\lambda_{exc} > \omega_0/c$) and can decay only at the ends of the chain. These excitations are hence predicted to be very long-lived [Bettles et al., 2016a, Asenjo-Garcia et al., 2017, Perczel et al., 2017] and could lead to metrological enhancement [Ostermann et al., 2013] in Ramsey spectroscopy. Our setup will be also particularly suited to study in-situ how collective spontaneous emission can build up correlations [Henriet et al., 2019], and how correlations emerge in a driven system in general.

2.4 Publications

Again, I reproduce here a selected number of publications from my work in Palaiseau, the complete list can be found at the end of this report in section 3.9.

Conclusion

This report summarizes the work that I have carried out in the 10 past years, following my PhD. Throughout these years, I have used the tools of laser cooling to experimentally study correlated ensembles of atoms. Since working as a permanent member at laboratoire Charles Fabry, I have encountered and explored the topic of collective light scattering in atomic ensembles. This field originates from decades-old, fundamental studies of collective light-matter interaction in quantum mechanics. It is nowadays pushed forward by the advent of novel techniques in atomic physics, and the promises of quantum technologies which call for novel light-matter interfaces. Current trends in our community focus greatly on quantum computing, which drives technical progresses at a fast pace. I hope we will be able to continue to make use of these progresses to tackle interesting fundamental problems in physics, along some of the lines that I have presented as prospects in the sections above.

All this is possible thanks to the students and postdocs that we have in the lab, I have highlighted in each section the persons who have been leading the effort. Supervising junior researchers is a very enjoyable part of my occupation, and has motivated me to obtain the *Habilitation à diriger des recherches*. Since the beginning of my career I am also involved in teaching, nowadays at the Institut d'Optique. It is very rewarding on its own, and it is also an inspiration for research as well as a way to meet new bright students who might join the team in the future. Now that my research activity has developed, I wish to be able to continue contributing to teaching. More details on my activities can be found in the administrative data below.

3 Administrative data

3.1 Research career

Oct. 2018 - present, Chargé de recherche de classe normale, CNRS.
Laboratoire Charles Fabry, CNRS, Institut d'Optique, Université Paris Saclay.
Palaiseau, France.
Dec. 2014 - Aug. 2018, Post-doctoral researcher, "group leader".
5. Physikaliches Institut, Stuttgart University, group of Tilman Pfau.
Stuttgart, Germany.
Sep. 2011 - Oct. 2014, Graduate student.
Laboratoire Kastler-Brossel, ENS Paris, advisors : Christophe Salomon and Frédéric Chevy.
Paris, France.

3.2 Teaching experience

2018 - present, Stuttgart University.
Graduate Lectures : Ultracold Atoms and Quantum Simulators. Undergraduate exercise sessions : Mathematics for physicists. Total $\sim 40\,\mathrm{h}$/year.
2015 - 2018, Institut d'optique Graduate School, Université Paris Saclay.
Graduate Lectures : Atomic physics and quantum gases. Undergraduate exercise sessions : Atomic physics, linear optics and non-linear optics. Total $\sim 40\,\mathrm{h}$/year.
2011 - 2014, ENS Paris, Université Paris Saclay.
Undergraduate experimental lab : Atomic physics, quantum optics. Undergraduate exercise sessions : Special relativity and E&M. Total $64\,\mathrm{h}$/year.

3.3 Education

2011-2014, PhD, ENS Paris, France.
Title : Mixtures of Bose and Fermi superfluids. Advisors : Christophe Salomon and Frédéric Chevy.
2010-2011, Master 2, ENS Paris, France.
Quantum Physics program.
2009-2010, Master 1, UC Berkeley, USA.
Education Abroad Program, exchange with Université Joseph Fourier.
2005-2009, Bachelor in Physics, Université Joseph Fourier, Grenoble, France .

3.4 Awards

Grand Prix Jacques Herbrand, French academy of sciences, 2022.
Prix Jeunes Chercheurs, IFRAF/GDR atomes froids, 2015.

3.5 Research contracts

Principal Investigator Grants

ERC Starting Grant, CORSAIR. European Commission, 1.5 M€, 2022 - 2026.
ANR JCJC, DEAR. Agence Nationale de la Recherche, 450 k€, 2021 - 2025.
Petit équipement grant, DSHAPE. DIM Sirteq, 25 k€, 2019 - 2022.
Marie Sklodovska-Curie Fellowship, DipInQuantum. European Union, 2016 - 2018.

Main collaborations

The Quantum Optics - Atoms team is part of several collaborations, I list here the ones in which I participate actively.

EIC Pathfinder, PANDA, European Union. DIM Sirteq, Coordinator : Nicolas Treps, Laboratoire de Kastler-Brossel. Consortium : LCF, LKB, ICFO, Pasqal, 2024 - 2028.

Moyen équipement grant, FSTOL. DIM Sirteq, Coordinator : Martin Robert de Saint Vincent, Laboratoire de Physique des Lasers, 2020 - 2023.

Others : Pasquans2.1 (European unin) QubitAF (PEPR Quantique).

3.6 Supervision

Postdocs

At Laboratoire Charles Fabry (co-supervised with Antoine Browaeys).

Giovanni Ferioli, Rubidium project, 2020-2023. Now at LENS, Florence.

Antoine Glicenstein, Rubidium project, 2022. Now at InPhyNi, Nice.

Graduate students

At Laboratoire Charles Fabry (co-supervised with Antoine Browaeys).

Adrien Gavalda, 2024-present, Rubidium, defense planned for spring 2027. CIFRE collaboration with Pasqal.

Britton Hofer, 2022-present, Dysprosium project, defense planned for fall 2025.

Sara Pancaldi, 2022-present, Rubidium project, defense planned for fall 2025.

Damien Bloch, 2021-present, Dysprosium project, defense planned for fall 2024.

Antoine Glicenstein, 2018-2022, Rubidium project, *'Collective spontaneous emission from dense ensembles of two-level atoms'*. Now postdoc at InPhyNi group of Robin Kaiser, Nice, France.

At Stuttgart University (co-supervised with Tilman Pfau).

Fabian Bötcher, 2016-2018, *'Supersolid Arrays of Dipolar Quantum Droplets'*.

Matthias Wenzel, 2014-2018, *'Macroscopic states of dipolar quantum gases'*.

Matthias Schmitt, 2014-2017, *'A self-bound quantum liquid of Dysprosium atoms'*.

Master and bachelor students

Master 2 students at LCF : Guillaume Tremblier (Université Paris Saclay), Yannis Bencherif (ENS Lyon), Valère Sautel (Université Paris Saclay), Britton Hofer (Telecom Strasbourg), Damien Bloch (ENS Paris Saclay), Maxime Lecomte (ENS Paris Saclay).

Master 1 students at LCF : Mogens From (Danish Technical University)'.

Bachelor students at LCF : Inés Vergara (Supoptique), Guillaume Chapelant (Supoptique), Matthis Brossaud (ENS Paris Saclay).

Other bachelor and master students at Stuttgart University.

3.7 Community service

Organisation of scientific events

Lecture series of the Quantum Saclay center, 2023 - present. Coordination with Sylvain Ravets and Benoit Valiron,

Mini-colloquim on latest advances in quantum technologies, Paris, France, 2023. Coordinator.
School on quantum physics with atoms and photons, Les Houches, France, 2023. Coordination with Sylvain Ravets and Quentin Glorieux.

Referee service

Physical Review Letters, Physical Review X, Physical Review A, Science, Nature, Nature Physics, New Journal of Physics, Optics Express, Europhysics Letters, Applied Physics B, Physics Letters A.

3.8 Outreach

2019-2023 Organizer of the open days for the Fête de la Science" at Institut d'Optique.
2011-2014 Organization and supervision of scientific weeks for high-school students in the Paris area offered by the association "Science ouverte".

3.9 Complete list of publications

Perspective pieces

1. *Ultradilute Quantum Droplets*,
   I. Ferrier-Barbut.
   Physics Today **72**, 46 (2018)
2. *Quantum liquids get thin*,
   I. Ferrier-Barbut and T. Pfau.
   Science **359**, 274 (2018)
3. *Smashing magnets*,
   I. Ferrier-Barbut.
   New J. Phys. **8**, 111004 (2016)

At LCF

1. *Anisotropic polarizability of Dy at 532 nm on the intercombination transition*,
   D. Bloch, B. Hofer, S. R. Cohen, M. Lepers, A. Browaeys and I. Ferrier-Barbut.
   In preparation.
2. *Non-Gaussian correlations in the steady-state of driven-dissipative clouds of two-level atoms*,
   G. Ferioli, S. Pancaldi, A. Glicenstein, D. Clément, A. Browaeys and I. Ferrier-Barbut.
   Phys. Rev. Lett. **132**, 133601 (2024), ArXiv:2311.13503.
3. *Trapping and Imaging Single Dysprosium Atoms in Optical Tweezer Arrays*,
   D. Bloch, B. Hofer, S. R. Cohen, A. Browaeys and I. Ferrier-Barbut.
   Phys. Rev. Lett. **131**, 203401 (2023), ArXiv:2307.04689.
4. *Optical control of collective states in one-dimensional ordered atomic chains beyond the linear regime*,
   N. Fayard, I. Ferrier-Barbut, A. Browaeys and J.-J. Greffet.
   Phys. Rev. A **108**, 023116 (2023), ArXiv:2212.13022.

5. *A non-equilibrium superradiant phase transition in free space*,
G. Ferioli, A. Glicenstein, I. Ferrier-Barbut and A. Browaeys.
Nature Physics **19**, 1345 (2023), ArXiv:2207.10361.
6. *From superradiance to subradiance : exploring the many-body Dicke Ladder*,
A. Glicenstein, G. Ferioli, A. Browaeys, and I. Ferrier-Barbut.
Optics Letters **45**, 1542 (2022), ArXiv:2112.10635.
7. *Laser-Driven Superradiant Ensembles of Two-Level Atoms near Dicke Regime*,
G. Ferioli, A. Glicenstein, F. Robicheaux, R.T. Sutherland, A. Browaeys, and I. Ferrier-Barbut.
Phys. Rev. Lett. **127**, 243602 (2021), ArXiv:2107.13392.
8. *Storage and release of subradiant excitations in dense atomic clouds*,
G. Ferioli, A. Glicenstein, L. Henriet, I. Ferrier-Barbut and A. Browaeys.
Phys. Rev. X **11**, 021031 (2021), ArXiv:2012.10222.
9. *Preparation of one-dimensional atomic chains and dense cold atomic clouds with a high numerical aperture four-lens system*,
A. Glicenstein, G. Ferioli, L. Brossard, Y. R. P. Sortais, D. Barredo, F. Nogrette, I. Ferrier-Barbut and A. Browaeys.
Phys. Rev. A **103**, 043301 (2021), ArXiv:2101.07544.
10. *Many-body signatures of collective decay in atomic chains*,
S. J. Masson, I. Ferrier-Barbut, L. Orozco, A. Browaeys and A. Asenjo-Garcia.
Phys. Rev. Lett. **125**, 263601 (2020), ArXiv:2008.08139.
11. *Collective shift in resonant light scattering by a one-dimensional atomic chain*,
A. Glicenstein, G. Ferioli, N. Sibalic, L. Brossard, I. Ferrier-Barbut, and A. Browaeys.
Phys. Rev. Lett. **124**, 253602 (2020), ArXiv:2004.05395.

Postdoc in Stuttgart

11. *Dipolar physics : A review of experiments with magnetic quantum gases*,
L. Chomaz, I. Ferrier-Barbut, F. Ferlaino, B. Laburthe-Tolra, B. L. Lev and T. Pfau.
Rep. Prog. Phys. **86** 026401 (2023), ArXiv:2201.02672.
12. *Quantum correlations in dilute dipolar quantum droplets beyond the extended Gross-Pitaevskii equation*,
F. Böttcher, M. Wenzel, J-N. Schmidt, M. Guo, T. Langen, I. Ferrier-Barbut, T. Pfau, R. Bombin, J. Sanchéz-Baena, J. Boronat, F. Mazzanti.
Phys. Rev. Res. **1**, 033088 (2019), ArXiv:1904.10349.
13. *A fermionic impurity in a dipolar quantum droplet*,
M. Wenzel, T. Pfau and I. Ferrier-Barbut.
Physica Scripta **113** 104004 (2018), ArXiv:1807.00631.
14. *Anisotropic superfluid behavior of a dipolar Bose-Einstein condensate*,
M. Wenzel, F. Böttcher, J. N. Schmidt, M. Eisenmann, T. Langen, T. Pfau and I. Ferrier-Barbut.
Phys. Rev. Lett. **121**, 030401 (2018), ArXiv:1804.04552.
15. *Scissors mode of a dipolar quantum droplet of dysprosium atoms*,
I. Ferrier-Barbut, M. Wenzel, F. Böttcher, T. Langen, M. Isoard, S. Stringari and T. Pfau.
Phys. Rev. Lett. **120**, 160402 (2018), ArXiv:1712.06927.

16. *Onset of a modulational instability in trapped dipolar Bose-Einstein condensates*,
I. Ferrier-Barbut, M. Wenzel, M. Schmitt, F. Böttcher, T. Pfau.
Phys. Rev. A **97**, 011604(R) (2018), ArXiv:1711.07275.

17. *Striped states in a many-body system of tilted dipoles*,
M. Wenzel, F. Böttcher, T. Langen, I. Ferrier-Barbut and T. Pfau.
Phys. Rev. A **96**, 053630 (2017), ArXiv:1706.09388.

18. *Self-bound droplets of a dilute magnetic quantum liquid*,
M. Schmitt, M. Wenzel, F. Böttcher, I. Ferrier-Barbut and T. Pfau.
Nature **539**, 259 (2016), ArXiv:1607.07355.

19. *Liquid quantum droplets of ultracold magnetic atoms*,
I. Ferrier-Barbut, M. Schmitt, M. Wenzel, H. Kadau and T. Pfau.
J. Phys. B. **49**, 214004 (2016), ArXiv:1609.03937.

20. *Observation of quantum droplets in a strongly dipolar Bose gas*,
I. Ferrier-Barbut, H. Kadau, M. Schmitt, M. Wenzel, and T. Pfau.
Phys. Rev. Lett. **116**, 215301 (2016), ArXiv:1601.03318.

21. *Observing the Rosensweig instability of a quantum ferrofluid*,
H. Kadau, M. Schmitt, M. Wenzel, C. Wink, T. Maier, I. Ferrier-Barbut and T. Pfau.
Nature **530**, 194 (2016), ArXiv:1508.05007.

22. *Broad universal Feshbach resonances in the chaotic spectrum of dysprosium atoms*,
T. Maier, I. Ferrier-Barbut, H. Kadau, M. Schmitt, M. Wenzel, C. Wink, T. Pfau, K. Jachymski, and P. S. Julienne.
Phys. Rev. A **92**, 060702 (2015), ArXiv:1506.01875.

23. *Emergence of chaotic scattering in ultracold Er and Dy*,
T. Maier, H. Kadau, M. Schmitt, M. Wenzel, I. Ferrier-Barbut, T. Pfau, A. Frisch, S. Baier, K. Aikawa, L. Chomaz, M. J. Mark, F. Ferlaino, C. Makrides, E. Tiesinga, A. Petrov, and S. Kotochigova.
Phys. Rev. X **5**, 041029 (2015), ArXiv:1506.05221.

PhD in Paris

24. *Universal loss dynamics in a unitary Bose gas*,
U. Eismann, L. Khaykovich, S. Laurent, I. Ferrier-Barbut, B. S. Rem, A. T. Grier, M. Delehaye, F. Chevy, C. Salomon, L.-C. Ha and C. Chin.
Phys. Rev. X **6**, 021025 (2016), ArXiv:1505.04523.

25. *Critical velocity and dissipation of an ultracold Bose-Fermi counterflow*,
M. Delehaye, S. Laurent, I. Ferrier-Barbut, S. Jin, F. Chevy, and C. Salomon.
Phys. Rev. Lett. **115**, 265303 (2015), ArXiv:1510.06709.

26. *The Landau critical velocity for a particle in a Fermi superfluid*,
Y. Castin, I. Ferrier-Barbut and C. Salomon.
Comptes Rendus Physique **16**, 241 (2015), ArXiv:1408.1326.

27. *A mixture of Bose and Fermi superfluids*,
I. Ferrier-Barbut, M. Delehaye, S. Laurent, A. T. Grier, M. Pierce, B. S. Rem, F. Chevy, and C. Salomon.
Science **345**, 1035 (2014), ArXiv:1404.2548

28. *Lambda-enhanced sub-Doppler cooling of lithium atoms in D1 gray molasses*,
A. T. Grier, I. Ferrier-Barbut, B. S. Rem, M. Delehaye, L. Khaykovich, F. Chevy, and C.

Salomon.
Phys. Rev. A **87**, 063411 (2013), ArXiv:1304.6971.

29. *Lifetime of the Bose Gas with resonant interactions* ,
B. S. Rem, A. Grier, I. Ferrier-Barbut, U. Eismann, T. Langen, N. Navon, L. Khaykovich, F. Werner, D. S. Petrov, F. Chevy, and C. Salomon.
Phys. Rev. Lett. **110**, 163202 (2013), ArXiv:1212.5274.

3.10 Presentations in conferences

Lectures

1. Giryd Summer School, Weizmann Institute, Rehovot, Israel (2022)
2. International school on quantum gases, Chlef, Algeria (2018)
3. Granada quantum matter summer school, Granada, Spain (2017)

Invited talks

1. Collective scattering of light CoScaLi 2023, Heraklion, Grece (2023)
2. Open quantum many-body physics, Institut Pascal, Orsay, France (2023)
3. Waveguide QED, WQED23, Erice, Sicily (2023)
4. Long-range interactions in the ultracold workshop, Innsbruck, Austria (2022)
5. Workshop on collective scattering of light COSCALI, Porquerolles, France (2021)
6. Optique 2021 Coloque Horizons de l'Optique, Dijon, France (2021)
7. Cold atoms online meeting, Online, France (2021)
8. WE-Heraeus Seminar, Collective Effects and Non-Equilibrium Quantum Dynamics, Bad Honnef (online), Germany (2021)
9. XXII conference on few-body problems in physics, Caen, France (2018)
10. Workshop on long-range interactions in atomic systems, Sao Carlos, Brazil (2017)
11. From few to many, exploring quantum systems one atom at a time, Obergurgl, Austria (2017)
12. 47th colloquium on the physics of quantum electronics PQE2017, Snowbird, Utah (2017)
13. Gauge field dynamics with ultracold gas systems, Bad Honnef, Germany (2016)
14. Long-range interactions in the ultracold workshop, Ercolano, Italy (2016),
15. Quantum gases and quantum coherence BEC, Salerno, Italy (2016)
16. Ultracold quantum gases, current trends and perspectives Quo Vadis BEC, Bad Honnef, Germany (2016)
17. Quantum Optics, Obergurgl, Austria (2016)
18. Workshop : Advanced atomic sources and extreme cooling of atoms and molecules, Les Houches, France (2016)
19. Synthetic Quantum Magnetism International Workshop, Dresden, Germany (2015),
20. International Symposium on Quantum Fluids and Solids QFS2015, Niagara Falls, NY (2015)

Contributed talks

1. 7th colloquium of the CNRS research network "quantum engineering, foundations and applications", Paris, France (2016)
2. Quantum technologies conference V, Krakow, Poland (2014)
3. Laser Physics international workshop LPHYS13, Prague, Czech Republic (2013)

Références

[Aharonovich et al., 2016] Aharonovich, I., Englund, D., & Toth, M. (2016). Solid-state single-photon emitters. *Nature Photonics*, 10(10), 631–641.

[Albrecht et al., 2019] Albrecht, A., Henriet, L., Asenjo-Garcia, A., Dieterle, P. B., Painter, O., & Chang, D. E. (2019). Subradiant states of quantum bits coupled to a one-dimensional waveguide. *New Journal of Physics*, 21(2), 025003.

[Allen & Eberly, 1975] Allen, L. & Eberly, J. H. (1975). *Optical resonance and two-level atoms*. New York : Wiley.

[Araújo et al., 2016] Araújo, M. O., Krešić, I., Kaiser, R., & Guerin, W. (2016). Superradiance in a large and dilute cloud of cold atoms in the linear-optics regime. *Phys. Rev. Lett.*, 117, 073002.

[Asenjo-Garcia et al., 2017] Asenjo-Garcia, A., Moreno-Cardoner, M., Albrecht, A., Kimble, H. J., & Chang, D. E. (2017). Exponential improvement in photon storage fidelities using subradiance and "selective radiance" in atomic arrays. *Phys. Rev. X*, 7, 031024.

[Asselie et al., 2022] Asselie, S., Cipris, A., & Guerin, W. (2022). Optical interpretation of linear-optics superradiance and subradiance. *Phys. Rev. A*, 106, 063712.

[Bali et al., 1996] Bali, S., Hoffmann, D., Simán, J., & Walker, T. (1996). Measurements of intensity correlations of scattered light from laser-cooled atoms. *Phys. Rev. A*, 53, 3469–3472.

[Ballantine & Ruostekoski, 2021] Ballantine, K. E. & Ruostekoski, J. (2021). Quantum single-photon control, storage, and entanglement generation with planar atomic arrays. *PRX Quantum*, 2, 040362.

[Barredo et al., 2016] Barredo, D., de Léséleuc, S., Lienhard, V., Lahaye, T., & Browaeys", A. (2016). An atom-by-atom assembler of defect-free arbitrary two-dimensional atomic arrays. *Science*, 354(6315), 1021–1023.

[Baumann et al., 2014] Baumann, K., Burdick, N. Q., Lu, M., & Lev, B. L. (2014). Observation of low-field fano-feshbach resonances in ultracold gases of dysprosium. *Phys. Rev. A*, 89, 020701.

[Becher et al., 2018] Becher, J. H., Baier, S., Aikawa, K., Lepers, M., Wyart, J.-F., Dulieu, O., & Ferlaino, F. (2018). Anisotropic polarizability of erbium atoms. *Phys. Rev. A*, 97, 012509.

[Bekenstein et al., 2020] Bekenstein, R., Pikovski, I., Pichler, H., Shahmoon, E., Yelin, S. F., & Lukin, M. D. (2020). Quantum metasurfaces with atom arrays. *Nature Physics*, 16(6), 676–681.

[Bettles et al., 2016a] Bettles, R. J., Gardiner, S. A., & Adams, C. S. (2016a). Cooperative eigenmodes and scattering in one-dimensional atomic arrays. *Phys. Rev. A*, 94, 043844.

[Bettles et al., 2016b] Bettles, R. J., Gardiner, S. A., & Adams, C. S. (2016b). Enhanced optical cross section via collective coupling of atomic dipoles in a 2d array. *Phys. Rev. Lett.*, 116, 103602.

[Biagioni et al., 2023] Biagioni, G., Antolini, N., Donelli, B., Pezzè, L., Smerzi, A., Fattori, M., Fioretti, A., Gabbanini, C., Inguscio, M., Tanzi, L., & Modugno, G. (2023). Sub-unity superfluid fraction of a supersolid from self-induced josephson effect.

[Bismut et al., 2012] Bismut, G., Laburthe-Tolra, B., Maréchal, E., Pedri, P., Gorceix, O., & Vernac, L. (2012). Anisotropic excitation spectrum of a dipolar quantum bose gas. *Phys. Rev. Lett.*, 109, 155302.

[Bloch et al., 2024] Bloch, D., Hofer, B., Cohen, S., Lepers, M., Browaeys, a., & Ferrier-Barbut, I. (2024). In preparation.

[Bloch et al., 2023] Bloch, D., Hofer, B., Cohen, S. R., Browaeys, A., & Ferrier-Barbut, I. (2023). Trapping and imaging single dysprosium atoms in optical tweezer arrays. *Phys. Rev. Lett.*, 131, 203401.

[Bloch et al., 2008] Bloch, I., Dalibard, J., & Zwerger, W. (2008). Many-body physics with ultracold gases. *Rev. Mod. Phys.*, 80, 885–964.

[Bohnet et al., 2012] Bohnet, J. G., Chen, Z., Weiner, J. M., Meiser, D., Holland, M. J., & Thompson, J. K. (2012). A steady-state superradiant laser with less than one intracavity photon. *Nature*, 484(7392), 78–81.

[Boiron et al., 1995] Boiron, D., Triché, C., Meacher, D. R., Verkerk, P., & Grynberg, G. (1995). Three-dimensional cooling of cesium atoms in four-beam gray optical molasses. *Physical Review A*, 52(5), R3425–R3428.

[Böttcher et al., 2020] Böttcher, F., Schmidt, J.-N., Hertkorn, J., Ng, K. S., Graham, S. D., Guo, M., Langen, T., & Pfau, T. (2020). New states of matter with fine-tuned interactions : quantum droplets and dipolar supersolids. *Reports on Progress in Physics*, 84(1), 012403.

[Böttcher et al., 2019] Böttcher, F., Schmidt, J.-N., Wenzel, M., Hertkorn, J., Guo, M., Langen, T., & Pfau, T. (2019). Transient supersolid properties in an array of dipolar quantum droplets. *Phys. Rev. X*, 9, 011051.

[Brossard, 2020] Brossard, L. (2020). *Study of light-induced dipolar interactions in cold atoms assemblies*. PhD thesis, Université Paris Saclay.

[Brown et al., 2019] Brown, M. O., Thiele, T., Kiehl, C., Hsu, T.-W., & Regal, C. A. (2019). Gray-Molasses Optical-Tweezer Loading : Controlling Collisions for Scaling Atom-Array Assembly. *Physical Review X*, 9(1), 011057.

[Buonaiuto et al., 2021] Buonaiuto, G., Carollo, F., Olmos, B., & Lesanovsky, I. (2021). Dynamical phases and quantum correlations in an emitter-waveguide system with feedback. *Phys. Rev. Lett.*, 127, 133601.

[Cabrera et al., 2018] Cabrera, C. R., Tanzi, L., Sanz, J., Naylor, B., Thomas, P., Cheiney, P., & Tarruell, L. (2018). Quantum liquid droplets in a mixture of Bose-Einstein condensates. *Science*, 359(6373), 301–304.

[Carmichael et al., 1978] Carmichael, H. J., Drummond, P., Meystre, P., & Walls, D. F. (1978). Intensity correlations in resonance fluorescence with atomic number fluctuations. *Journal of Physics A : Mathematical and General*, 11(5), L121.

[Chalopin et al., 2018] Chalopin, T., Makhalov, V., Bouazza, C., Evrard, A., Barker, A., Lepers, M., Wyart, J.-F. m. c., Dulieu, O., Dalibard, J., Lopes, R., & Nascimbene, S. (2018). Anisotropic light shift and magic polarization of the intercombination line of dysprosium atoms in a far-detuned dipole trap. *Phys. Rev. A*, 98, 040502.

[Chin et al., 2010] Chin, C., Grimm, R., Julienne, P., & Tiesinga, E. (2010). Feshbach resonances in ultracold gases. *Rev. Mod. Phys.*, 82, 1225–1286.

[Chomaz et al., 2016] Chomaz, L., Baier, S., Petter, D., Mark, M. J., Wächtler, F., Santos, L., & Ferlaino, F. (2016). Quantum-Fluctuation-Driven Crossover from a Dilute Bose-Einstein Condensate to a Macrodroplet in a Dipolar Quantum Fluid. *Physical Review X*, 6(4), 041039.

[Chomaz et al., 2022] Chomaz, L., Ferrier-Barbut, I., Ferlaino, F., Laburthe-Tolra, B., Lev, B. L., & Pfau, T. (2022). Dipolar physics : a review of experiments with magnetic quantum gases. *Reports on Progress in Physics*, 86(2), 026401.

[Chomaz et al., 2019] Chomaz, L., Petter, D., Ilzhöfer, P., Natale, G., Trautmann, A., Politi, C., Durastante, G., van Bijnen, R. M. W., Patscheider, A., Sohmen, M., Mark, M. J., & Ferlaino, F. (2019). Long-lived and transient supersolid behaviors in dipolar quantum gases. *Phys. Rev. X*, 9, 021012.

[Chomaz et al., 2018] Chomaz, L., van Bijnen, R. M. W., Petter, D., Faraoni, G., Baier, S., Becher, J. H., Mark, M. J., Wächtler, F., Santos, L., & Ferlaino, F. (2018). Observation of roton mode population in a dipolar quantum gas. *Nature Physics*, 14(5), 442–446.

[Cipris et al., 2021] Cipris, A., Moreira, N. A., Santo, T. S. d. E., Weiss, P., Villas-Boas, C. J., Kaiser, R., Guerin, W., & Bachelard, R. (2021). Subradiance with Saturated Atoms : Population Enhancement of the Long-Lived States. *Physical Review Letters*, 126(10), 103604.

[Cooper et al., 2018] Cooper, A., Covey, J. P., Madjarov, I. S., Porsev, S. G., Safronova, M. S., & Endres, M. (2018). Alkaline-earth atoms in optical tweezers. *Phys. Rev. X*, 8, 041055.

[Dalibard, 2024] Dalibard, J. (2024). Cours du Collège de France 2024 : Interactions magnétiques entre atomes froids : gouttelettes quantiques et états supersolides.

[Das et al., 2020] Das, D., Lemberger, B., & Yavuz, D. D. (2020). Subradiance and superradiance-to-subradiance transition in dilute atomic clouds. *Physical Review A*, 102(4), 043708.

[de Paz et al., 2013] de Paz, A., Sharma, A., Chotia, A., Maréchal, E., Huckans, J. H., Pedri, P., Santos, L., Gorceix, O., Vernac, L., & Laburthe-Tolra, B. (2013). Nonequilibrium quantum magnetism in a dipolar lattice gas. *Phys. Rev. Lett.*, 111, 185305.

[DeVoe & Brewer, 1996] DeVoe, R. G. & Brewer, R. G. (1996). Observation of Superradiant and Subradiant Spontaneous Emission of Two Trapped Ions. *Physical Review Letters*, 76(12), 2049–2052.

[Dicke, 1954] Dicke, R. H. (1954). Coherence in spontaneous radiation processes. *Phys. Rev.*, 93, 99–110.

[Diedrich et al., 1989] Diedrich, F., Bergquist, J. C., Itano, W. M., & Wineland, D. J. (1989). Laser cooling to the zero-point energy of motion. *Phys. Rev. Lett.*, 62, 403–406.

[Diedrich & Walther, 1987] Diedrich, F. & Walther, H. (1987). Nonclassical radiation of a single stored ion. *Phys. Rev. Lett.*, 58, 203–206.

[Endres et al., 2016] Endres, M., Bernien, H., Keesling, A., Levine, H., Anschuetz, E. R., Krajenbrink, A., Senko, C., Vuletic, V., Greiner, M., & Lukin, M. D. (2016). Atom-by-atom assembly of defect-free one-dimensional cold atom arrays. *Science*, 354(6315), 1024–1027.

[Esslinger et al., 1996] Esslinger, T., Ritsch, H., Weidemüller, M., Sander, F., Hemmerich, A., & Hänsch, T. W. (1996). Purely optical dark lattice. *Optics Letters*, 21(13), 991.

[Facchinetti et al., 2016] Facchinetti, G., Jenkins, S. D., & Ruostekoski, J. (2016). Storing Light with Subradiant Correlations in Arrays of Atoms. *Physical Review Letters*, 117(24), 243601.

[Fayard et al., 2023] Fayard, N., Ferrier-Barbut, I., Browaeys, A., & Greffet, J.-J. (2023). Optical control of collective states in one-dimensional ordered atomic chains beyond the linear regime. *Phys. Rev. A*, 108, 023116.

[Ferioli et al., 2023] Ferioli, G., Glicenstein, A., Ferrier-Barbut, I., & Browaeys, A. (2023). A non-equilibrium superradiant phase transition in free space. *Nature Physics*, 19(9), 1345–1349.

[Ferioli et al., 2021a] Ferioli, G., Glicenstein, A., Henriet, L., Ferrier-Barbut, I., & Browaeys, A. (2021a). Storage and Release of Subradiant Excitations in a Dense Atomic Cloud. *Physical Review X*, 11(2), 021031.

[Ferioli et al., 2021b] Ferioli, G., Glicenstein, A., Robicheaux, F., Sutherland, R. T., Browaeys, A., & Ferrier-Barbut, I. (2021b). Laser-Driven Superradiant Ensembles of Two-Level Atoms near Dicke Regime. *Physical Review Letters*, 127(24), 243602.

[Ferioli et al., 2024] Ferioli, G., Pancaldi, S., Glicenstein, A., Clement, D., Browaeys, A., & Ferrier-Barbut, I. (2024). Non-gaussian correlations in the steady-state of driven-dissipative clouds of two-level atoms.

[Fernandes et al., 2012] Fernandes, D. R., Sievers, F., Kretzschmar, N., Wu, S., Salomon, C., & Chevy, F. (2012). Sub-Doppler laser cooling of fermionic 40K atoms in three-dimensional gray optical molasses. *EPL*, 100(6), 63001.

[Ferreira et al., 2020] Ferreira, D., Bachelard, R., Guerin, W., Kaiser, R., & FouchÃľ, M. (2020). Connecting field and intensity correlations : The siegert relation and how to test it. *American Journal of Physics*, 88(10), 831–837.

[Ferrier-Barbut, 2019] Ferrier-Barbut, I. (2019). Ultradilute quantum droplets. *Physics Today*, 72(4), 46–52.

[Ferrier-Barbut et al., 2016] Ferrier-Barbut, I., Kadau, H., Schmitt, M., Wenzel, M., & Pfau, T. (2016). Observation of quantum droplets in a strongly dipolar bose gas. *Phys. Rev. Lett.*, 116, 215301.

[Frisch et al., 2014] Frisch, A., Mark, M., Aikawa, K., Ferlaino, F., Bohn, J. L., Makrides, C., Petrov, A., & Kotochigova, S. (2014). Quantum chaos in ultracold collisions of gas-phase erbium atoms. *Nature*, 507(7493), 475–479.

[Gazzano et al., 2013] Gazzano, O., Michaelis de Vasconcellos, S., Arnold, C., Nowak, A., Galopin, E., Sagnes, I., Lanco, L., Lemaître, A., & Senellart, P. (2013). Bright solid-state sources of indistinguishable single photons. *Nature Communications*, 4(1), 1425.

[Glicenstein, 2022] Glicenstein, A. (2022). *Collective spontaneous emission from dense ensembles of two-level atoms*. PhD thesis, Université Paris Saclay.

[Glicenstein et al., 2021] Glicenstein, A., Ferioli, G., Brossard, L., Sortais, Y. R. P., Barredo, D., Nogrette, F., Ferrier-Barbut, I., & Browaeys, A. (2021). Preparation of one-dimensional chains and dense cold atomic clouds with a high numerical aperture four-lens system. *Phys. Rev. A*, 103, 043301.

[Glicenstein et al., 2022] Glicenstein, A., Ferioli, G., Browaeys, A., & Ferrier-Barbut, I. (2022). From superradiance to subradiance : exploring the many-body dicke ladder. *Opt. Lett.*, 47(6), 1541–1544.

[Glicenstein et al., 2020] Glicenstein, A., Ferioli, G., Šibalić, N., Brossard, L., Ferrier-Barbut, I., & Browaeys, A. (2020). Collective shift in resonant light scattering by a one-dimensional atomic chain. *Phys. Rev. Lett.*, 124, 253602.

[Góral et al., 2000] Góral, K., Rzążewski, K., & Pfau, T. (2000). Bose-einstein condensation with magnetic dipole-dipole forces. *Phys. Rev. A*, 61, 051601.

[Grier et al., 2013] Grier, A. T., Ferrier-Barbut, I., Rem, B. S., Delehaye, M., Khaykovich, L., Chevy, F., & Salomon, C. (2013). Λ-enhanced sub-Doppler cooling of lithium atoms in D1 gray molasses. *Physical Review A*.

[Gross & Haroche, 1982] Gross, M. & Haroche, S. (1982). Superradiance : An essay on the theory of collective spontaneous emission. *Physics Reports*, 93(5), 301–396.

[Grover et al., 2015] Grover, J. A., Solano, P., Orozco, L. A., & Rolston, S. L. (2015). Photon-correlation measurements of atomic-cloud temperature using an optical nanofiber. *Phys. Rev. A*, 92, 013850.

[Guerin et al., 2016] Guerin, W., Araújo, M. O., & Kaiser, R. (2016). Subradiance in a large cloud of cold atoms. *Phys. Rev. Lett.*, 116, 083601.

[Guerin et al., 2017] Guerin, W., Rouabah, M., & Kaiser, R. (2017). Light interacting with atomic ensembles : collective, cooperative and mesoscopic effects. *Journal of Modern Optics*, 64(9), 895–907.

[Hanbury Brown & Twiss, 1956] Hanbury Brown, R. & Twiss, R. Q. (1956). A test of a new type of stellar interferometer on sirius. *Nature*, 178(4541), 1046–1048.

[Hannukainen & Larson, 2018] Hannukainen, J. & Larson, J. (2018). Dissipation-driven quantum phase transitions and symmetry breaking. *Phys. Rev. A*, 98, 042113.

[Hazzard et al., 2014] Hazzard, K. R. A., van den Worm, M., Foss-Feig, M., Manmana, S. R., Dalla Torre, E. G., Pfau, T., Kastner, M., & Rey, A. M. (2014). Quantum correlations and entanglement in far-from-equilibrium spin systems. *Phys. Rev. A*, 90, 063622.

[He et al., 2020] He, Y., Ji, L., Wang, Y., Qiu, L., Zhao, J., Ma, Y., Huang, X., Wu, S., & Chang, D. E. (2020). Geometric control of collective spontaneous emission. *Phys. Rev. Lett.*, 125, 213602.

[Henriet et al., 2019] Henriet, L., Douglas, J. S., Chang, D. E., & Albrecht, A. (2019). Critical open-system dynamics in a one-dimensional optical-lattice clock. *Physical Review A*, 99(2), 023802.

[Hong et al., 2006] Hong, H.-G., Seo, W., Lee, M., Choi, W., Lee, J.-H., & An, K. (2006). Spectral line-shape measurement of an extremely weak amplitude-fluctuating light source by photon-counting-based second-order correlation spectroscopy. *Opt. Lett.*, 31(21), 3182–3184.

[Jenkins et al., 2016] Jenkins, S. D., Ruostekoski, J., Javanainen, J., Bourgain, R., Jennewein, S., Sortais, Y. R. P., & Browaeys, A. (2016). Optical resonance shifts in the fluorescence of thermal and cold atomic gases. *Phys. Rev. Lett.*, 116, 183601.

[Jennewein et al., 2016] Jennewein, S., Sortais, Y. R. P., Greffet, J.-J., & Browaeys, A. (2016). Propagation of light through small clouds of cold interacting atoms. *Phys. Rev. A*, 94, 053828.

[Kadau et al., 2016] Kadau, H., Schmitt, M., Wenzel, M., Wink, C., Maier, T., Ferrier-Barbut, I., & Pfau, T. (2016). Observing the rosensweig instability of a quantum ferrofluid. *Nature*, 530(7589), 194–197.

[Kao et al., 2017] Kao, W., Tang, Y., Burdick, N. Q., & Lev, B. L. (2017). Anisotropic dependence of tune-out wavelength near dy 741-nm transition. *Opt. Express*, 25(4), 3411–3419.

[Kiffner et al., 2010] Kiffner, M., Macovei, M., Evers, J., & Keitel, C. (2010). Chapter 3 - vacuum-induced processes in multilevel atoms. volume 55 of *Progress in Optics* (pp. 85–197). Elsevier.

[Kimble et al., 1977] Kimble, H. J., Dagenais, M., & Mandel, L. (1977). Photon antibunching in resonance fluorescence. *Phys. Rev. Lett.*, 39, 691–695.

[Kotochigova & Petrov, 2011] Kotochigova, S. & Petrov, A. (2011). Anisotropy in the interaction of ultracold dysprosium. *Phys. Chem. Chem. Phys.*, 13, 19165–19170.

[Kubo, 1962] Kubo, R. (1962). Generalized cumulant expansion method. *Journal of the Physical Society of Japan*, 17(7), 1100–1120.

[Labuhn et al., 2016] Labuhn, H., Barredo, D., Ravets, S., de Léséleuc, S., Macrì, T., Lahaye, T., & Browaeys, A. (2016). Tunable two-dimensional arrays of single rydberg atoms for realizing quantum ising models. *Nature*, 534(7609), 667–670.

[Lahaye et al., 2009] Lahaye, T., Menotti, C., Santos, L., Lewenstein, M., & Pfau, T. (2009). The physics of dipolar bosonic quantum gases. *Reports on Progress in Physics*, 72(12), 126401.

[Lahaye et al., 2008] Lahaye, T., Metz, J., Fröhlich, B., Koch, T., Meister, M., Griesmaier, A., Pfau, T., Saito, H., Kawaguchi, Y., & Ueda, M. (2008). *d*-wave collapse and explosion of a dipolar bose-einstein condensate. *Phys. Rev. Lett.*, 101, 080401.

[Laske et al., 2019] Laske, T., Winter, H., & Hemmerich, A. (2019). Pulse delay time statistics in a superradiant laser with calcium atoms. *Phys. Rev. Lett.*, 123, 103601.

[Lee et al., 1957] Lee, T. D., Huang, K., & Yang, C. N. (1957). Eigenvalues and eigenfunctions of a bose system of hard spheres and its low-temperature properties. *Phys. Rev.*, 106, 1135–1145.

[Lemieux & Durian, 1999] Lemieux, P.-A. & Durian, D. J. (1999). Investigating non-gaussian scattering processes by using nth-order intensity correlation functions. *J. Opt. Soc. Am. A*, 16(7), 1651–1664.

[Lepers et al., 2014] Lepers, M., Wyart, J.-F., & Dulieu, O. (2014). Anisotropic optical trapping of ultracold erbium atoms. *Phys. Rev. A*, 89, 022505.

[Li et al., 2016] Li, H., Wyart, J.-F., Dulieu, O., Nascimbène, S., & Lepers, M. (2016). Optical trapping of ultracold dysprosium atoms : transition probabilities, dynamic dipole polarizabilities and van der waals c6 coefficients. *Journal of Physics B : Atomic, Molecular and Optical Physics*, 50(1), 014005.

[Lima & Pelster, 2011] Lima, A. R. P. & Pelster, A. (2011). Quantum fluctuations in dipolar bose gases. *Phys. Rev. A*, 84, 041604.

[Lima & Pelster, 2012] Lima, A. R. P. & Pelster, A. (2012). Beyond mean-field low-lying excitations of dipolar bose gases. *Phys. Rev. A*, 86, 063609.

[Loudon, 2000] Loudon, R. (2000). *The quantum theory of light*. OUP Oxford.

[Ludlow et al., 2015] Ludlow, A. D., Boyd, M. M., Ye, J., Peik, E., & Schmidt, P. O. (2015). Optical atomic clocks. *Rev. Mod. Phys.*, 87, 637–701.

[Ma et al., 2022] Ma, S., Burgers, A. P., Liu, G., Wilson, J., Zhang, B., & Thompson, J. D. (2022). Universal gate operations on nuclear spin qubits in an optical tweezer array of ^{171}Yb atoms. *Phys. Rev. X*, 12, 021028.

[Maier et al., 2015a] Maier, T., Ferrier-Barbut, I., Kadau, H., Schmitt, M., Wenzel, M., Wink, C., Pfau, T., Jachymski, K., & Julienne, P. S. (2015a). Broad universal feshbach resonances in the chaotic spectrum of dysprosium atoms. *Phys. Rev. A*, 92, 060702.

[Maier et al., 2015b] Maier, T., Kadau, H., Schmitt, M., Wenzel, M., Ferrier-Barbut, I., Pfau, T., Frisch, A., Baier, S., Aikawa, K., Chomaz, L., Mark, M. J., Ferlaino, F., Makrides, C., Tiesinga, E., Petrov, A., & Kotochigova, S. (2015b). Emergence of chaotic scattering in ultracold er and dy. *Phys. Rev. X*, 5, 041029.

[McGuyer et al., 2015] McGuyer, B. H., McDonald, M., Iwata, G. Z., Tarallo, M. G., Skomorowski, W., Moszynski, R., & Zelevinsky, T. (2015). Precise study of asymptotic physics with subradiant ultracold molecules. *Nature Physics*, 11(1), 32–36.

[Meiser et al., 2009] Meiser, D., Ye, J., Carlson, D. R., & Holland, M. J. (2009). Prospects for a millihertz-linewidth laser. *Phys. Rev. Lett.*, 102, 163601.

[Mink & Fleischhauer, 2023] Mink, C. D. & Fleischhauer, M. (2023). Collective radiative interactions in the discrete truncated Wigner approximation. *SciPost Phys.*, 15, 233.

[Mitra et al., 2016] Mitra, D., Brown, P. T., Schauß, P., Kondov, S. S., & Bakr, W. S. (2016). Phase separation and pair condensation in a spin-imbalanced 2d fermi gas. *Phys. Rev. Lett.*, 117, 093601.

[Moreno-Cardoner et al., 2021] Moreno-Cardoner, M., Goncalves, D., & Chang, D. E. (2021). Quantum nonlinear optics based on two-dimensional rydberg atom arrays. *Phys. Rev. Lett.*, 127, 263602.

[Nagourney et al., 1986] Nagourney, W., Sandberg, J., & Dehmelt, H. (1986). Shelved optical electron amplifier : Observation of quantum jumps. *Phys. Rev. Lett.*, 56, 2797–2799.

[Nogrette et al., 2014] Nogrette, F., Labuhn, H., Ravets, S., Barredo, D., Béguin, L., Vernier, A., Lahaye, T., & Browaeys, A. (2014). Single-atom trapping in holographic 2d arrays of microtraps with arbitrary geometries. *Phys. Rev. X*, 4, 021034.

[Norcia & Thompson, 2016] Norcia, M. A. & Thompson, J. K. (2016). Cold-strontium laser in the superradiant crossover regime. *Phys. Rev. X*, 6, 011025.

[Norcia et al., 2018] Norcia, M. A., Young, A. W., & Kaufman, A. M. (2018). Microscopic control and detection of ultracold strontium in optical-tweezer arrays. *Phys. Rev. X*, 8, 041054.

[Ortiz-Gutiérrez et al., 2019] Ortiz-Gutiérrez, L., Teixeira, R. C., Eloy, A., da Silva, D. F., Kaiser, R., Bachelard, R., & Fouché, M. (2019). Mollow triplet in cold atoms. *New Journal of Physics*, 21(9), 093019.

[Ostermann et al., 2013] Ostermann, L., Ritsch, H., & Genes, C. (2013). Protected state enhanced quantum metrology with interacting two-level ensembles. *Phys. Rev. Lett.*, 111, 123601.

[Ostermann et al., 2023] Ostermann, S., Rubies-Bigorda, O., Zhang, V., & Yelin, S. F. (2023). Breakdown of steady-state superradiance in extended driven atomic arrays.

[Pavolini et al., 1985] Pavolini, D., Crubellier, A., Pillet, P., Cabaret, L., & Liberman, S. (1985). Experimental Evidence for Subradiance. *Physical Review Letters*, 54(17), 1917–1920.

[Pellegrino et al., 2014] Pellegrino, J., Bourgain, R., Jennewein, S., Sortais, Y. R. P., Browaeys, A., Jenkins, S. D., & Ruostekoski, J. (2014). Observation of suppression of light scattering induced by dipole-dipole interactions in a cold-atom ensemble. *Phys. Rev. Lett.*, 113, 133602.

[Perczel et al., 2017] Perczel, J., Borregaard, J., Chang, D. E., Pichler, H., Yelin, S. F., Zoller, P., & Lukin, M. D. (2017). Photonic band structure of two-dimensional atomic lattices. *Phys. Rev. A*, 96, 063801.

[Petrov, 2015] Petrov, D. S. (2015). Quantum mechanical stabilization of a collapsing bose-bose mixture. *Phys. Rev. Lett.*, 115, 155302.

[Petter et al., 2019] Petter, D., Natale, G., van Bijnen, R. M. W., Patscheider, A., Mark, M. J., Chomaz, L., & Ferlaino, F. (2019). Probing the roton excitation spectrum of a stable dipolar bose gas. *Phys. Rev. Lett.*, 122, 183401.

[Pitaevskii & Stringari, 2016] Pitaevskii, L. & Stringari, S. (2016). *Bose-Einstein condensation and superfluidity*, volume 164. Oxford University Press.

[Plankensteiner et al., 2022] Plankensteiner, D., Hotter, C., & Ritsch, H. (2022). QuantumCumulants.jl : A Julia framework for generalized mean-field equations in open quantum systems. *Quantum*, 6, 617.

[Robicheaux & Suresh, 2021] Robicheaux, F. & Suresh, D. A. (2021). Beyond lowest order mean-field theory for light interacting with atom arrays. *Phys. Rev. A*, 104, 023702.

[Roccuzzo & Ancilotto, 2019] Roccuzzo, S. M. & Ancilotto, F. (2019). Supersolid behavior of a dipolar bose-einstein condensate confined in a tube. *Phys. Rev. A*, 99, 041601.

[Roof et al., 2016] Roof, S. J., Kemp, K. J., Havey, M. D., & Sokolov, I. M. (2016). Observation of single-photon superradiance and the cooperative lamb shift in an extended sample of cold atoms. *Phys. Rev. Lett.*, 117, 073003.

[Rubies-Bigorda et al., 2022] Rubies-Bigorda, O., Walther, V., Patti, T. L., & Yelin, S. F. (2022). Photon control and coherent interactions via lattice dark states in atomic arrays. *Phys. Rev. Res.*, 4, 013110.

[Rui et al., 2020] Rui, J., Wei, D., Rubio-Abadal, A., Hollerith, S., Zeiher, J., Stamper-Kurn, D. M., Gross, C., & Bloch, I. (2020). A subradiant optical mirror formed by a single structured atomic layer. *Nature*, 583(7816), 369–374.

[Santos et al., 2003] Santos, L., Shlyapnikov, G. V., & Lewenstein, M. (2003). Roton-maxon spectrum and stability of trapped dipolar bose-einstein condensates. *Phys. Rev. Lett.*, 90, 250403.

[Saskin et al., 2019] Saskin, S., Wilson, J. T., Grinkemeyer, B., & Thompson, J. D. (2019). Narrow-line cooling and imaging of ytterbium atoms in an optical tweezer array. *Phys. Rev. Lett.*, 122, 143002.

[Sauter et al., 1986] Sauter, T., Neuhauser, W., Blatt, R., & Toschek, P. E. (1986). Observation of quantum jumps. *Phys. Rev. Lett.*, 57, 1696–1698.

[Schäffer et al., 2020] Schäffer, S. A., Tang, M., Henriksen, M. R., Jørgensen, A. A., Christensen, B. T. R., & Thomsen, J. W. (2020). Lasing on a narrow transition in a cold thermal strontium ensemble. *Phys. Rev. A*, 101, 013819.

[Schlosser et al., 2001] Schlosser, N., Reymond, G., Protsenko, I., & Grangier, P. (2001). Sub-poissonian loading of single atoms in a microscopic dipole trap. *Nature*.

[Schmitt et al., 2016] Schmitt, M., Wenzel, M., Böttcher, F., Ferrier-Barbut, I., & Pfau, T. (2016). Self-bound droplets of a dilute magnetic quantum liquid. *Nature*, 539(7628), 259–262.

[Semeghini et al., 2018] Semeghini, G., Ferioli, G., Masi, L., Mazzinghi, C., Wolswijk, L., Minardi, F., Modugno, M., Modugno, G., Inguscio, M., & Fattori, M. (2018). Self-Bound Quantum Droplets of Atomic Mixtures in Free Space. *Physical Review Letters*, 120(23), 235301.

[Shahmoon et al., 2017] Shahmoon, E., Wild, D. S., Lukin, M. D., & Yelin, S. F. (2017). Cooperative resonances in light scattering from two-dimensional atomic arrays. *Phys. Rev. Lett.*, 118, 113601.

[Siegert, 1943] Siegert, A. (1943). *On the fluctuations in signals returned by many independently moving scatterers*. Radiation Laboratory, Massachusetts Institute of Technology.

[Sievers et al., 2015] Sievers, F., Kretzschmar, N., Fernandes, D. R., Suchet, D., Rabinovic, M., Wu, S., Parker, C. V., Khaykovich, L., Salomon, C., & Chevy, F. (2015). Simultaneous sub-doppler laser cooling of fermionic ^{6}Li and ^{40}K on the D_1 line : Theory and experiment. *Phys. Rev. A*, 91, 023426.

[Somech & Shahmoon, 2022] Somech, O. & Shahmoon, E. (2022). Quantum entangled states of a classically radiating macroscopic spin.

[Sortais et al., 2007] Sortais, Y. R. P., Marion, H., Tuchendler, C., Lance, A. M., Lamare, M., Fournet, P., Armellin, C., Mercier, R., Messin, G., Browaeys, A., & Grangier, P. (2007). Diffraction-limited optics for single-atom manipulation. *Phys. Rev. A*, 75, 013406.

[Steck, 2007] Steck, D. A. (2007). Quantum and atom optics.

[Stitely et al., 2023] Stitely, K. C., Finger, F., Rosa-Medina, R., Ferri, F., Donner, T., Esslinger, T., Parkins, S., & Krauskopf, B. (2023). Quantum fluctuation dynamics of dispersive superradiant pulses in a hybrid light-matter system. *Phys. Rev. Lett.*, 131, 143604.

[Sutherland & Robicheaux, 2016] Sutherland, R. T. & Robicheaux, F. (2016). Collective dipole-dipole interactions in an atomic array. *Physical Review A*, 94(1), 013847.

[Sutherland & Robicheaux, 2017] Sutherland, R. T. & Robicheaux, F. (2017). Superradiance in inverted multilevel atomic clouds. *Phys. Rev. A*, 95, 033839.

[Takasu et al., 2012] Takasu, Y., Saito, Y., Takahashi, Y., Borkowski, M., Ciurylo, R., & Julienne, P. S. (2012). Controlled Production of Subradiant States of a Diatomic Molecule in an Optical Lattice. *Physical Review Letters*, 108(17), 173002.

[Tanji-Suzuki et al., 2011] Tanji-Suzuki, H., Leroux, I. D., Schleier-Smith, M. H., Cetina, M., Grier, A. T., Simon, J., & Vuletić, V. (2011). Chapter 4 - interaction between atomic ensembles and optical resonators : Classical description. In E. Arimondo, P. Berman, & C. Lin (Eds.), *Advances in Atomic, Molecular, and Optical Physics*, volume 60 of *Advances In Atomic, Molecular, and Optical Physics* (pp. 201–237). Academic Press.

[Tanzi et al., 2019] Tanzi, L., Lucioni, E., Famà, F., Catani, J., Fioretti, A., Gabbanini, C., Bisset, R. N., Santos, L., & Modugno, G. (2019). Observation of a dipolar quantum gas with metastable supersolid properties. *Phys. Rev. Lett.*, 122, 130405.

[Ville et al., 2017] Ville, J. L., Bienaimé, T., Saint-Jalm, R., Corman, L., Aidelsburger, M., Chomaz, L., Kleinlein, K., Perconte, D., Nascimbène, S., Dalibard, J., & Beugnon, J. (2017). Loading and compression of a single two-dimensional bose gas in an optical accordion. *Phys. Rev. A*, 95, 013632.

[Walschaers, 2021] Walschaers, M. (2021). Non-gaussian quantum states and where to find them. *PRX Quantum*, 2, 030204.

[Wenzel et al., 2017] Wenzel, M., Böttcher, F., Langen, T., Ferrier-Barbut, I., & Pfau, T. (2017). Striped states in a many-body system of tilted dipoles. *Phys. Rev. A*, 96, 053630.

[Wenzel et al., 2018] Wenzel, M., Böttcher, F., Schmidt, J.-N., Eisenmann, M., Langen, T., Pfau, T., & Ferrier-Barbut, I. (2018). Anisotropic superfluid behavior of a dipolar bose-einstein condensate. *Phys. Rev. Lett.*, 121, 030401.

[Yi & You, 2000] Yi, S. & You, L. (2000). Trapped atomic condensates with anisotropic interactions. *Phys. Rev. A*, 61, 041604.

[Yu, 2017] Yu, Z.-Q. (2017). Landau criterion for an anisotropic bose-einstein condensate. *Phys. Rev. A*, 95, 033618.

[Zhang & Mølmer, 2019] Zhang, Y.-X. & Mølmer, K. (2019). Theory of Subradiant States of a One-Dimensional Two-Level Atom Chain. *Physical Review Letters*, 122(20), 203605.

université
PARIS-SACLAY

Titre : Expériences d'atomes froids sur les corrélations dans des ensembles de dipolaires.

Mots clés : physique atomique, physique quantique, interaction lumière-matière.

Résumé : Ce mémoire d'habilitation retrace les travaux de recherches auxquels j'ai participé depuis mon doctorat. Il présente d'une part les travaux effectués lors de mon séjour post-doctoral à l'Université de Stuttgart, avant de se focaliser sur nos travaux sur la diffusion de la lumière, au Laboratoire Charles Fabry. Ces travaux ont majoritairement pour but la mise en évidence expérimentale de corrélations et de leurs effets macroscopiques dans des systèmes à N corps interagissant via une interaction dipolaire. Ils sont le fruit d'un travail en équipe dont j'ai pris part à la supervision, ce qui est présenté dans le mémoire.

Title : Cold-atom experiments on correlations in magnetic and light-induced dipoles.

Keywords : atomic physics, quantum physics, light-matter interaction.

Abstract : This report summarizes the research works that I took part in in the past 10 years. I first review results from my post-doctoral stay in Stuttgart University, before focusing on the research project that we develop in Laboratoire Charles Fabry. The unifying theme of these works is the search for microscopic and macroscopic manifestations of correlations in many-body ensembles of atomic dipoles. The report presents how I shared the supervision of the teams that carried-out the experimental work.